To the Graduate Council:

I am submitting herewith a dissertation written by Maharaj Krishen Bhat entitled "On Transonic Flow over Segmented Slotted Wind Tunnel Wall with Mass Transfer." I have examined the final copy of this dissertation for form and content and recommend that it be accepted in partial fulfillment of the requirements for the degree of Doctor of Philosophy with a major in Aerospace Engineering.

Jain-Ming Wu

Jain-Ming Wu, Major Professor

We have read this dissertation
and recommend its acceptance:

Frank G. Collins

A. D. Vakili

[illegible]

Joe C Reddy

Accepted for the Council:

C W Minkel

Vice Provost
and Dean of the Graduate School

ON TRANSONIC FLOW OVER SEGMENTED SLOTTED WIND TUNNEL WALL WITH MASS TRANSFER

A Dissertation
Presented for the
Doctor of Philosophy
Degree
The University of Tennessee, Knoxville

Maharaj Krishen Bhat

December 1988

ACKNOWLEDGMENTS

The author is grateful to his major professor, Dr. Jain-Ming Wu, for his invaluable support and guidance.

The author is indebted to Dr. F. G. Collins for his technical advice and help. Sincere appreciation is expressed to Dr. T. H. Moulden and Dr. K. C. Reddy for their constructive criticism and advice. The effort of Dr. T. H. Moulden to correct the manuscript is gratefully acknowledged. Sincere thanks are extended to Dr. A. D. Vakili for his encouragement and useful discussions.

The author expresses sincere thanks to Mr. Richard G. Ray, Mr. Harold Sartain and Mr. Ricky Meeker, of the University of Tennessee Space Institute transonic wind tunnel laboratory, for their help in conducting the experiments reported herein. Also a special thanks to George Shi for his support and help with all the last minute concerns.

The work reported herein was partially supported by the NASA Ames Research Center.

The author extends special thanks to Ms. Linda Williams and Ms. Melissa Weatherford for their help in typing the manuscript.

ABSTRACT

The flowfield on a single and a segmented multi-slotted wind tunnel wall have been studied at transonic speeds by traversing the wall viscous layer using five port cone probes. As expected, the slotted wall flowfield was observed to be three-dimensional in nature for a significant distance above the slot. The boundary layer characteristics measured on the single slotted wall have been found to be very sensitive to the applied suction through the slot. The velocity component perturbations generated due to the flow through the slot decay rapidly in the transverse direction. A vortex-like flow existed on the single slotted wall for natural ventilation but diminished with increased suction flow rate. For flow on a segmented multi-slotted wall, the normal velocity component changes were found to be maximum for measurement points located between the segmented slots atop the active chamber. The lateral influence due to applied suction and blowing, through a compartment, exceeded only slightly that in the downstream direction. Limited upstream influence was observed. Influence coefficients were determined from the data in the least-square sense for blowing and suction applied through one and two compartments. This was found to be an adequate determination of the influence coefficients for the range of mass flows considered.

TABLE OF CONTENTS

LIST OF FIGURES

LIST OF SYMBOLS

c_p	pressure coefficient
c_α	pitch angularity coefficient $\Delta P_{1-3}/(P_5 - \overline{P})$
c_β	yaw angularity coefficient $\Delta P_{2-4}/(P_5 - \overline{P})$
c_M	compressibility factor $(P_5 - \overline{P})/P_5$
M	Mach number
$\dot{m}$	applied suction or blowing mass flow rate (lbm/min.)
m^*	normalized mass flow rate $(\dot{m}/\dot{m}_{\text{tunnel}})$
P	static pressure
P_1, P_2, P_3, P_4	static port pressures on cone probe
P_5	pitot port pressure on cone probe
$\overline{P}$	average of static port pressures on cone probe
$\tilde{P}$	normalized static pressure (P/q)
P_t	total pressure
ΔP_{1-3}	differential pressure between ports 1 and 3 on cone probe
ΔP_{2-4}	differential pressure across ports 2 and 4 on cone probe
q	dynamic pressure $(\frac{\gamma}{2}PM^2)$
Q	volume flow rate (CFM), SCFM - referred to standard pressure and temperature conditions
$Re/ft.$	unit Reynolds number $(\rho V/\mu)$
T	static temperature
V	magnitude of total velocity
u, v, w	velocity components in X, Y, Z directions
Δw	change in w velocity component

(x, y, z)	distance in X, Y, Z directions
α	pitch angle
β	yaw angle
θ	total probe incidence
δ	boundary layer thickness
δ^*	boundary layer displacement thickness
ξ, η, ς	vorticity components in X, Y, Z directions
Subscripts	
c	cone coordinate system
0	initial values
∞	freestream
e	edge of wall viscous layer
slot	just above the slot

CHAPTER I

INTRODUCTION

Of necessity, a wind tunnel wall will confine streamlines at some distance from the test model. The earliest tunnels, all used for low speed testing, had solid walls and well understood corrections were developed. As test speeds increased it was evident that test-section chocking was a limit both to test Mach number and of the viability of theoretical correction methods. Introduction (see Goethert 1961) of non-solid test sections removed the first difficulty but not the second.

The interfering effect of the slotted wind tunnel walls has presented a continuous problem in transonic wind tunnel testing. The problem of wall interference appears in the imposing constraint presented by the partially ventilated walls which takes the form of a resistance to the flow normal to the walls. The result is a change in the streamline curvature of the test section flowfield from that which would have occurred in free flight. The wall interference depends on model size, model incidence, Mach number, blockage ratio and pertinent tunnel characteristics. These include the type of ventilation (slotted or perforated) and the percentage and distribution of this ventilation. The wall geometries of conventional tunnels are optimized so as to minimize the wall interference at transonic speeds over a range of parameters. In general the blockage ratio is restricted to 1%. However, the wall interference can be significant in the testing of high lift configurations at transonic speed.

A. TECHNICAL BACKGROUND

The modern methods of assessing the wall interference, as reported by Smith (1982), require knowledge of flow near the walls where any local effects of slots or perforations are not present. These data are then used as boundary conditions to calculate the wall interference. Kemp (1978) and Stahara (1979) employed nonlinear theories, pressure measurements near the wall and at the model to assess the wall interference. The flow passes through the ventilated wall due to the flowfield generated on the model. The magnitude of this flow depends on a number of factors such as the number of slots, size of slots, and length of working test section. Firmin et al. (1984) report that it is very difficult to estimate accurately the magnitude of this flow and it is a common practice to make measurements of boundary conditions where it can safely be assumed that the flow is homogeneous in form, that is where any local disturbances from the slots have died away. Figure 1.1 shows the isobars of pitot pressure measured by Firmin et al. (1984) near the slot of the upper tunnel wall. Although Firmin et al. (1984) indicated that there was some incidence error in pitot readings the above mentioned isobars indicate the depth of influence of the slot flowfield. The reason for regions of lower total pressure, as described by the authors, appears to be either due to that air from the slot which has been entrained within the slat boundary layer or lower energy air has entered the test section from the plenum chamber under the influence of the pressure difference across the walls. It is also clear that the slot flow increases in penetration into the main flow significantly further downstream. Very little information is available to guide the wind tunnel engineer in deciding how far away from the walls such measurements should be made. It is further reported that the low energy air from the plenum can enter the test section downstream of the model and its influence felt in regions far from the wall. The problem is lessened with segmented slotted walls.

As reported by Satyanarayana, et al. (1981), the applicability of the assessment methods is limited to attached flows, also there is some uncertainty involved a = slot width

w = distance between centerline of slots

d = distance from tunnel wall

P = local pitot pressure

c = airfoil chord

$M_\infty = 0.7$

s = lateral distance

x = longitudinal distance

H = free stream total pressure

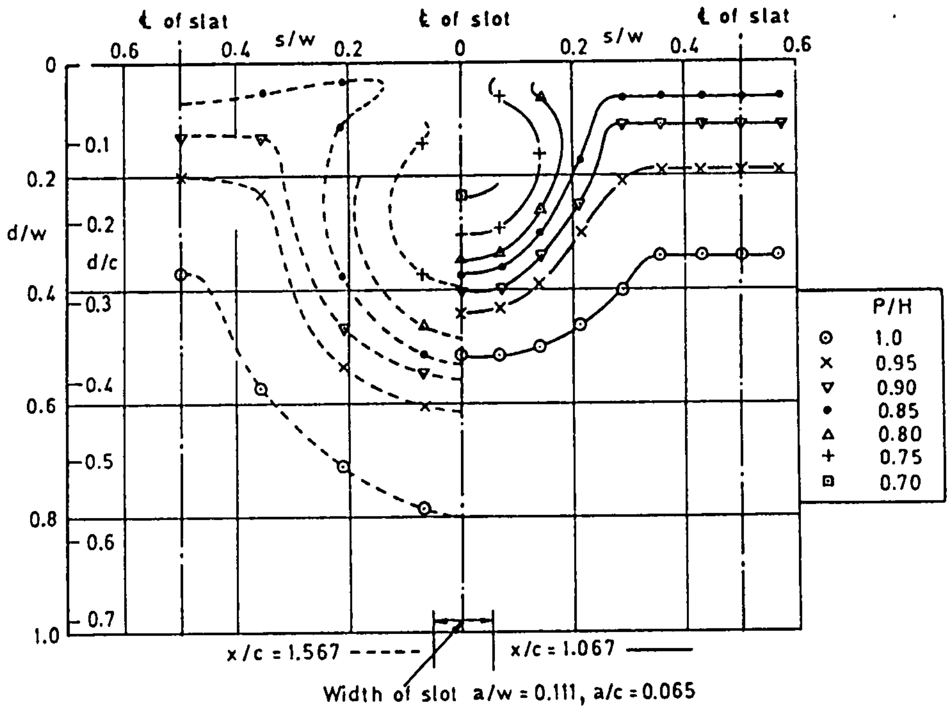

Figure 1.1. Isobars of Pitot pressure near upper tunnel wall, (Firmin et al. 1984).

and therefore a technique such as an adaptive wall technique which reduces or eliminates interference presents a better alternative. In an adaptive wall, the wall boundary conditions are adjusted to minimize the interference produced by constraining walls. The boundary conditions at the walls are changed by adjusting the shape of the walls (flexible solid walls), distributed blowing or suction along segmented slots, local crossflow characteristics (porosity and hole angle), or some combinations of the above.

Ganzer (1984) produced a nearly interference free flow, i.e., one that compared well with the numerical results, in a solid flexible octagonal test section at $M_\infty = 0.7$ on an aircraft model. The wall displacements required were less than 2 mm. One of the results obtained by Ganzer is shown in Figure 1.2. The influence of streamsurface curvature control near the tunnel wall in reducing the wall interference is illustrated. Goodyer (1985) numerically studied the influence of jack movements, in a flexible wind tunnel wall, on the changes in axial and normal velocity components and obtained the influence coefficient matrix required to characterize the wall.

An annotated bibliography of reducing wall interference by the use of adaptive walls is given by Tuttle et al. (1982). Satyanarayana et al. (1981) conducted a 2-D adaptive wall transonic wind tunnel experiment. Unconfined flow conditions in the test section were obtained by systematically adjusting the local wall flow characteristics until the measured velocity components at a control surface corresponded to that which would exist in free air. The required pressure changes within the plenum chamber for blowing or suction necessary to produce velocity changes for interference free test section flow conditions were predicted by the use of a measured influence coefficient matrix. The influence coefficient matrix was determined by performing calibration runs in the empty tunnel with controlled

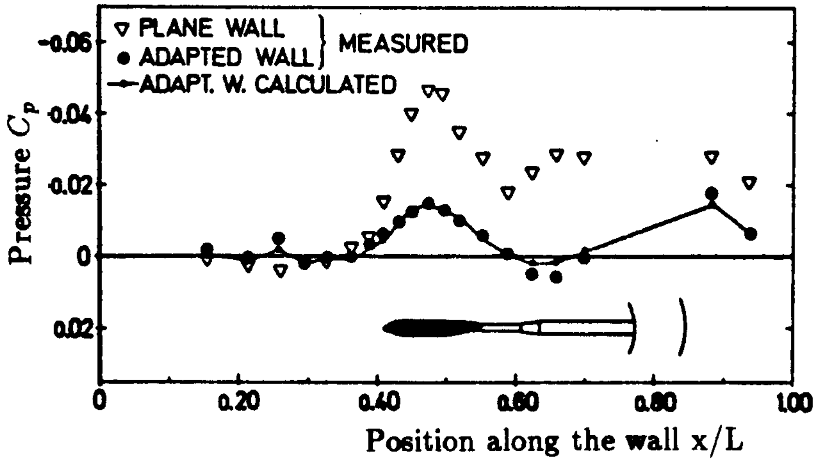

Figure 1.2. Pressure distribution along upper wall with a model at $M_\infty = 0.7$ and $\alpha = 0^o$, (Ganzer 1984).

blowing or suction applied through one or two chambers at a time. The change in w-component produced as a result of blowing or suction applied through chosen chambers is shown in Figure 1.3. It is also reported that pressure changes in one compartment produced pressure changes within adjacent compartments as is clear from Figure 1.4. This indicated that blowing or suction lead to the modification of the slotted wall flowfield which resulted in inflow or outflow from other plenum compartments.

The flow on slotted walls has been studied by many authors. The related ones among those are discussed below. Neyberg (1976), Berndt (1977), and Berndt and Sorensen (1975) examined the flow through slots to formulate a homogeneous wall boundary condition for accurate numerical calculations of inviscid transonic flows around models in slotted test sections. The slot flow was examined with oil flow pictures of the flow through the slots and with pressure measurements made in and around the slots. Also, a special probe was used to measure the slot flow angle in the plenum chamber. For their experiments the test section pressure upstream of the model was greater than the plenum pressure and, consequently, there was an outflow from the test section into the plenum chamber. The flow entered the plenum chamber by entrainment and deflection. Near the model, and for a short distance downstream, the plenum pressure was greater than the test section pressure, thus causing inflow into the test section from the plenum chamber. The inflow into the test section was reported to be a mixed flow, consisting in part of fast air removed earlier (upstream) from the test section and of low momentum air from the plenum. This low momentum air formed a "bubble" which spread laterally and was driven farther into the wall boundary layer. A schematic of the slot flow as illustrated by Berndt (1982) is shown in Figure 1.5. He also inferred that high momentum air going into the slot might split into two streams, one

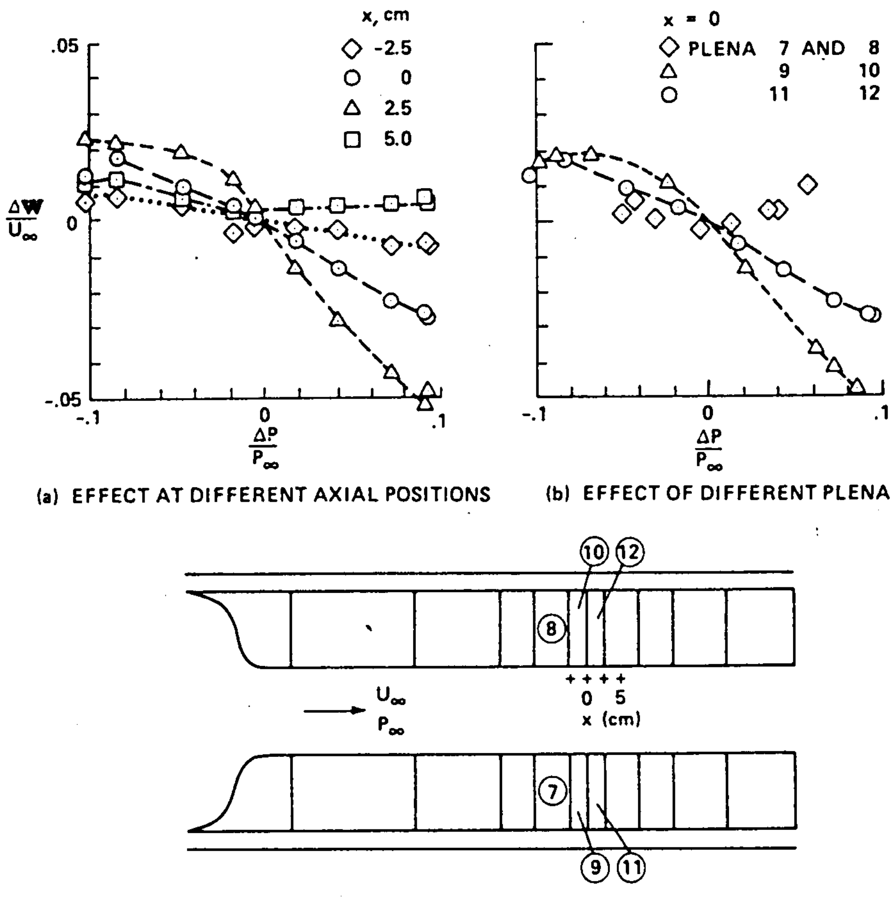

Figure 1.3. Normal velocity component and pressure changes close to upper wall for controlled blowing or suction applied through chosen chambers (Satyanarayana 1981).

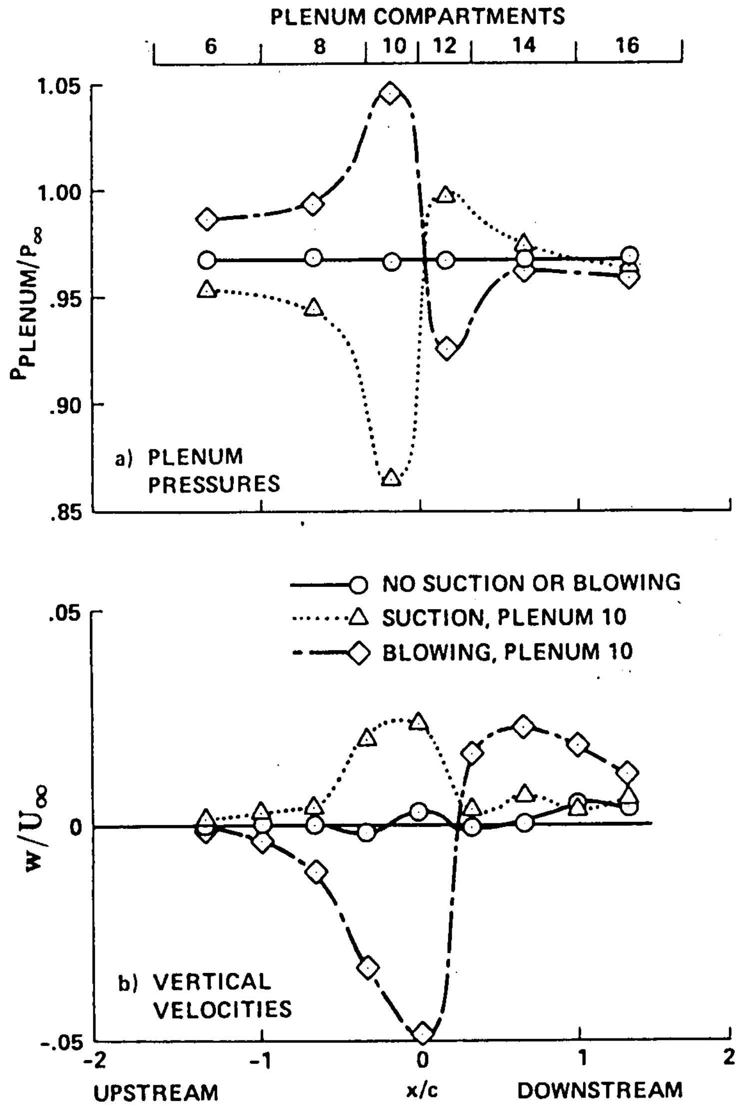

Figure 1.4. Plenum pressure and vertical velocity distribution resulting from suction or blowing applied through compartment 10 (Satyanaryana 1981).

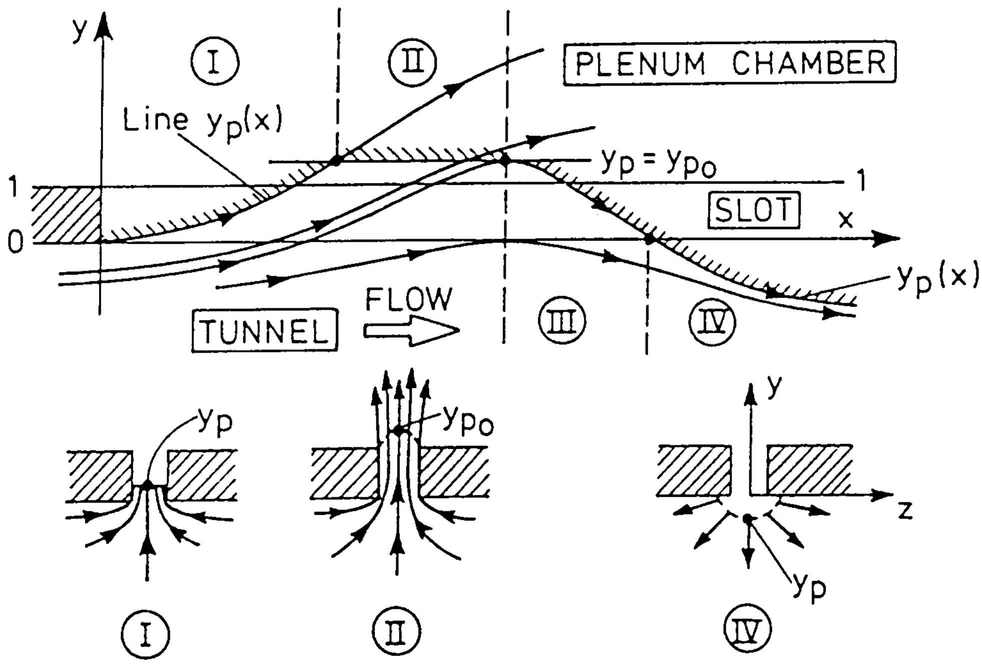

Figure 1.5. Generalized slot flow model (Berndt 1982).

going into the plenum as a jet and one turning back into the test section, there forming a narrow longitudinal bubble filled with quiescent plenum air. Based on the slot flow velocity measurements, Berndt (1977) inferred that the viscous effects caused a 15% reduction in effective slot width for outflow from the test section. No measurements of the inflow into the test section were carried out.

Matyk and Kobayashi (1977) studied the boundary layer and crossflow characteristics of the Ames 2×2 ft and 11×11 ft transonic tunnel configurations. They reported that the boundary-layer displacement thickness downstream of the slots was approximately twice as large as that at the centerline of the solid portion between the slots. This result was attributed to the aspirating effect and was considered to be a result of the natural development of the slot boundary layer. The crossflow differential pressure drop across the slot was found to be nonlinear with mass outflow and the fluctuating component of the crossflow velocity was as large as 30%. Their measurements were obtained with a traversing straight pitot probe, and therefore, the complex three-dimensional nature of the flow was not detected.

The boundary-layer displacement thickness has a strong influence on the slot crossflow characteristics. This becomes particularly significant due to the influence of the wall boundary layer. Furthermore, there are other slot flow problems that remain unanswered. Among these are the following: there are possibilities that the air returning to the test section contains vorticity and that there may be separation at the slot edges. The exact location of the surface where the plenum pressure exists in the slot flow is unknown. The crossflow may be too large for linearization, as is frequently assumed in the theoretical treatment. In spite of the vital role that the boundary layer on the slotted walls may play in understanding the features of the transonic wind tunnel wall flowfield, the experimental data on the flow near slotted walls is scarce and incomplete, especially in view of the three-dimensional nature of the flowfield in the presence of mass transfer across the slots.

It is obvious that the wall boundary conditions are different for various flow conditions and models placed in the test section. Therefore, the best way to accommodate various wall boundary conditions would be to place segmented compartments beneath the slotted wall and to apply local pressure controls to each compartment.

B. PRESENT OBJECTIVES

With the above in view, the present investigation studies the three-dimensional flowfield on slotted transonic wind tunnel wall in two parts. In Part 1, the flow on a single slotted wall is studied. The objectives of this study are the following

(a) determine the manner of decay in the transverse direction of the perturbation generated as a result of mass removal (suction) on a single slotted wall.

(b) determine the extent and influence of the slot flowfield in a direction normal to the wall and extending into free stream.

(c) obtain flowfield information which may better help visualize the slot flowfield.

The results on single slotted walls are applicable to wind tunnel walls with widely spaced slots. As mentioned earlier, flow control near the walls can be accomplished using inclined holes or slots. Zig–zag baffles provide a means of directing the flow within slots at a desired angle. Zig-zag baffles making a 14 degree angle (configuration used in NASA Ames transonic wind tunnel) with the normal to wall have been placed inside the slot of the single slotted wall. This study should help in the use of multi-slotted walls to design slots with inclined edges to minimize interference as has also been indicated by Berndt (1982).

In Part II, the experiments on a segmented slotted wind tunnel wall have been carried out. The objectives of this study has been the following

(a) obtain flowfield information in lateral, downstream and upstream directions of the segmented compartment through which blowing or suction was applied. This information should help to visualize the characteristics of the cross plane flowfield resulting from blowing or suction through a compartment.

(b) determine at selected measurement traversing locations, the influence of controlled blowing or suction on the normal velocity component. This should provide information required to form an influence coefficient matrix for blowing and suction applied through more than one compartment.

Due to the fact that the flow over a slotted wall is three dimensional in nature, a five port cone probe was used to measure the flow velocity through the wall boundary layer. The local flow conditions, i.e., the Mach number and the flow angularity both in pitch and yaw were deduced from these cone probe measurements. In Part I of the studies, for flow on a single slotted wall, the boundary layer traverses were made above the slot and at three equally spaced transverse stations away from the slot. All measurements were made at one longitudinal station.

In the second part of the study, the experiments were carried out on a slotted wall with six longitudinal slots whose underneath plenum chamber was divided into 6 (longitudinal direction) x 3 (transverse direction) compartments. The influence of controlled blowing and suction through 4 chosen compartments on the flowfield were studied. Measurements were made at 2 longitudinal stations. At each longitudinal station, measurements at three transverse stations were conducted simultaneously. Five-port-cone probes were used to measure local total pressure, Mach number and 3–D flow angularity. No turbulence measurements were made and only mean quantities are reported in this study.

CHAPTER II

EXPERIMENTAL SET-UP AND DATA REDUCTION TECHNIQUE

Brief descriptions of the test facility, single slotted and segmented slotted model wall geometries, applied suction and blowing control mechanisms, and the instrumentation used to conduct three dimensional transonic flow measurements are given below.

A. WIND TUNNEL FACILITY

This experimental investigation was performed in The University of Tennessee Space Institute (UTSI) transonic wind tunnel. The tunnel is of the blow-down type. The test section is nominally 12 inches in width and 11 inches in height. It has a useful testing length of 144 inches. Details of the UTSI transonic wind tunnel facility can be found in References that have been furnished by Shen (1974); therefore, only remarks relevant to the present experiments are given below.

Figure 2.1 gives a cross-sectional view of the tunnel. The test section is topped along its entire length with a plenum chamber for ventilation purposes. The plenum chamber lower wall is perforated with about 30% open area. This wall was modified for the Part II tests. Slots were provided to let the traversing probe holders to pass through (see Section C of Chapter II). The test section ends in a variable area section which is used to control the mass flow rate and the test section Mach number, followed by a diffuser and finally the exhaust stack. Stagnation pressure is controlled through a 4 inch control valve upstream of the stilling chamber.

The present tests required boundary layer surveys on single slotted and segmented multi-slotted wall models. Controlled suction was applied in the case of

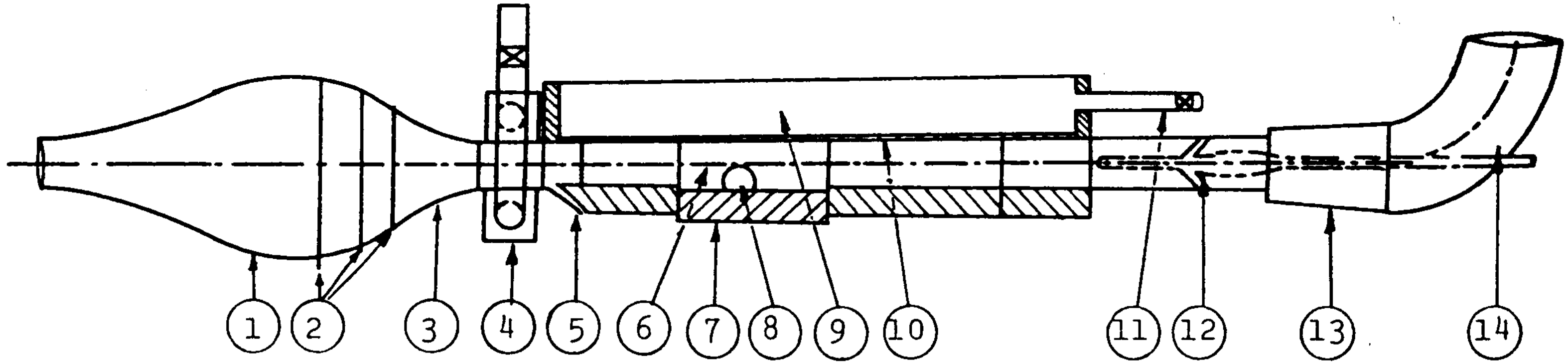

1	Settling Chamber	8	Schlieren Window
2	Smoothing Screens	9	Plenum Chamber
3	Contraction Cone	10	Perforated Ceiling
4	Supersonic Nozzle	11	Plenum Ventilation Pipe
5	B. L. Suction Device	12	Translating Centerbody
6	Test Section	13	Diffuser
7	Typical Floor Plate	14	Exhaust Stack

Figure 2.1. Sectional view of the University of Tennessee Space Institute Transonic Wind Tunnel.

the single slotted model wall and both blowing and suction at chosen slot segments were applied in tests on segmented slotted walls. In each case the model wall was flush mounted on the test section floor. The mounting of the segmented slotted model wall on the test section floor is shown in Figure 2.2. The details are given in the next three sections.

B. SINGLE SLOTTED MODEL WALL

The single slotted model wall was 40 inches long and 12.25 inches wide. With proper inserts, an open slot 14 inches long and 0.26 inches wide was provided. Baffles were used to direct the flow into the slot. In the present experiment baffles making an angle of 14 degrees to the wall normal were used. Figure 2.3 shows the geometry of the slot and the baffle used. Four rows of static pressure taps ran longitudinally on the wall at $y = \pm 1$ and $y = \pm 3$ inches.

Attached underneath the model wall was the plenum chamber. The plenum chamber was 40 inches long, 12.25 inches wide and 24 inches deep. A sliding block was mounted on two shafts which ran longitudinally parallel to the model wall and were fixed to the plenum chamber end walls. This sliding block was used to support the traversing probe holder assembly. A lead screw and nut arrangement permitted the placement of the traversing probe anywhere along the length of the slot. In this experiment, the probe was located in the longitudinal direction at $x = 7.5$ inches (measured from the slot beginning).

In order to be able to traverse the boundary layer at a streamwise location, but at different stations in the transverse direction, four extension pieces of different lengths that could be attached to the probe holder were constructed. These extension pieces allowed the probe to be traversed either on the slot, or at distances of 0.5 inches, 1 inch, 1.5 inches away from the slot center line in the transverse

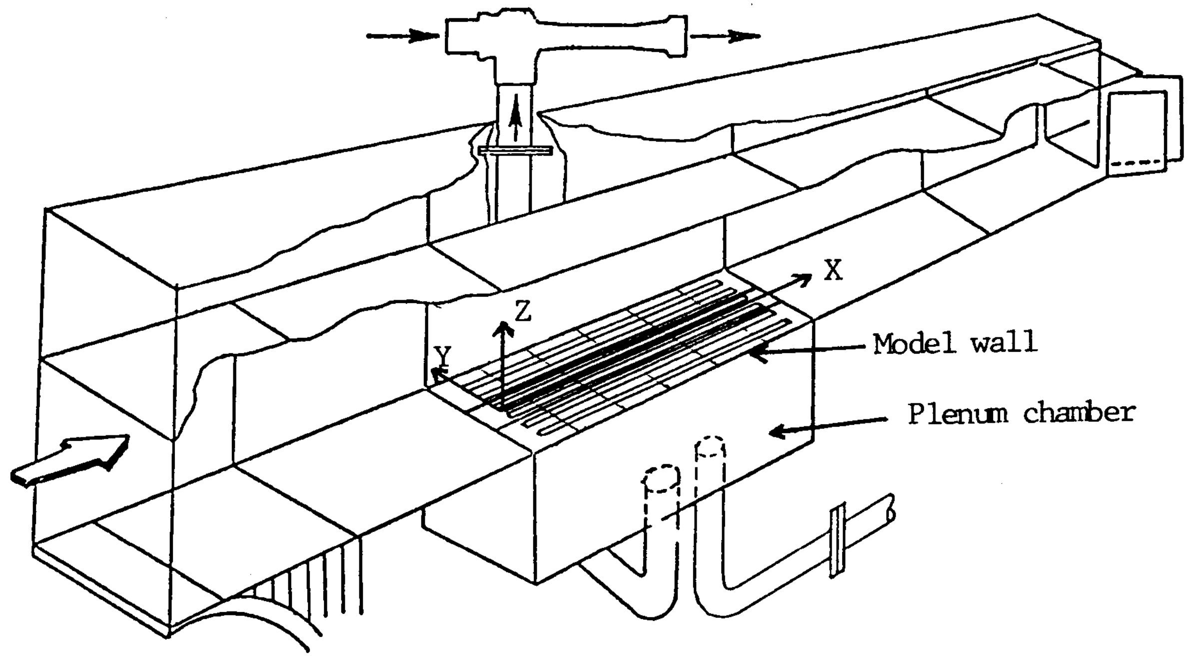

Figure 2.2. Segmented slotted model wall flush mounted on the tunnel floor.

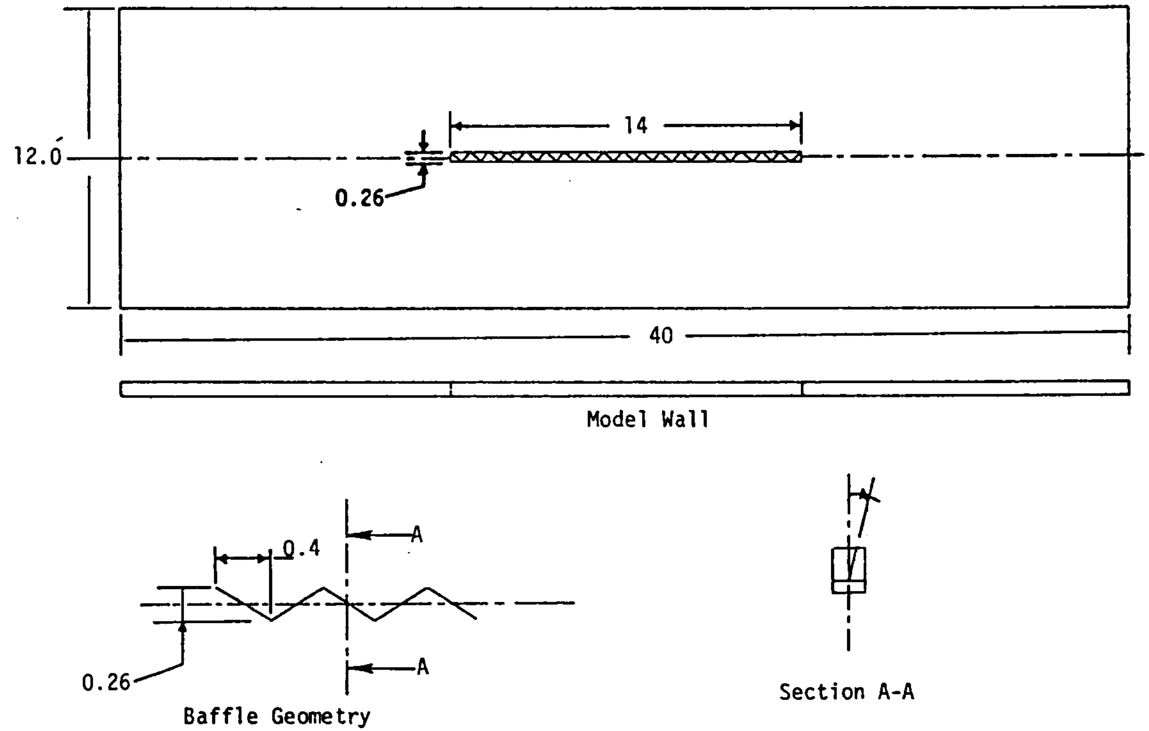

Figure 2.3. Schematic of the single slotted model wall.

direction. The probe holder was driven vertically up or down using an electric motor.

C. SLOTTED SEGMENTED MODEL WALL

The model wall was 40 inches long and 12.25 inches wide. Six longitudinal slots were provided. The central 4 slots were 0.25 inches wide and the outer two slots (one on each side of the center line) were each 0.375 inches wide. A schematic of the model wall is shown in Figure 2.4. The segmentation of the slotted model wall was achieved by using a segmented plenum chamber attached underneath the model wall. The plenum chamber was 40 inches long, 12.25 inches wide and 24 inches deep. The plenum chamber was divided into 18 independent compartments, i.e., 6 longitudinal x 3 transverse segments. Each segmented chamber contained 2 slots on top; that is, the surface that was a portion of the wind tunnel lower wall.

For reasons of the symmetry of the slotted segmented wall, four segments were chosen where controlled blowing or suction could be applied. These selected compartments had 1.5 inch outer diameter outlets that could be either closed or connected to blowing or suction devices through connecting ducts. Figure 2.5 shows a schematic of the side view of the compartments.

In the Part II test, the perforated upper wall of the tunnel above the slotted model wall was replaced by a slotted plate for traversing the probes. This upper slotted plate had 4 longitudinal slots. Each slot was 35 inches in length and 0.4 inches in width.

The probe traversing assembly, consisting of the traverse sliding mechanism and computer controlled electric motor, were located in the upper plenum chamber. The traverse assembly was located 1.5 inches above the upper slotted plate to permit unrestricted flow into the upper plenum chamber. Three probe holders

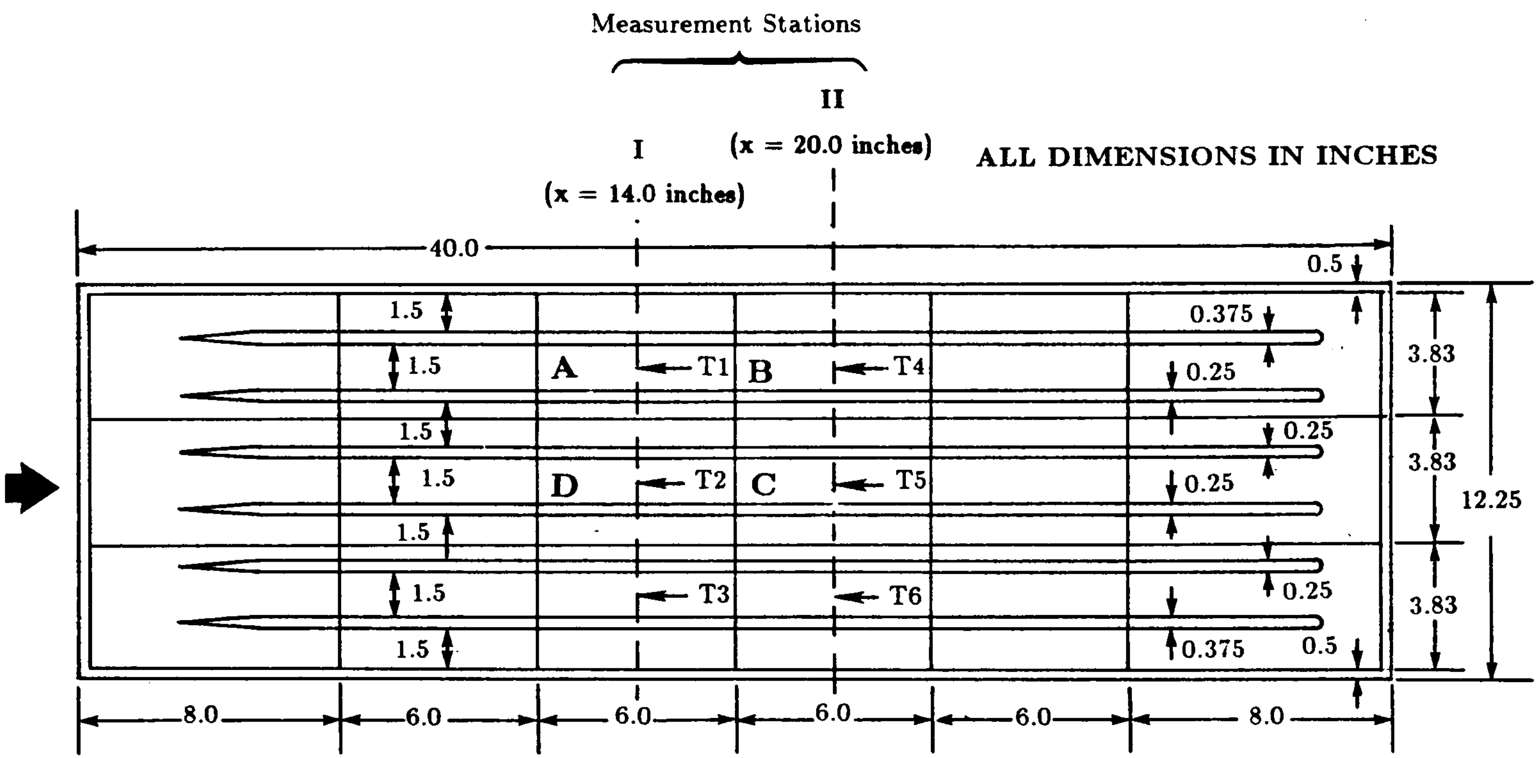

Figure 2.4. Schematic of the segmented slotted model wall.

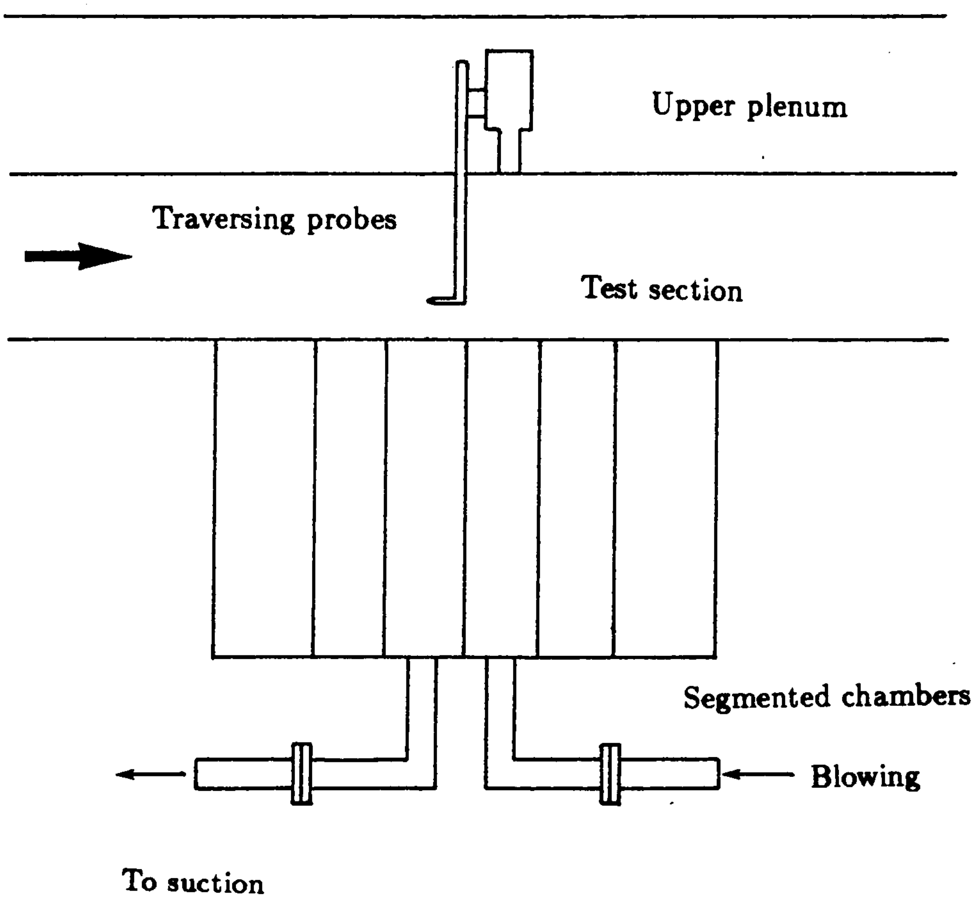

Figure 2.5. Longitudinal view of the segmented slotted model wall and lower plenum chambers.

were attached to the traverse assembly and passed through slots in the upper slotted wall. Three cone probes uniquely attached to their respective probe holders permitting simultaneous boundary layer traverse measurements at three transverse stations. The transverse locations of these stations, measured from the slotted wall centerline were

$$y = +3.5 \text{ inch}, \quad y = -0.19 \text{ inch}, \quad \text{and} \quad y = -3.81 \text{ inch}.$$

The probe traverse assembly could be held fixed at two stations so that the boundary layer traverses could be obtained at two stream-wise stations, of $x =$ 14.0 inch and $x = 20.0$ inch, x being measured from the slot beginning, as indicated in Figure 2.4.

D. SUCTION AND BLOWING MECHANISM

In the Part I test on the single slotted model wall the plenum chamber under the model wall acted as the suction chamber. A 3 inch inner diameter pipe connected the suction chamber via an orifice flow meter to the suction device. In Part II of the present investigation for the case of tests on segmented slotted wall, the individual plenum chambers under the slot sections of the segmented slotted wall acted as suction or blowing chambers. 1.5 inch inner diameter pipes connected the blowing or suction chambers via respective orifice flow meters to the pumping/blowing devices.

Suction was provided by two air operated ejectors which were operated in parallel for increased pumping. The pumps were Pemberthy Hondaille 4 inch air-ejectors. The pumping media was high pressure air that was bled off from the tunnel high pressure air supply. The ejector inlet air pressure was controlled with a 1.5 inch Grove dome controller that was operated with a Grove autoloader.

Blowing was applied from a 120 psi supply line and manually controlled through a 2 inch dome type regulator.

The suction or blowing flow rates were measured by using sharp-edge orifice plate flow rate meters. The orifice diameter in the flow meters was approximately 0.8 times the pipe diameter which was approximately 2 inches. Pressure transducers were placed one pipe diameter upstream and one-half pipe diameters downstream of the orifice plate. The flow rate was determined using the following equations which are valid for compressible flow. These equations and the discharge coefficients have been taken from Bean (1971).

$$Q = 60\frac{KA_0\rho_u\sigma}{\rho_s}\sqrt{\frac{2(P_u - P_d)}{\rho_u}};\ \text{standard SCFM (ft}^3\text{/min)}$$

where,

Q = flow rate in SCFM

$K = CF$, with C = discharge coefficient, F = velocity-of-approach factor

$$F = 1 - \left(\frac{A_0}{A_p}\right)^2$$

A_0 = orifice area

A_p = pipe area

ρ_u = air density upstream of orifice plate

ρ_s = standard atmospheric density

P_u, P_d = air pressure upstream and downstream, respectively of orifice plate

σ = expansion factor

$$= 1 - \left[0.41 + 0.35\left(\frac{A_0}{A_p}\right)^2\right]\frac{(P_u - P_d)}{P_u\gamma}\ ;\quad \gamma = 1.4$$

The upstream air density was estimated from the measured pressure and the stagnation temperature.

E. INSTRUMENTATION

The major instrumentation used in this study were the traversing cone probes. The other instruments were the pressure transducers and thermocouples. The details are described below.

F. MEASUREMENT OF LOCAL FLOW CONDITIONS USING CONE PROBE

The boundary layer on the slotted wall with suction or blowing is three dimensional in nature. The requirement is to be able to measure the complete velocity vector in one probe positioning as the probe traverses through the boundary layer.

A five-port-cone probe allowed the determination of the local flow conditions, i.e., Mach number, static pressure and the flow angularity both in pitch and yaw. A suitable model for the velocity-temperature relation using boundary layer concepts was utilized (see Section H of Chapter II) which then allowed the determination of the complete local velocity vector.

When the flow is inclined to a cone the pressure difference between the symmetrically placed orifices on the opposite sides can be utilized to determine flow angularity. Using the cone probe measurements the local flow angle can be determined from a probe calibration. This method of operation is known as the fixed mode. In the second kind of operation, namely the null mode, the flow angularity is determined by orienting the probe until the pressure measured on the opposite sets of orifices is balanced. Rotation must be performed in two planes for three-dimensional flows. In general the null method is more accurate than the fixed one, however, the fixed mode of operation is faster in operation. In the present investigation the fixed mode of operation was employed.

A 0.16 inch diameter cone probe of half angle 20 degrees and the surface pressure orifices located at $X/L = 0.65$ was used here. The present geometry of the cone probe used exhibited reasonably high sensitivity and the cone surface pressure distribution changed only slightly at the orifice locations. In Part I of this study, in the test on the single slotted wall, the cone probe measurements were analyzed using the numerically generated calibration data. The calibration data were obtained using the computer program of Wu and Lock (1974). In Part II of this investigation, the cone probe measurements were analyzed using experimental calibration data.

Figure 2.6 shows the schematic of the five-port-cone probe used. The orifice on the cone probe include one total pressure pitot tube orifice and four static pressure orifices placed 90 degrees azimuthally apart on the cone surface at $x/L = 0.654$ from the cone apex.

The limitations of the use of probes in flows with gradients normal to the flow direction have been discussed by Reed et al. (1977) and the flow induced vibrations on a cone-cylinder combination have been studied by Rittenhouse (1969). However, no significant probe vibrations were observed and the probe is estimated to be adequate and yield reasonable accuracy for measurements.

G. PRESSURE AND TEMPERATURE MEASUREMENT

The experiments required accurate measurement of many pressures and temperatures. The measurement of pressures included tunnel total and static pressures, the total, port static and differential pressures for each cone probe, model wall surface static pressures, blowing or suction orifice flow rate meter pressures

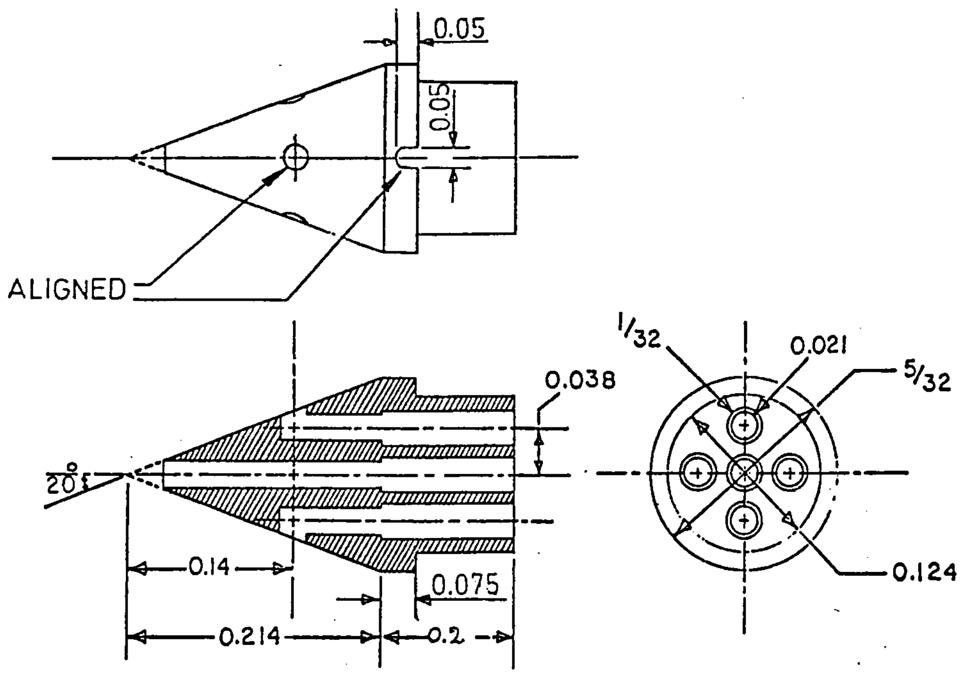

Figure 2.6. Schematic of the cone probe.

and atmospheric pressure.

All the pressures, except the tunnel total pressure, were measured using Validyne DP Series differential pressure transducers with either ± 15 psid or ± 5 psid diaphragms. The tunnel total and static pressures were measured with Tabor and ± 12.5 psid Stathem differential transducers (referenced to atmosphere), respectively. All the transducer signals were conditioned, digitized and stored in the data acquisitions system.

The model wall pressures were connected to a scanivalve that was scanned at a rate of 16 channels per second. The cone probe differential pressure measurements were made accurate by calibrating the transducers in the ± 5 psid range. High signal amplification factors were used and the time constant of the measurements was reduced by using large diameter tubing to the transducers and by reducing the internal volume of the transducers by adding special inlet connectors. The error in differential pressure measurements was less than ± 1%.

All the temperatures were measured using Chromel–Alumel thermocouples. The temperature measurements were made in the test section, the stilling chamber, the suction or blowing orifice flow meter pipelines and the atmosphere.

H. LOCAL AND FREE STREAM CONDITIONS, BOUNDARY LAYER DATA ANALYSIS

The equations that were used to calculate the flow variables using the measurements are given in this section. The computer program using these equations was originally used in the Propulsion Wind Tunnel Facility at the Arnold Engineering Development Center. This program was developed by Whitfield (1976), and modified to be used by the Gas Dynamics division of UTSI by Dowgwillo (1977).

The freestream Mach number was calculated from the isentronic flow relation:

$$M_\infty = \left\{ \left[\left(\frac{P_t}{P_\infty} \right)^{\frac{\gamma-1}{\gamma}} - 1 \right] \frac{2}{\gamma + 1} \right\}^{\frac{1}{2}}$$

where P_t is the total pressure, P_∞ is the freestream pressure and the specific heat ratio, γ was taken to be 1.4. The pressure coefficient is taken in the usual way,

$$C_p = \frac{P - P_\infty}{q_\infty} = \frac{P - P_\infty}{\frac{1}{2}\gamma P_\infty M_\infty^2}.$$

The normalized pressure is obtained by using the relation,

$$\widetilde{P} = \frac{P}{q_\infty} = \frac{P}{\frac{1}{2}\gamma P_\infty M_\infty^2}.$$

The Reynolds number per foot was found from

$$Re/ft = \frac{1.7784 \times 10^9 P_{t_\infty} M_\infty}{(T_t + 460)^{1.315}(1 + .2M_\infty^2)^{2.185}}$$

with the total pressure in psia and the total temperature in ^0F.

The Mach number distribution together with the orientation of the velocity vector across the skewed boundary layer was obtained from cone probe data analysis (see Section I of Chapter II).

The velocity ratio is calculated by:

$$\frac{V}{V_e} = \frac{M}{M_e}\left(\frac{T}{T_e}\right)^{\frac{1}{2}} \tag{1}$$

where the subscript e indicates the condition at the edge of the boundary layer.

For an adiabatic wall, the temperature and velocity ratios are related by Whitfield and High (1974)

$$\frac{T}{T_e} = 1 + \frac{(\gamma - 1)}{2} M_e^2 \left[1 - \left(\frac{V}{V_e}\right)^2\right] + (1 - Pr_m) \times$$

$$\left\{ \frac{\beta(\gamma-1)M_e^2}{(\alpha+1)(\alpha+2)} \left[1 - \left(\frac{V}{V_e}\right)^{\alpha+2}\right] + \frac{\gamma-1}{2} M_e^2 \left[1 - \left(\frac{V}{V_e}\right)^2\right] \right.$$
$$\left. + f(1) - f\left(\frac{V}{V_e}\right) \right\} \tag{2}$$

where,

$$f\left(\frac{V}{V_e}\right) = \frac{\Delta}{(\gamma-1)M_e^2} \left[(\varsigma - \Delta)\ell n|\varsigma - \Delta| - (\varsigma + \Delta)\ell n|\varsigma + \Delta|\right]$$
$$\varsigma = -(\gamma-1)M_e^2 \frac{V}{V_e}$$
$$\Delta = \left[2(\gamma-1)M_e^2 \frac{T_{t,e}}{T_e}\right]^{\frac{1}{2}}$$

and where the subscript e indicates the condition at the edge of the shear layer. The mixed or "turbulent" Prandtl number is defined by

$$Pr_m = \frac{C_p(\mu + \mu_t)}{(\kappa + \kappa_t)},$$

while subscript t here refers to turbulent value, and the parameters α and β above are taken to be

$$\alpha \equiv (5/2)m|_{m=10} = 25$$
$$\beta \equiv 10m|_{m=10} = 100$$

where m is the index for the relation,

$$\frac{V}{V_e} = \left(\frac{z}{\delta}\right)^{\frac{1}{m}}.$$

The velocity ratio is then found by solving Equations (1) and (2) simultaneously by iteration while preserving the corresponding orientation angle of the velocity vectors.

Boundary layer thickness, δ, is defined as

$$\delta = z|_{(u/u_e)=0.99}$$

An appropriate definition of the boundary layer thickness parameters for a three-dimensional boundary layer flow have been discussed by Lighthill (1958). These definitions involve the longitudinal development of the boundary layer. Since in Part I of this study the measurements have been carried out only at one longitudinal station, therefore the longitudinal gradients of the flow parameters were not available and the boundary layer displacement thickness for three dimensional flow could not be calculated. In the present study, the definition of the boundary layer thickness parameters based only on the u-component of the velocity vector are adapted. These are as follows:

The boundary layer displacement thickness, δ^*, is defined as

$$\delta^* = \int_0^{z_e} \left(1 - \frac{\rho u}{\rho_e u_e}\right) dz$$

and the momentum thickness as

$$\theta = \int_0^{z_3} \left(\frac{\rho u}{\rho_e u_e}\right) \left(1 - \frac{u}{u_e}\right) dz.$$

Both are evaluated by numerical integration using the trapezoidal rule. The shape factor H is then defined as $H = \delta^*/\theta$.

I. DATA ANALYSIS OF CONE PROBE MEASUREMENTS

The analysis of the cone probe measured data using the theoretical calibration (interpolation technique) is described by Wu et al. (1981). The cone probe was calibrated experimentally in an open jet tunnel. The details are given in the Appendix. The analysis of cone probe measurements using the experimental calibration is described below.

The pressures measured on the five-hole-cone probe (Figure 2.6) are the pitot pressure $P_T = P_5$, surface port pressures P_1 and P_2, and differential pressures ΔP_{1-3} and ΔP_{2-4}.

The local flow conditions, i.e., total pressure P_T, static pressure P, the three dimensional flow angularity expressed in the pitch (α) and yaw (β) angles were determined from the experimental calibration data. The calibration data was represented by 3rd order algebraic polynomials which were fitted through the P_T, P, α and β data in the least square sense. Each of these polynomials had 20 coefficients. These polynomial representations were used here to reduce the cone probe data.

The analysis of the measured cone probe data is made as follows:

The following normalized coefficients are formed,

$$C_\alpha = \frac{P_1 - P_3}{P_5 - \overline{P}} = \frac{\Delta P_{1-3}}{P_5 - \overline{P}}$$
$$C_\beta = \frac{P_2 - P_4}{P_5 - \overline{P}} = \frac{\Delta P_{2-4}}{P_5 - \overline{P}}$$
$$C_M = \frac{P_5 - \overline{P}}{P_5}$$

where,

$$\overline{P} = \frac{P_1 + P_2 + P_3 + P_4}{4}.$$

These normalized cone probe data are substituted into a polynomial expression of the following form,

$$\begin{aligned}
F = K_0 &+ K_1 C_\alpha + K_2 C_\beta + K_3 C_M \\
&+ K_4 C_\alpha^2 + K_5 C_\beta^2 + K_6 C_M^2 \\
&+ K_7 C_\alpha C_\beta + K_8 C_\alpha C_M + K_9 C_\beta C_M \\
&+ K_{10} C_\alpha^3 + K_{11} C_\beta^3 + K_{12} C_M^3 \\
&+ K_{13} C_\alpha^2 C_\beta + K_{14} C_\alpha^2 C_M + K_{15} C_\beta^2 C_\alpha \\
&+ K_{16} C_\beta^2 C_M + K_{17} C_M^2 C_\alpha + K_{18} C_M^2 C_\beta \\
&+ K_{19} C_\alpha C_\beta C_M \qquad (1)
\end{aligned}$$

where the K_i are the appropriate coefficients known from the calibration data for each $F = \alpha,\ \beta,\ C_0$ and C_q.

For each measured cone probe data, the α, β, C_0 and C_q are derived. The local total and static pressures are then determined from C_0 and C_q by

$$P_T = P_5 - C_0(P_5 - \overline{P})$$
$$P = P_T - \frac{P_5 - \overline{P}}{C_q}.$$

In order to facilitate automation to handle large amounts of data (measurements being made at 48 locations in one boundary layer traverse for each cone probe), a computer program was written to analyze the cone measurements.

J. ROTATION FROM CONE COORDINATE SYSTEM TO THE TUNNEL COORDINATE SYSTEM

The three dimensional flow angularity measurements were made with respect to the cone coordinate system. However the cone coordinate system could not be the reference coordinate system since in each mounting of the probe at the measurement station the cone coordinate system orientation changed.

The tunnel coordinate system was therefore selected to express the u, v and w components of the velocity vector. The x-axis of the tunnel coordinate system coincided with the longitudinal center line of the slotted wall model, directed in the direction of tunnel flow, and the y and z–axis formed the horizontal and vertical axis respectively, together to form a right handed coordinate system, as shown in Figure 2.2. The origin coincided with the beginning of the slot.

The orientation of the cone coordinate system (measurement coordinate system) relative to the tunnel coordinate system (reference coordinate system) was required. Since tunnel coordinate system was aligned with the tunnel freestream flow, the x-axis coincided with the u-component of the tunnel freestream velocity.

In case of the tunnel lower wall being a flat plate (closed slots of the model wall), the tunnel v and w components in the freestream, far from the wall shear layer should be negligible. Therefore any v and w velocity components measured using the cone probe were essentially due to the misalignment of the cone probe and its coordinate system.

There will always be certain misalignments introduced in the mounting of the cone probe. These misalignments may be in pitch, yaw or roll angle. In the present experiments the cone probe was uniquely attached to its stem. The stem had a projection that fitted into the groove on the cone probe. The probe stem was fastened onto the probe holder being guided by two pins. This arrangement permitted negligible roll misalignments of the probe. However, small pitch and yaw misalignments were unavoidable and were corrected in the interpretation of the data.

In order to express the velocity vector components in the reference tunnel coordinate system, a coordinate transformation from the measurement coordinate system distinguished by the subscript c, to the tunnel coordinate system was required and formed an additional step in the data reduction. As described earlier the flow angularity measured by the cone probe in the free stream for tests made on a flat plate is essentially due to the misalignment of the cone probe and its coordinate system. Therefore in each probe mounting, a test run with a traversing on a flat plate was made to determine zeros or the measure of misalignment in pitch and yaw.

If α_0 and β_0 are the misalignment angles in pitch and yaw respectively, then the coordinate transformation is represented by,

$$\begin{bmatrix} u \\ v \\ w \end{bmatrix} = \begin{bmatrix} \cos(\alpha_0)\cos(\beta_0) & \sin(\beta_0) & \cos(\beta_0)\sin(\alpha_0) \\ -\cos(\alpha_0)\sin(\beta_0) & \cos(\beta_0) & -\sin(\beta_0)\sin(\alpha_0) \\ -\sin(\alpha_0) & 0 & \cos(\alpha_0) \end{bmatrix} \begin{bmatrix} u_c \\ v_c \\ w_c \end{bmatrix}$$

where,

$$\alpha_0 = \tan^{-1}[\tan(\theta_0)\cos(\phi_0)]$$

$$\beta_0 = \sin^{-1}[\sin(\theta_0)\sin(\phi_0)].$$

The coordinate transformation from the cone coordinate system, distinguished by the subscript c, to the tunnel coordinate system is shown graphically in Figure 2.7. In the final phase of data analysis, the required coordinate transformation was made.

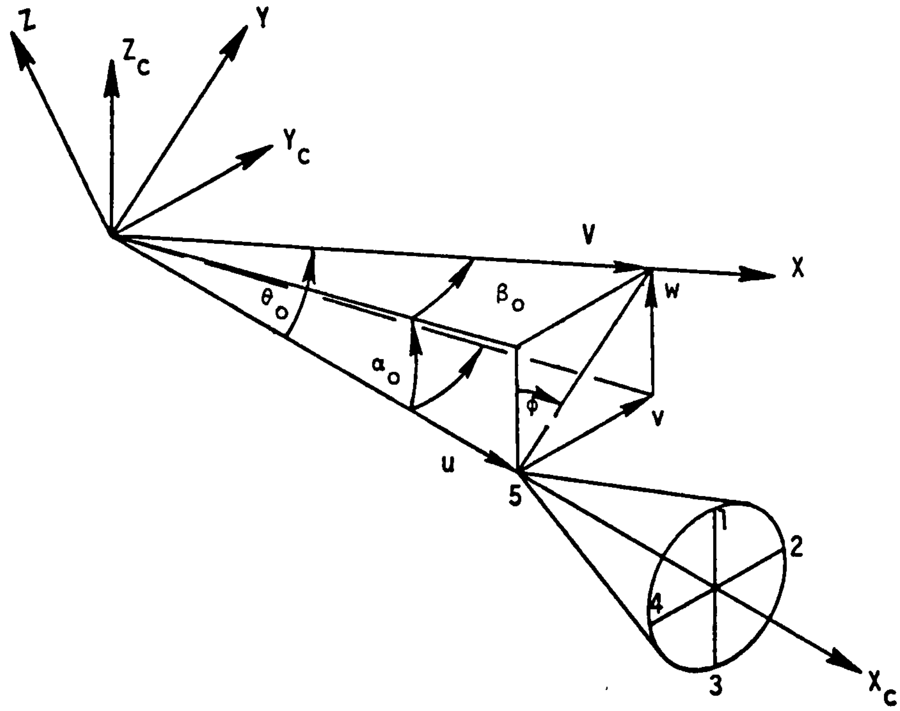

Figure 2.7. Rotation from cone coordinate system, distinguished by subscript c, to the tunnel coordinate system.

CHAPTER III

RESULTS FOR FLOW ON SINGLE SLOTTED WALL

Several test runs at various Mach number and Reynolds number conditions were made. The Mach number conditions were approximately 0.6, 0.76, and 0.9. The applied suction through slots varied from zero, to moderate ($Q = 75$ SCFM, $m^* = 0.002$) and to high (250 SCFM, $m^* = 0.006$). The tunnel unit Reynolds number changed from 5×10^6 to 9.6×10^6 per foot. The measurements were carried out using a 5 port cone probe. The cone probe data was reduced using the theoretical calibration as described in Wu et al. (1981). As has been indicated earlier, the mean flow measurements were carried out at 4 stations in the transverse plane (plane normal to the principle flow direction) at distances 0.0, 0.5, 1.0, and 1.5 inches from the slot longitudinal axis, the transverse plane being located at longitudinal station $x = 7.5$ inches from the slot beginning. Traverses were made above the slot and the slat on the test section side of the slotted wall. Figure 3.1 shows a schematic of the longitudinal view of the slotted wall viscous layer being traversed. The experimental data analyzed and the results obtained are described in the following sections.

A. THREE-DIMENSIONAL VELOCITY COMPONENTS

From the magnitude and orientation of the velocity vector the u, v and w velocity components are determined. Any contributions to these arising due to the initial mounting misalignments of the probe have been accounted for through the coordinate transformation. A positive component represents the velocity component directed in the positive y-direction in a plane parallel to the tunnel wall and normal to the slot orientation (see Figures 2.2 for coordinate axis and slot

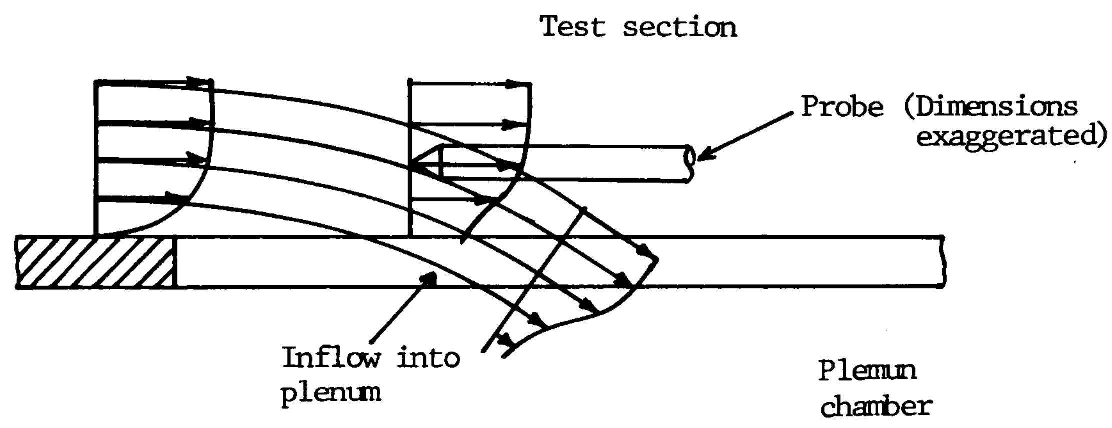

Figure 3.1. Schematic of the longitudinal view of the single slotted wall viscous layer being traversed.

orientation) and a positive w–component is the normal velocity component directed away from the wall. The velocity components have been normalized by the magnitude of the freestream velocity. Many plots of these normalized velocity components have been obtained. A typical result of three velocity components is shown in Figure 3.2. The nature of the wall shear layer velocity vector was analyzed using these measured velocity components. It should be noted that in the immediate neighborhood of the wall the cone probe results become spurious due to the probe-wall interference. A detailed discussion of the flowfield velocity vector distribution is presented in the Section C of Chapter III. Both normalized v and w components reduce with distance away from the slotted wall as expected. The boundary layer thickness characteristics are discussed below.

B. BOUNDARY LAYER THICKNESS CHARACTERISTICS

The distribution of the boundary layer thickness in the transverse (measurement) plane is shown in Figures 3.3a and 3.3b for flow over a single slotted model wall at the $M_\infty = 0.6$ and $M_\infty = 0.9$ run conditions respectively. For no applied suction through the slot (natural ventilation alone, $Q = 0.0$ SCFM), the boundary layer thickness remained relatively unchanged in the lateral direction. This is obvious from Figure 3.3a for $M_\infty = 0.6$, with no applied suction. With applied suction, the boundary layer thickness decreases in the close vicinity of the slot. The influence reduces with distance away from the slot. At high suction, the boundary layer thickness on the slot reduces significantly. This pronounced effect is also apparent for the $M_\infty = 0.9$, $Q = 250$ SCFM, $m^* = 0.004$ run condition in which the viscous layer above the slot almost disappears.

The u velocity component distribution is used to evaluate the boundary layer displacement thickness whose characteristics are discussed below.

$M_{\infty} = 0.81$, Re/ft. $= 8.14 \times 10^6$, Q = 56 SCFM, y = -0.5 inches, $m^* = 0.0011$

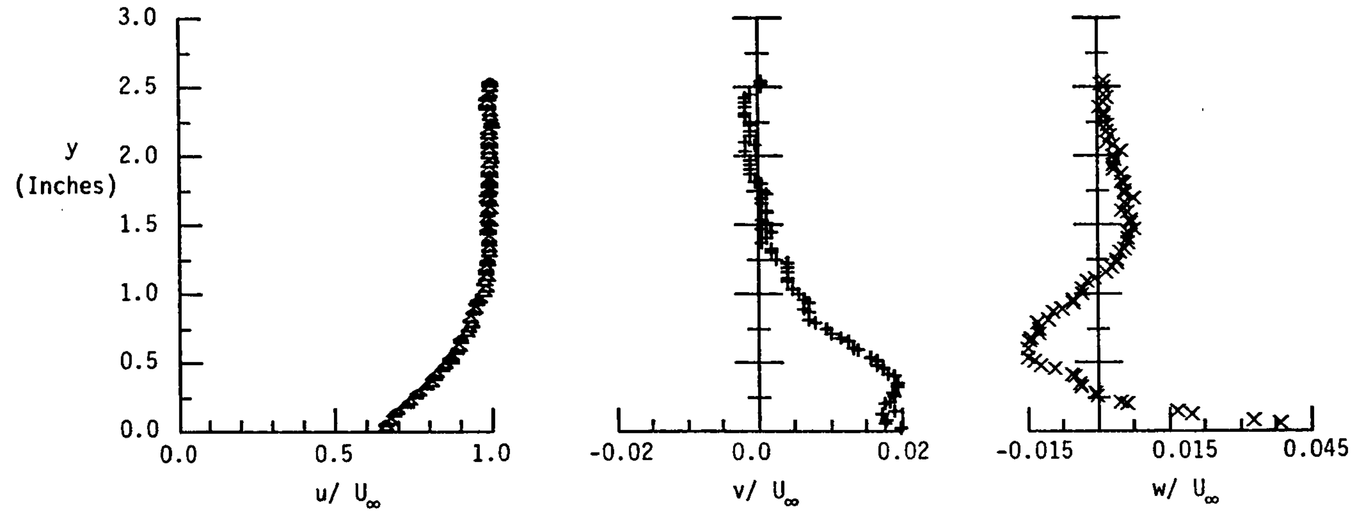

Figure 3.2. Typical velocity component distribution on the single slotted wall model.

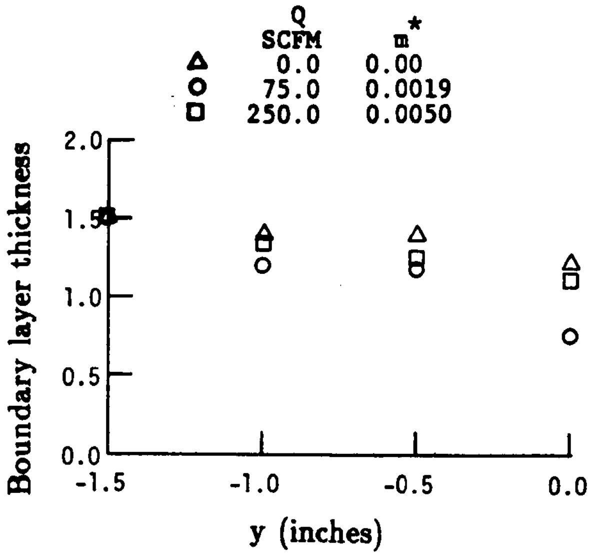

(a) $M_\infty = 0.6$

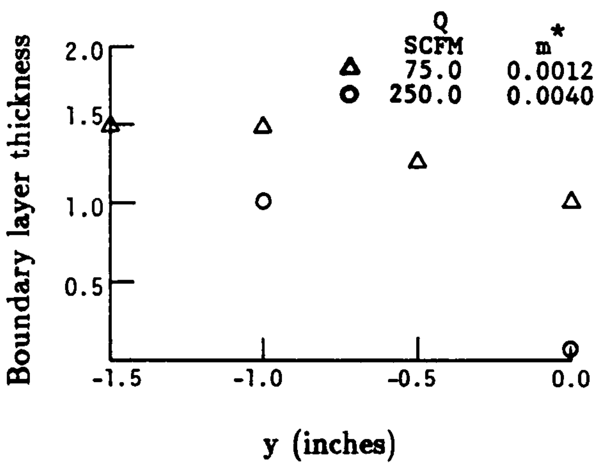

(b) $M_\infty = 0.9$

Figure 3.3. Boundary layer thickness distribution in the transverse plane.

Since the v and w velocity components decrease rapidly away from the wall and their contribution is significant only in the shear layer, their inclusion will in effect make the velocity larger than the u–component alone and will thereby reduce the velocity defect in the shear layer. It is thus realized that, based on the u–component alone, the value of δ^* is slightly overestimated.

The variation of boundary layer displacement thickness on the slot with the increasing suction mass flow rate through the slot for two different Mach numbers, $M_\infty = 0.6$ and $M_\infty = 0.76$, is shown in Figures 3.4a and 3.4b respectively. It is evident from these figures that δ^* on the slot is highly sensitive to the outflow rate from the slot. However, as determined from the analyzed velocity distributions, it is found that there is outflow from the test section into the plenum chamber at this longitudinal location in the empty tunnel. This is due to the boundary layer development on the slotted test section wall. The corresponding flat plate δ^* at approximately the same run conditions is also indicated in these figures. It is clear that for the case of no auxiliary suction through the slot ($Q = 0.0$ SCFM), the δ^* on the slot is approximately 3.3 and 2.0 times the corresponding flat plate value at $M_\infty = 0.76$, Re/ft. $= 7.82 \times 10^6$, and $M_\infty = 0.6$, Re/ft. $= 5.26 \times 10^6$, run conditions respectively. The reason for lower δ^* value on the slot for the case of $M_\infty = 0.6$ is due to the presence of a larger natural suction velocity because of a relatively thicker boundary layer. From the comparison of the velocity distribution near the slot in the two cases, it is found that at $M_\infty = 0.615$ the vertical component of velocity directed into the slot is 1.13 times greater than that at $M_\infty = 0.75$ run case.

The boundary layer is thicker at the lower Mach number of 0.6 compared to that at $M_\infty = 0.76$. This is evidenced by comparison of the flat plate case test results; the δ^* at $M_\infty = 0.6$, Re/ft. $= 6.59 \times 10^6$ is 1.48 times greater than that

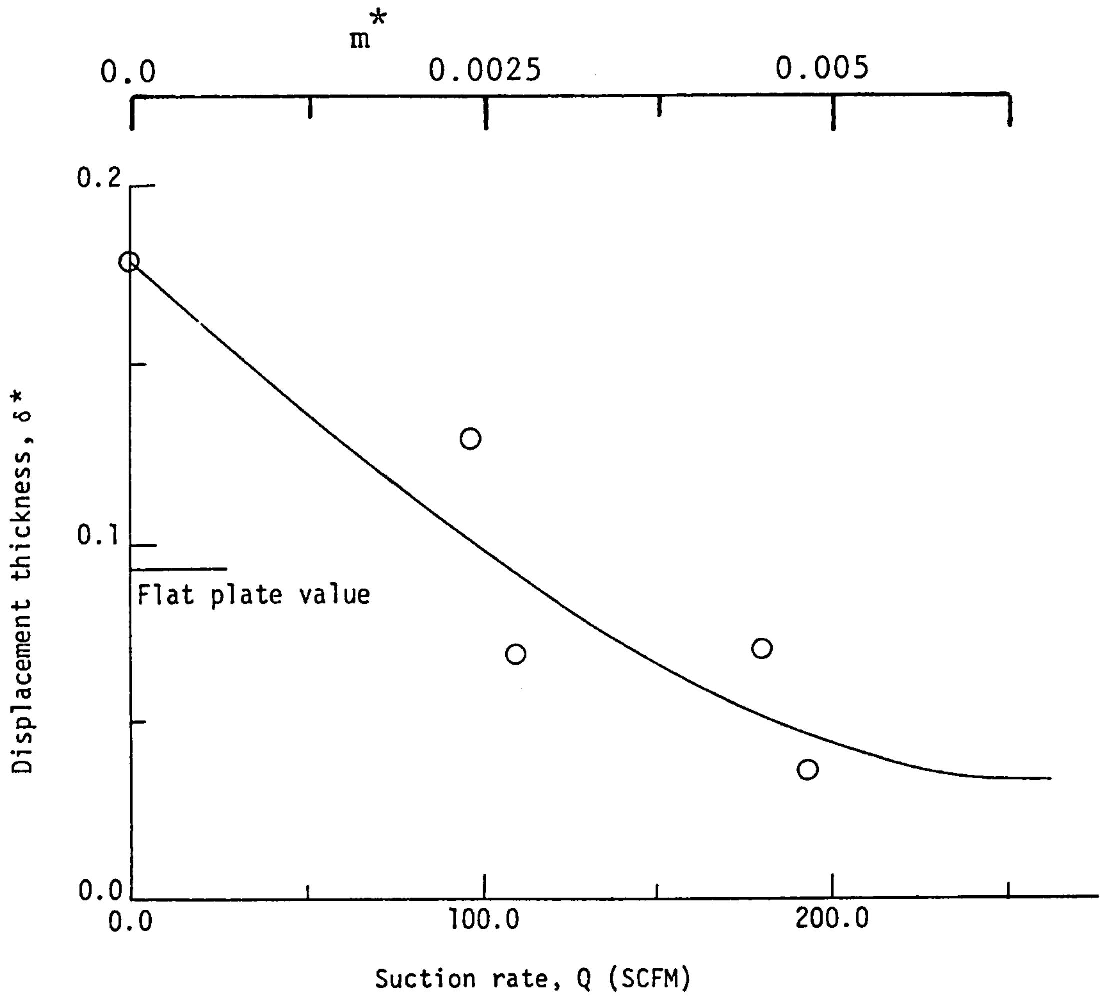

(a) $M_\infty = 0.6$, Re/ft. $= 7.1 \times 10^6$

Figure 3.4. Influence of suction flow rate upon the boundary layer displacement thickness over the slot for flow over the single slotted wall.

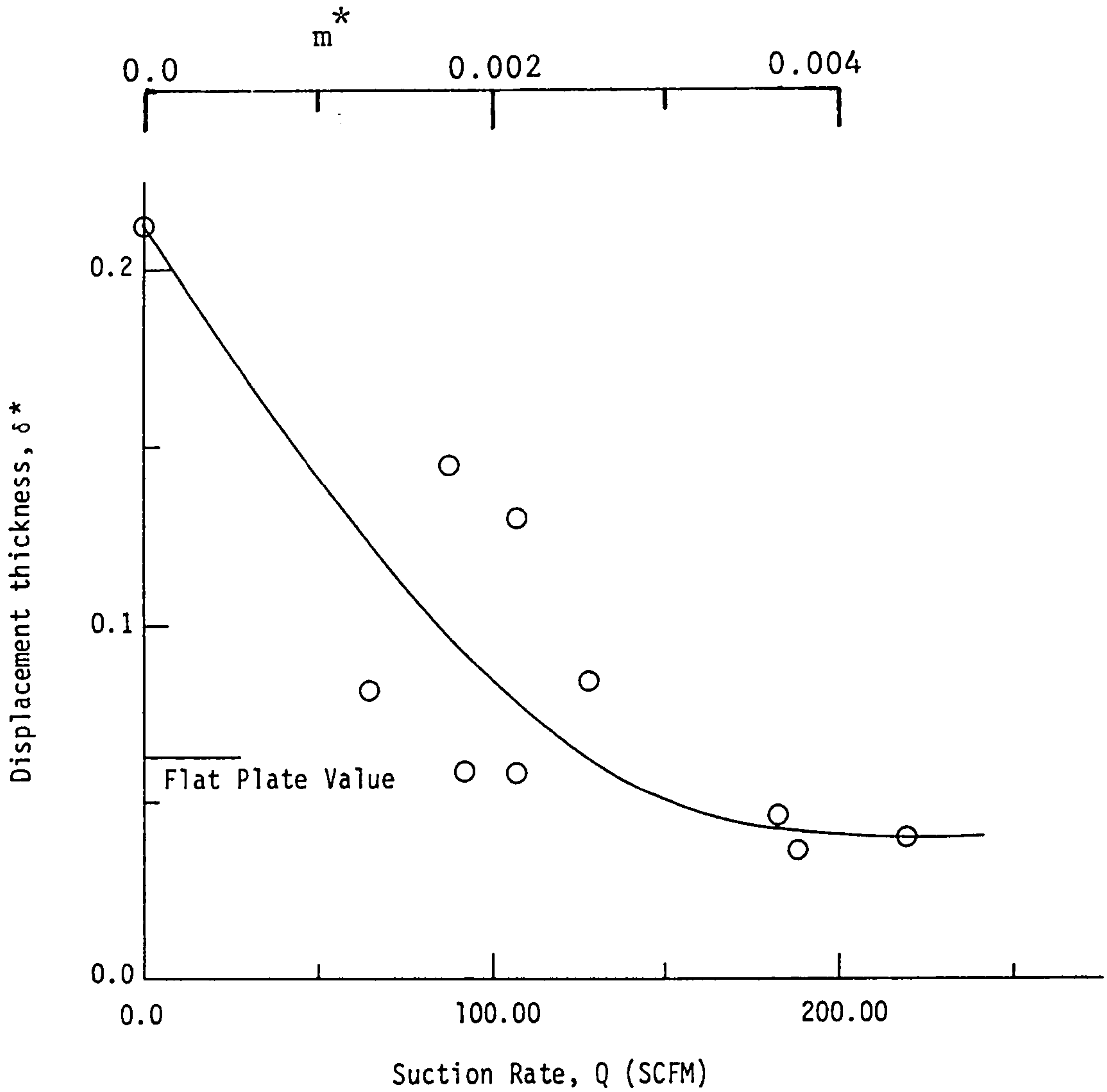

(b) $M_\infty = 0.76$, Re/ft. $= 9.85 \times 10^6$

Figure 3.4. (Continued)

at $M_\infty = 0.76$, Re/ft. $= 7.63 \times 10^6$. The larger velocity defect at $M_\infty = 0.6$ indicates that a greater amount of fluid mass that has been removed from the viscous layer has entered the slot. As a result, at the lower Mach number of 0.6, a larger suction velocity exists.

Due to this large build up of boundary layer on the model wall, there exists a sizable pressure gradient in the downstream direction which results in a lower downstream test section pressure. Associated with this pressure distribution is a larger inflow into the test section from the plenum chamber and a corresponding outflow from the test section. This outflow occurs at the upstream end of the slot.

The boundary layer displacement thickness on the slot decreases rapidly with increase in the suction mass flow rate through the slot. The δ^* of the boundary layer at the slot reduces from 0.218 inches at no auxiliary suction to 0.041 inches (reduction ratio of 5.32) at a suction flow rate of 200 SCFM or $m^* = 0.004$ (approximately equivalent to $w/U_\infty = 0.30$) through the slot at $M_\infty = 0.76$. This ratio is found to be 4.15 for the $M_\infty = 0.6$ run condition. At larger suction through the slot, the boundary layer almost disappears

The boundary layer displacement thickness distribution in the transverse plane, at $x = 7.5$ inches measured from the slot beginning, are shown for different cases of suction rate through the slot in Figures 3.5a to 3.5g. The decrease in the displacement thickness with higher suction rate is apparent. It is interesting to note how the velocity defect thickness changes over the slotted wall in these plots. These are explained in detail below.

At no auxiliary suction ($Q = 0.0$ SCFM), δ^* decreases monotonically with increase in distance away from the slot axis. However, for the case of $M_\infty = 0.6$ in Figure 3.5a, the decrease in δ^* close to the slot is due to reasons of larger suction velocity, explained earlier. Matyk and Kobayashi (1977) observed that the δ^* of

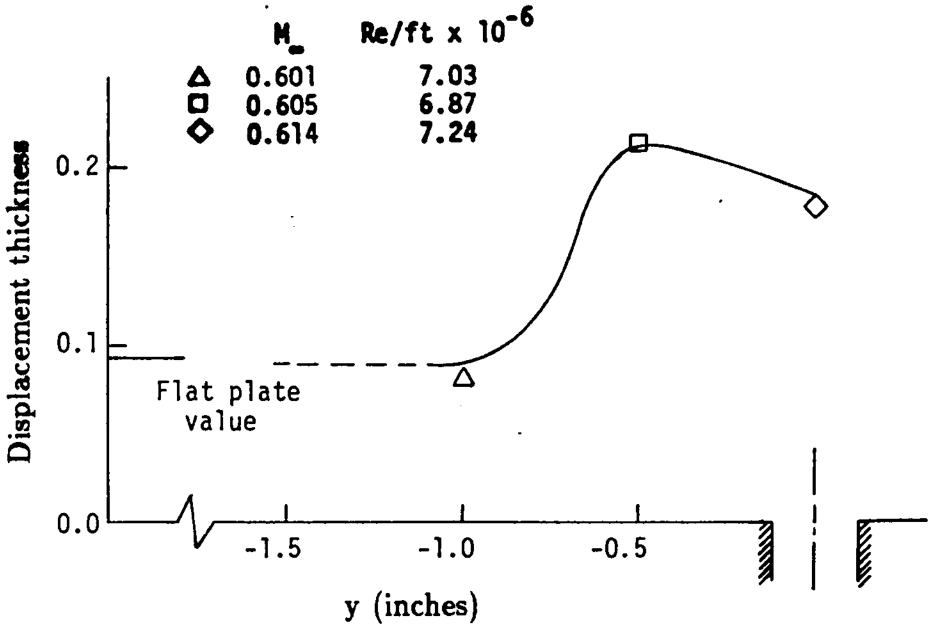

(a) $M_\infty = 0.62$, Re/ft. $= 7.0 \times 10^6$, $Q = 0.0$

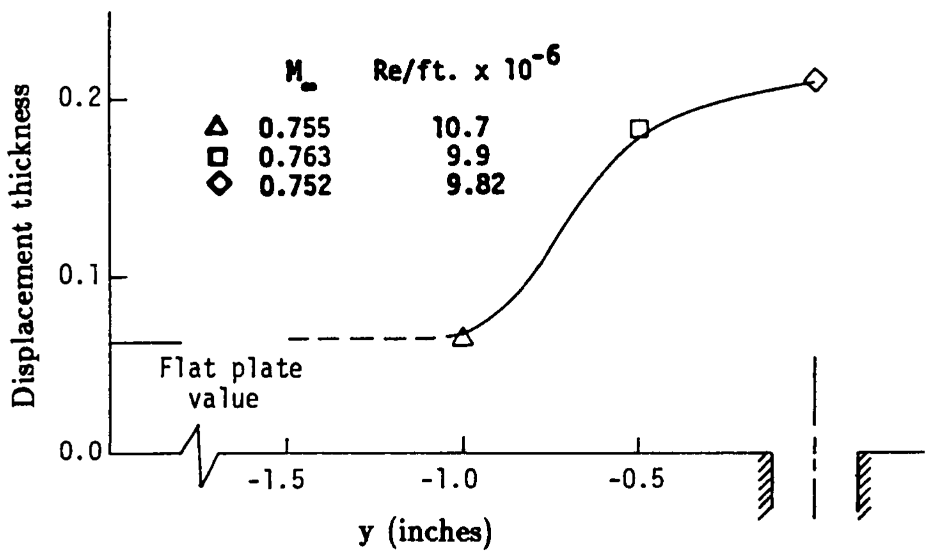

(b) $M_\infty = 0.76$, Re/ft. $= 10.0 \times 10^6$, $Q = 0.0$

Figure 3.5. Boundary layer displacement thickness distribution in the transverse plane at $x = 7.5$ inches for flow over the single slotted wall.

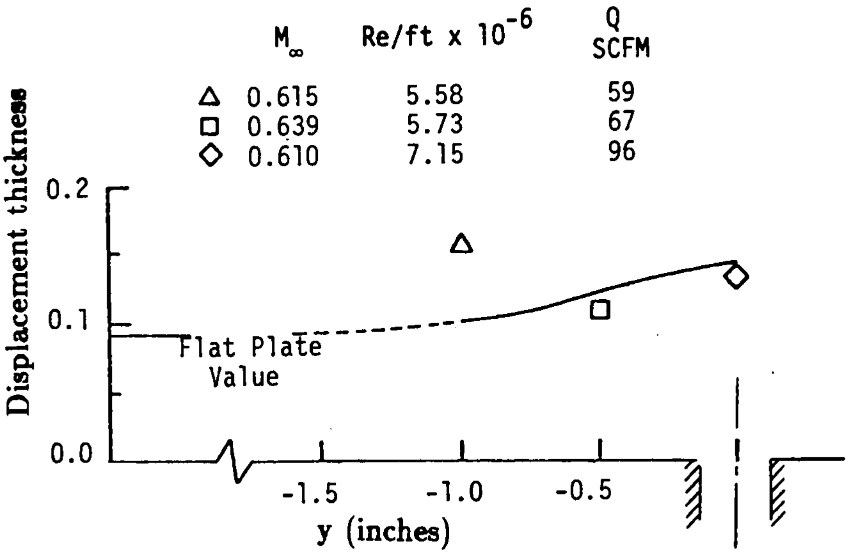

(c) M_∞ = 0.62, Re/ft. = 6.0 $\times 10^6$, Q = 60.0 SCFM, m^* =0.0015

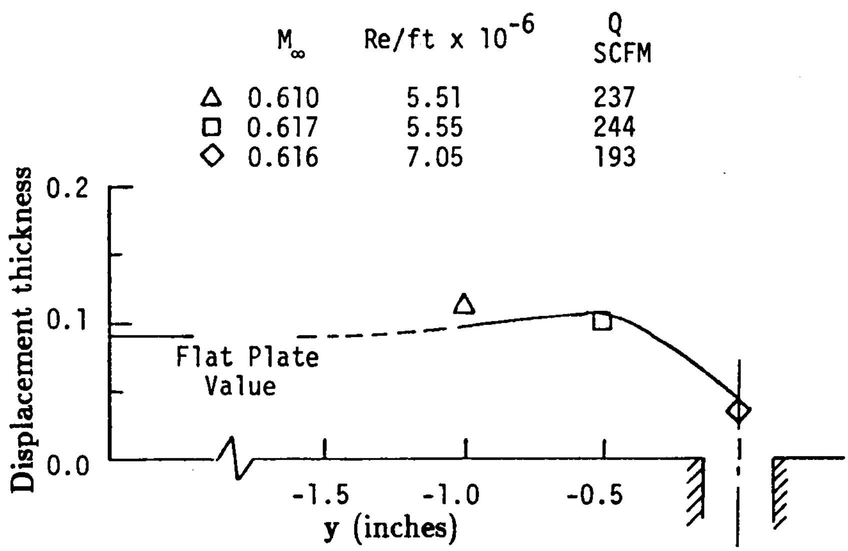

(d) M_∞ = 0.62, Re/ft. = 6.0 $\times 10^6$, Q = 240.0 SCFM, m^* =0.0058

Figure 3.5. (Continued)

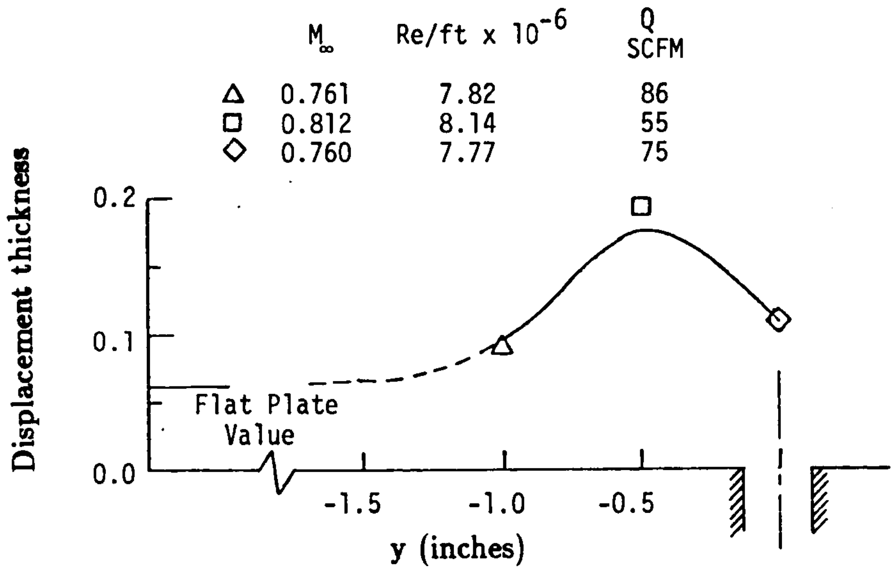

(e) $M_\infty = 0.76$, Re/ft. $= 8.0 \times 10^6$, $Q = 80.0$ SCFM, $m^* = 0.0016$

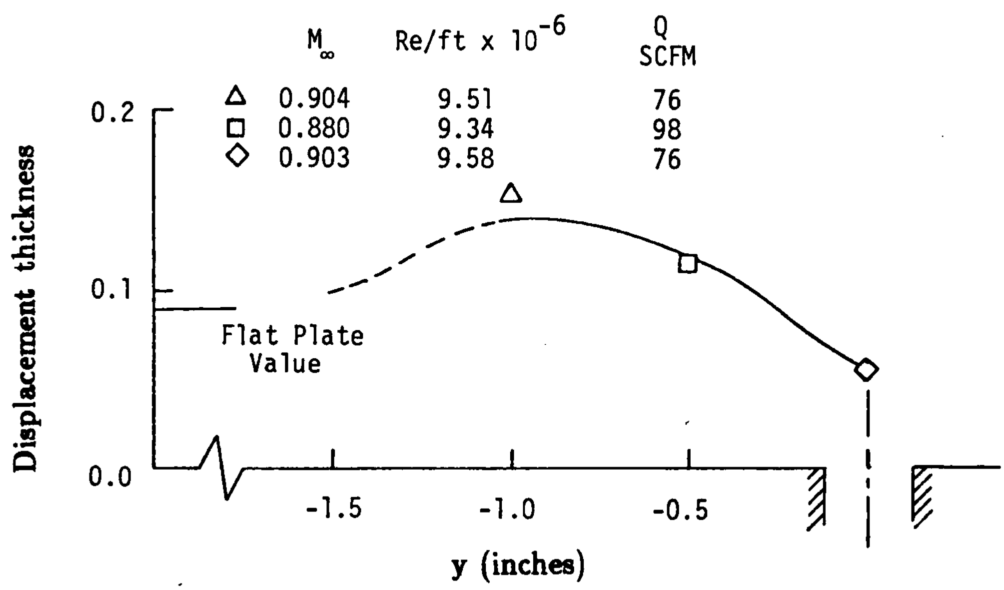

(f) $M_\infty = 0.9$, Re/ft. $= 9.5 \times 10^6$, $Q = 80.0$ SCFM, $m^* = 0.0013$

Figure 3.5. (Continued)

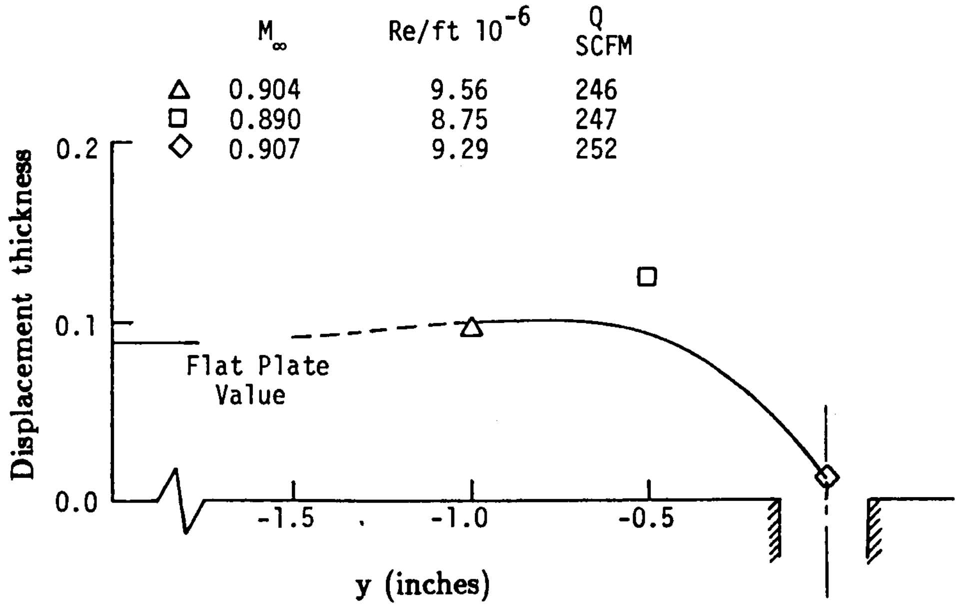

(g) $M_\infty = 0.9$, Re/ft. $= 9.5 \times 10^6$, $Q = 250.0$ SCFM, $m^* = 0.004$

Figure 3.5. (Continued)

the slot boundary layer increased to nearly twice the δ^* of the slat boundary layer. It must be noted that they had one traversing probe placed on the slat (between the two adjacent slots) and the other probe downstream of the slot. The δ^* obtained from the downstream probe was found to be twice that obtained by the first probe. The increase in δ^* was attributed to the aspirating effect. However, in the present investigation all the measurements were made at four locations in a transverse plane at the same longitudinal station and it was observed that the δ^* increased toward the slot and was a maximum at the slot centerline.

The reason for the increase in δ^* in the vicinity of the slot can be explained as follows. The boundary layer on the slotted wall is similar to the boundary layer flow on a solid plate which contains a deep, long cavity. For no applied suction (natural ventilation) the flow entering into the plenum chamber is mostly drawn from the slotted wall boundary layer and very little comes in from the outer stream flow. This is supported by the δ distribution (Figure 3.3) which indicates only a slight variation in δ with y for low applied suction through the slot. The drawing of mass from the boundary layer together with only a slight change in δ for zero to moderate amount of applied suction through the slot results in an increased velocity defect in the shear layer and consequently in an increase in δ^*.

The influence of the applied suction at the $M_\infty = 0.6$ condition is realized by comparing the data in Figures 3.5a, 3.5c and 3.5d. It is observed that the δ^* decreases in the neighborhood of the slot. The influence of suction in the lateral direction seems to be limited to about 4 to 5 slot widths. Figures 3.5b and 3.5e compare the δ^* distributions at $M_\infty = 0.76$, with and without applied suction. Figures 3.5f and 3.5g exhibit the results at $M_\infty = 0.9$ with applied suction as shown. The same trend in δ^* distribution as explained earlier is maintained.

C. VELOCITY VECTOR DISTRIBUTION

While the u–component is used to evaluate the boundary layer displacement thickness characteristics, as explained, the v– and w–components serve to illustrate the flow pattern in the transverse plane. The three-dimensional velocity of the flowfield at the measurement plane (transverse plane at x = 7.5 inches) is shown in Figures 3.6a for the Q = 250 SCFM or m^* = 0.006 run conditions. The plot contains the results from four independent test runs. The test conditions of the plotted data in each plot are approximately the same. The plot exhibits the three-dimensional nature of the flowfield on the single slotted model wall in a qualitative sense.

The plot further indicate that the velocity vector is skewed toward the slot for measurement locations away from the slot. The extent of skewness seemingly decreased with distance away form the slot. At the slot itself the flow was directed into the slot by the baffles. As indicated earlier, there was flow outward from the test section through the slot at this longitudinal measuring station for all present measurements even without applied suction due to the development of the boundary layer over the slotted wall.

The behavior of the flowfield is better visualized by considering the projection of the resultant of v/U_∞ and w/U_∞ velocity components onto the transverse plane. These plots at the corresponding run conditions are shown in Figures 3.7a and 3.7h. In these plots the main flow direction is coming out of the plane of paper. It is obvious from these figures that the magnitude of the v and w velocity components can be significantly large on a slotted tunnel wall, e.g., on a single slotted wall at the slot. For the run conditions $M_\infty = 0.77$, Re/ft. = 7.8 $\times 10^6$, Q = 87 SCFM or m^* = 0.002, the normalized w–component is w/U_∞ = 0.16; and for

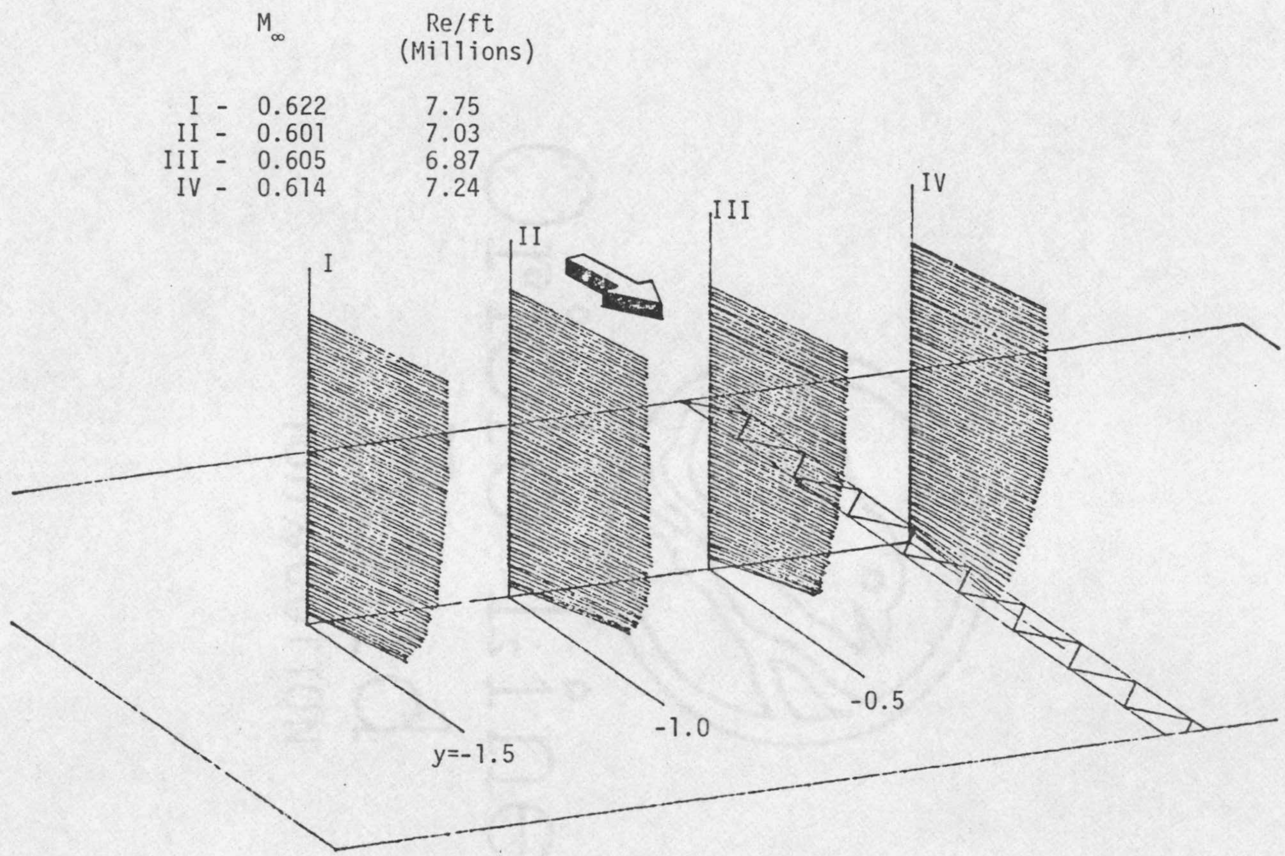

Figure 3.6. Three-dimensional velocity profiles on the single slotted wall.

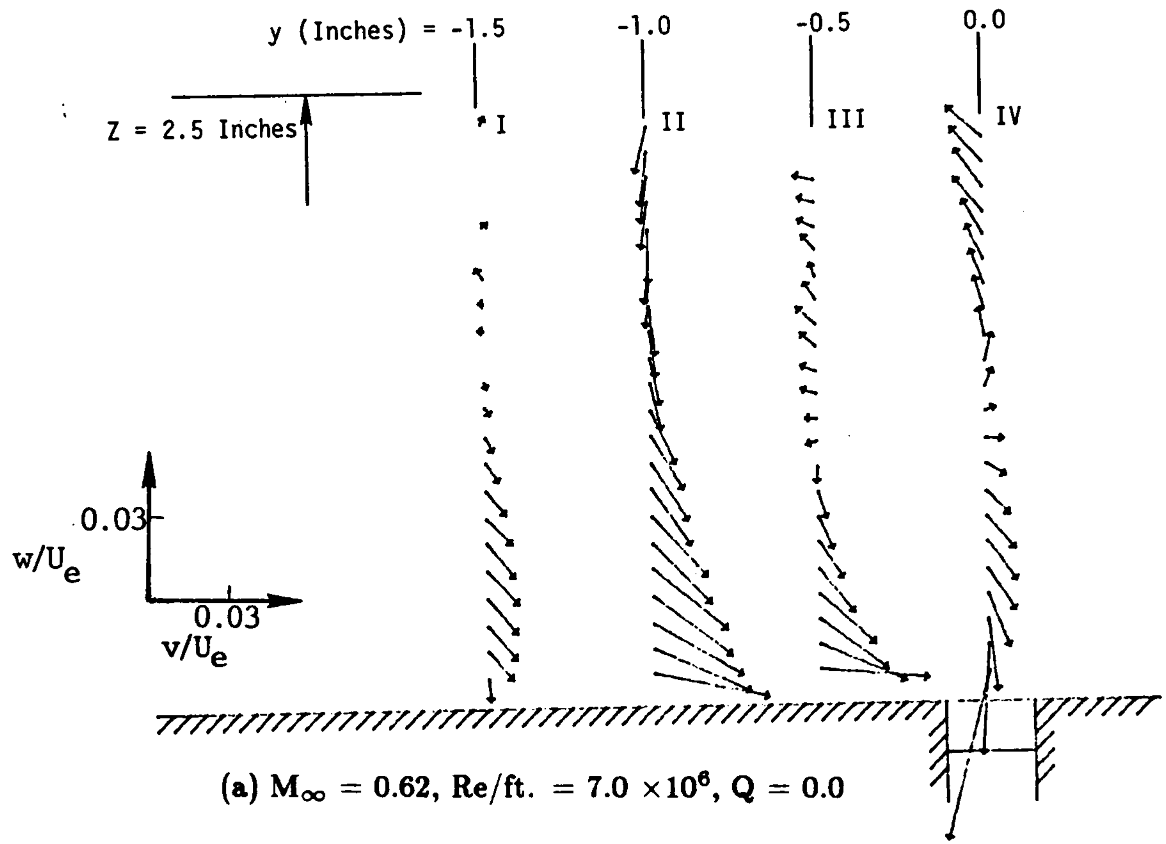

(a) $M_\infty = 0.62$, Re/ft. $= 7.0 \times 10^6$, $Q = 0.0$

Figure 3.7. Velocity vector distribution in the transverse plane at the longitudinal station $x = 7.5$ inches, for flow over single slotted wall.

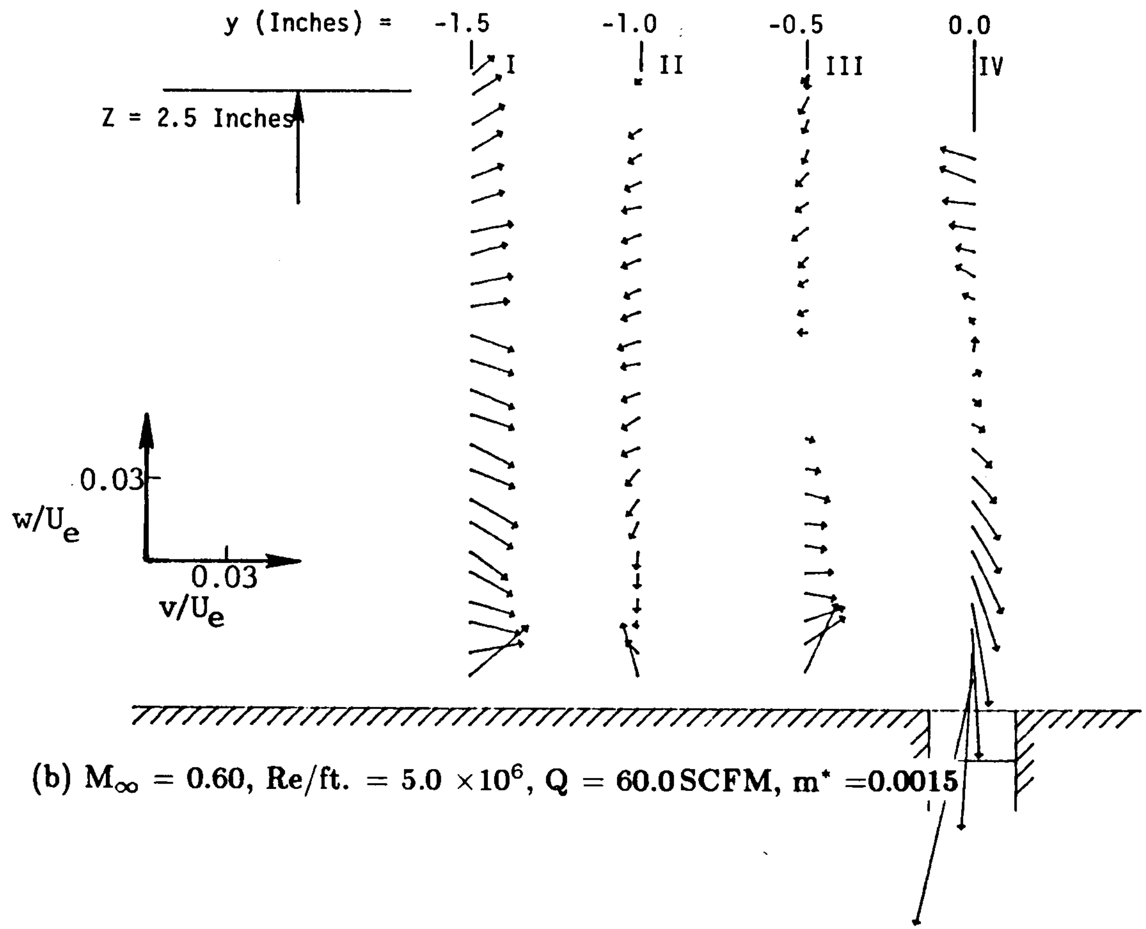

(b) $M_\infty = 0.60$, Re/ft. $= 5.0 \times 10^6$, Q $= 60.0$ SCFM, $m^* = 0.0015$

Figure 3.7. (Continued)

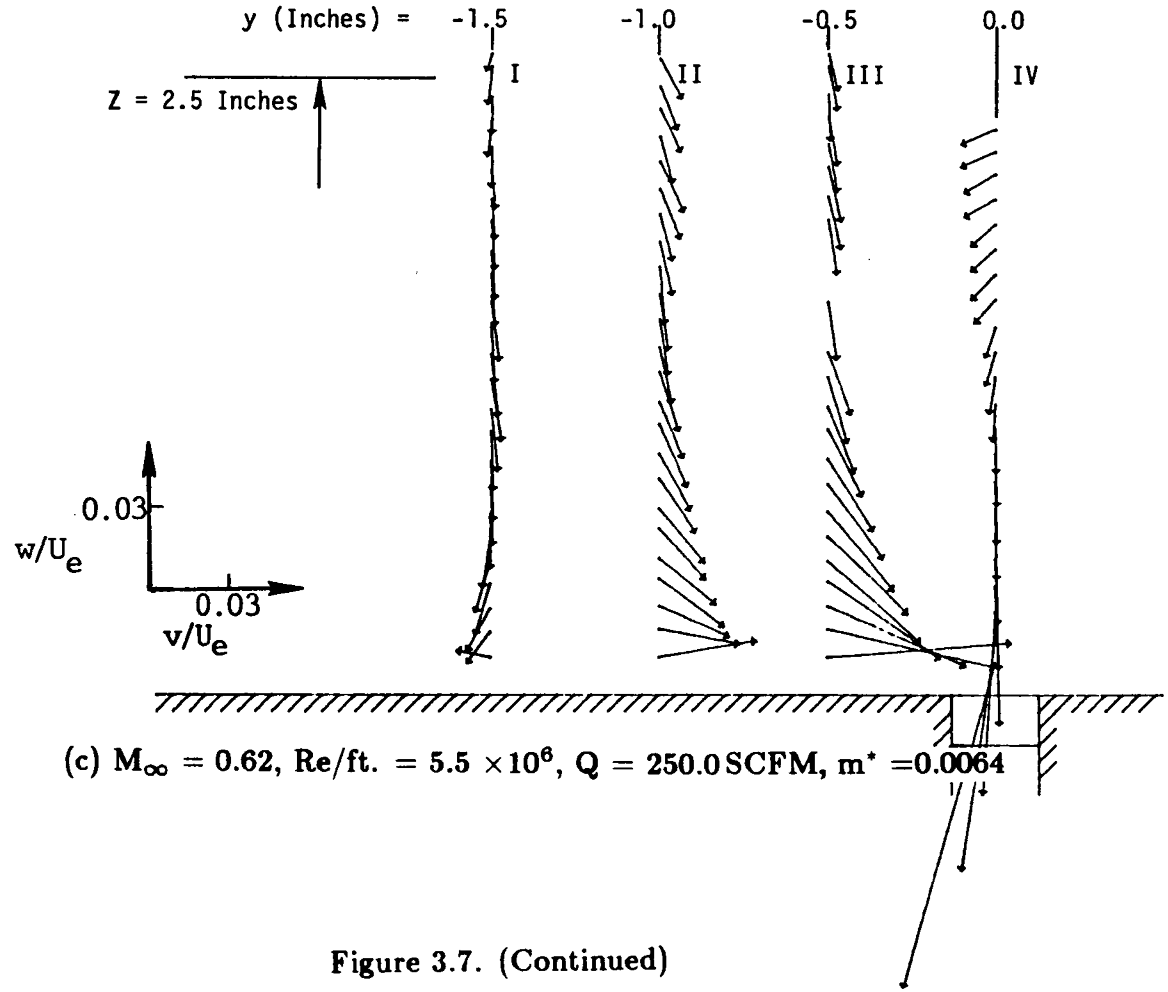

(c) $M_\infty = 0.62$, Re/ft. $= 5.5 \times 10^6$, Q = 250.0 SCFM, $m^* = 0.0064$

Figure 3.7. (Continued)

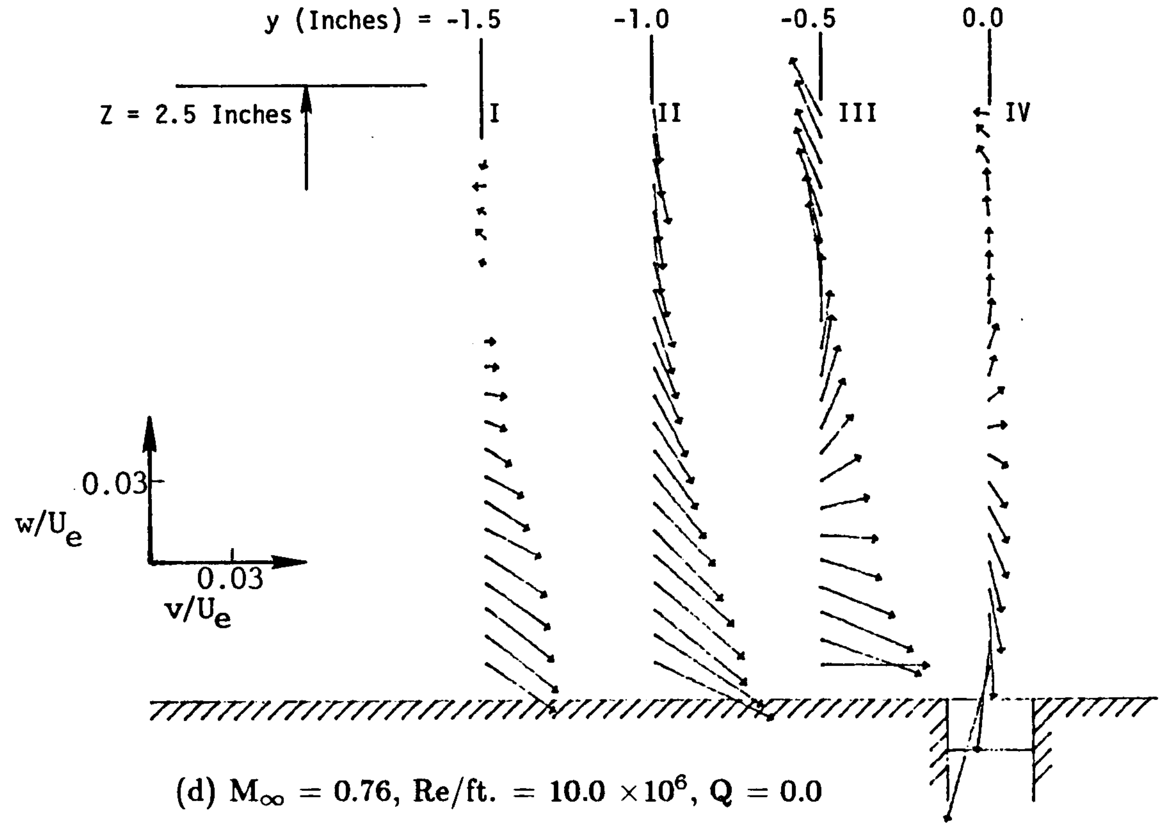

(d) $M_\infty = 0.76$, Re/ft. $= 10.0 \times 10^6$, $Q = 0.0$

Figure 3.7. (Continued)

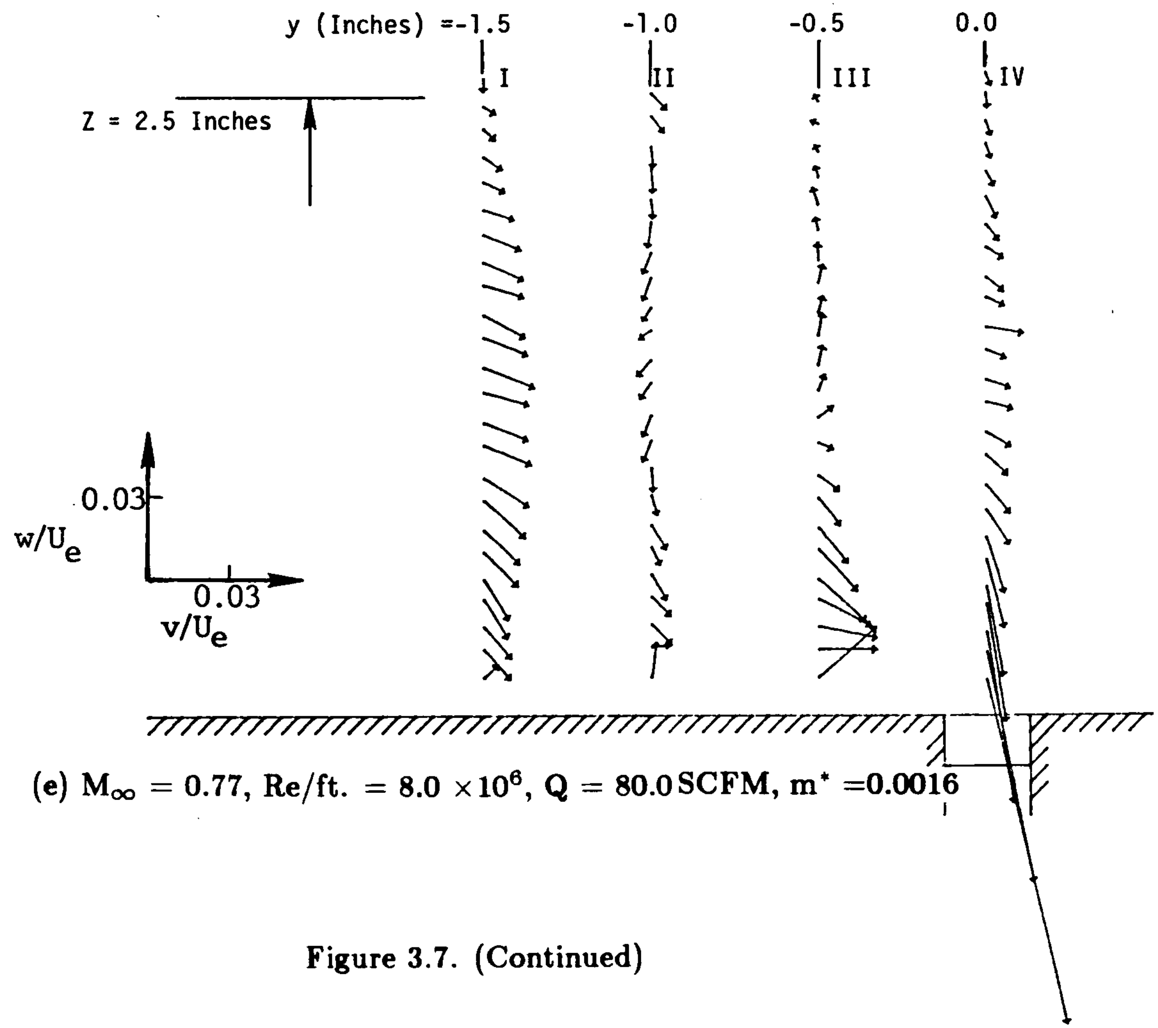

(e) $M_\infty = 0.77$, Re/ft. $= 8.0 \times 10^6$, $Q = 80.0$ SCFM, $m^* = 0.0016$

Figure 3.7. (Continued)

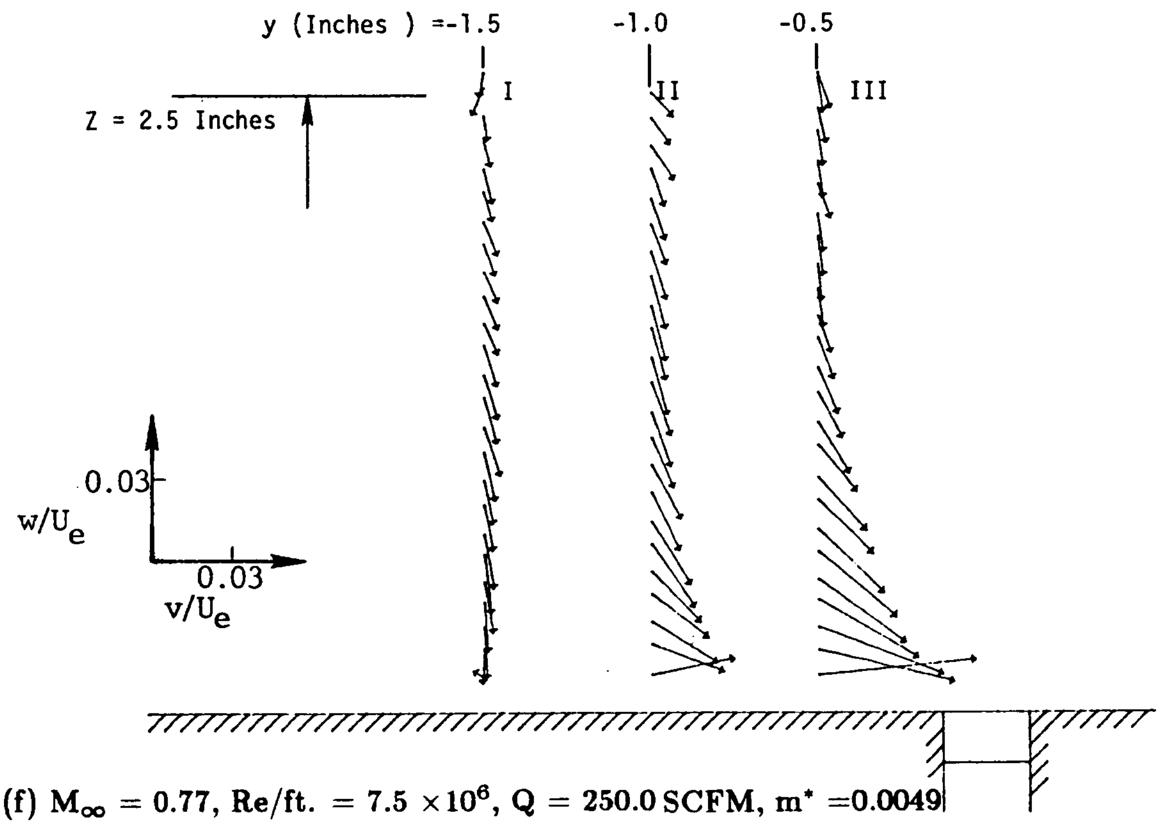

(f) $M_\infty = 0.77$, Re/ft. $= 7.5 \times 10^6$, Q $= 250.0$ SCFM, $m^* = 0.0049$

Figure 3.7. (Continued)

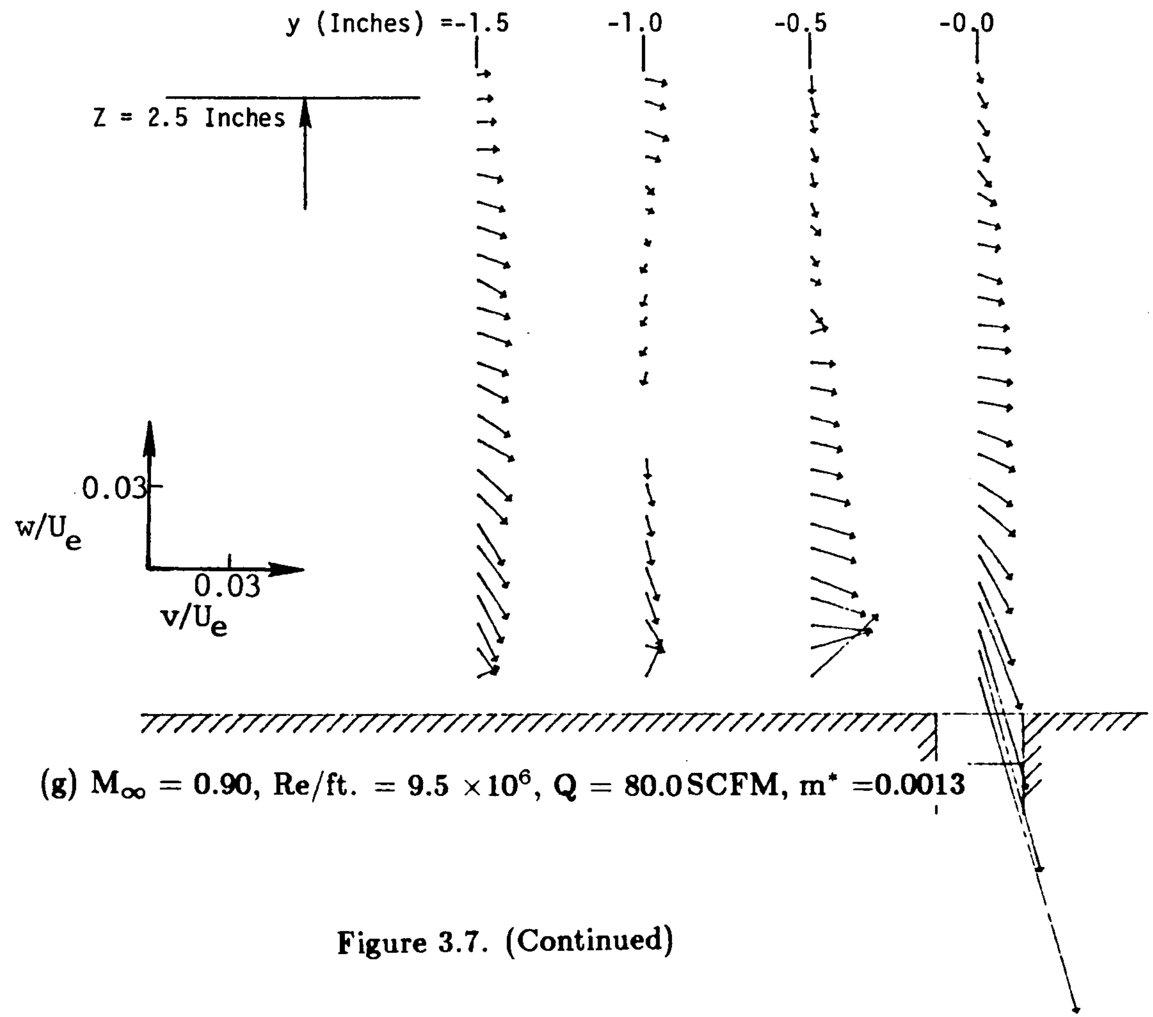

(g) $M_\infty = 0.90$, Re/ft. $= 9.5 \times 10^6$, Q = 80.0 SCFM, $m^* = 0.0013$

Figure 3.7. (Continued)

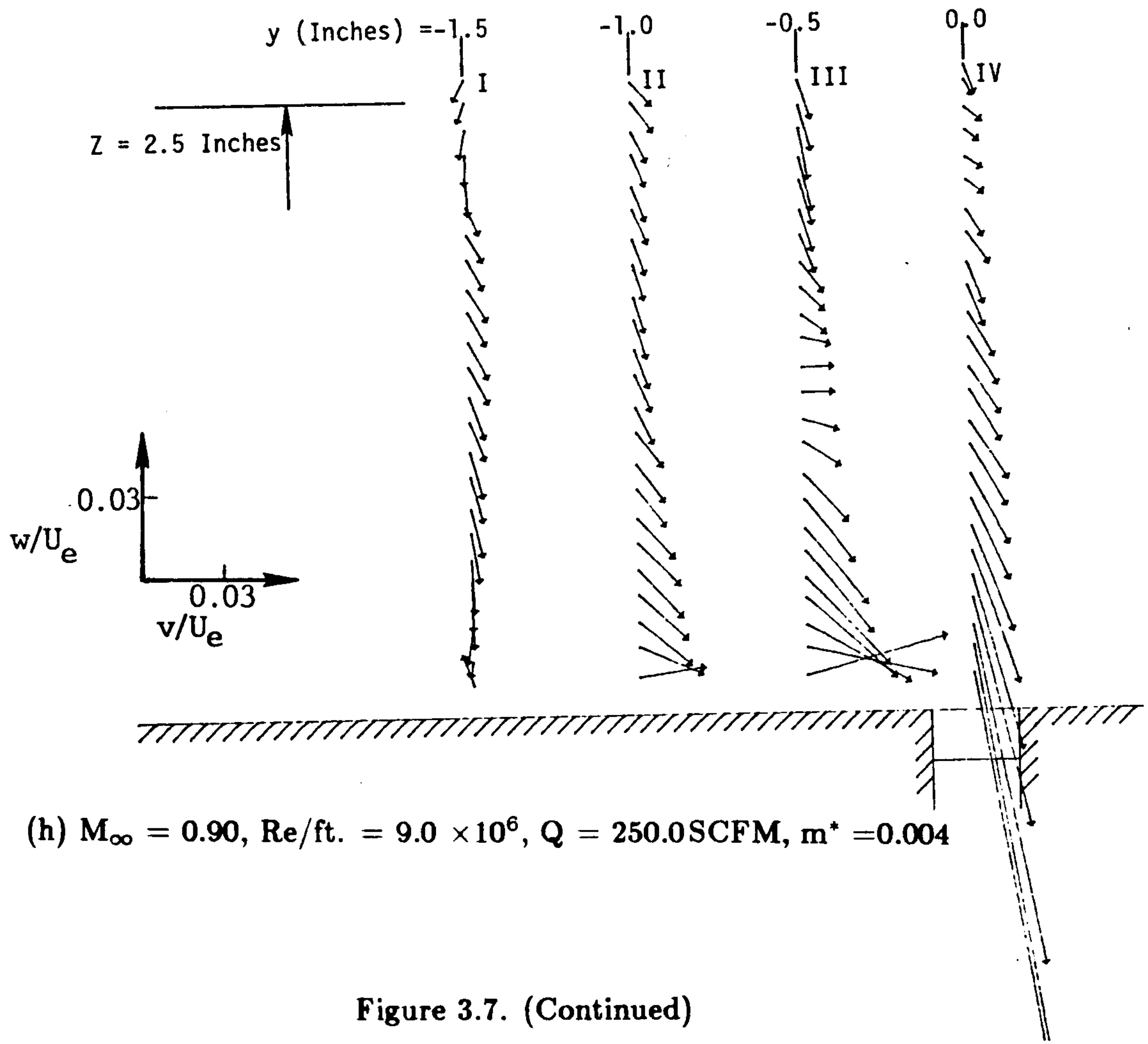

(h) $M_\infty = 0.90$, Re/ft. $= 9.0 \times 10^6$, Q = 250.0SCFM, $m^* = 0.004$

Figure 3.7. (Continued)

$M_\infty = 0.631$, Re/ft. $= 5.52 \times 10^6$, $Q = 234$ SCFM or $m^* = 0.006$ run conditions the w–component is $w/U_\infty = 0.33$, while at a distance of 0.5 inches from the slot center line in the transverse direction for $M_\infty = 0.761$, Re/ft. $= 7.82 \times 10^6$, $Q = 86$ SCFM or $m^* = 0.002$ conditions, the w–component is reduced to $w/U_\infty = 0.0423$ and for $M_\infty = 0.615$, Re/ft. $= 5.58 \times 10^6$, $Q = 54$ SCFM or $m^* = 0.002$ condition the normalized w–component is $w/U_\infty = 0.0397$.

The velocity vectors in the immediate neighborhood of the wall in these plots show a rather erroneous scattering from the general trend. This is because the cone probe results become spurious due to the probe-wall interference when the probe is very close to the wall, as explained previously.

The geometry of the slot as well as the baffle shape can influence the local flow significantly. The baffles direct the flow through the slot at a desired angle. Satyanarayana et al. (1981) described that the flow angle and Berndt (1982) reported that the slot shape can effectively be used to control the flow near a wind tunnel wall and therefore may be viable competitive tools in adaptive wall testing. Zig–zag baffles used within the slots in the present study had a configuration similar to that used in the NASA AMES Transonic wind tunnel.

In the present experiments the orifice location of the cone probe was located almost on the baffle dividing line on the slot. At the slot the flow was directed by the baffle in its proximity. The baffle angle was about 14 degrees and the measured angle of the resultant v-w components at the slot was slightly greater than 14 degrees.

In the Figures 3.7e, 3.7g and 3.7h the direction of the velocity vector in the transverse plane at the slot is different from that in the others. The reason for this is that the cone probe was perhaps mounted in such a way that the orifices shifted towards the other side of the baffle dividing line of the slot. The flow angle locally within the slot is significantly influenced by the angle of the part of the baffle which faces the flow entering the slot.

D. SECONDARY FLOW IN THE TRANSVERSE PLANE

The flow pattern in the transverse plane exhibited in Figures 3.7a - 3.7h indicates a vortex-like flow. On close observation it is seen that, for no applied suction, the vortex-like flow is strong and confined to rather outer regions extending into the freestream. Close to the slotted wall the flow tends to form a definite streamline pattern, in the transverse plane, directed toward and into the slot. At $M_\infty = 0.6$ and 0.76, and with moderate suction $Q = 75$ SCFM or $m^* = 0.002$, the vortex-like tendency of the outer flow is rather decreased, and at high suction $Q = 240$ SCFM or $m^* = 0.005 - 0.006$, this phenomenon has almost disappeared. It was understood earlier that at these high suction flow rates the boundary layer almost disappears. It is therefore inferred that this secondary vortex flow may be attributed to the irregularity of the slotted wall viscous layer namely the skewing of the mean flow and inhomogeneity of the boundary layer. It is to be noted that the center core of this vortex-like flow is outside the conventional wall shear layer.

In the present experiments slots with flat rectangular ends were used. It is plausible that the vortices were generated from the slot lip, similar in fashion to horse-shoe-vortices, as a consequence of flow into the slot and that they then propagate outwards from the wall while traveling downstream. However, such vortices should become stronger for increased suction rate through the slot. It is realized that this is not the case from the present observations. The formation of secondary flow can arise in turbulent flows from mean flow skewing and from anisotropy of wall turbulence in the presence of an inhomogeneous boundary layer, in the sense that δ is not constant in the transverse plane. The steady secondary flow vortices, as categorized by Prandtl, caused by the former (i.e., mean skewing) is referred to as the secondary flow of first kind and those caused by the later (i.e., inhomogeneous boundary layer in the transverse plane and wall turbulence anisotropy) is called the secondary flow of the second kind. Perkins (1970) obtained qualitatively the direction of the vortices for the secondary flow of the second kind in a nominal two-dimensional boundary layer. Following the analysis of Perkins it is possible to explain the formation and the attenuation with increased applied suction of the secondary vortex flow observed in the present results.

In steady incompressible flow the mean streamwise vorticity equation is:

$$\begin{aligned} u\frac{\partial \xi}{\partial x} + v\frac{\partial \xi}{\partial y} + w\frac{\partial \xi}{\partial z} &= \nu\nabla^2\xi + \xi\frac{\partial u}{\partial x} + \eta\frac{\partial u}{\partial y} \\ &+ \varsigma\frac{\partial u}{\partial z} + \frac{\partial}{\partial x}\left(\frac{\partial \overline{u'v'}}{\partial z} - \frac{\partial \overline{u'w'}}{\partial y}\right) \\ &+ \frac{\partial^2}{\partial y \partial z}(\overline{v'^2} - \overline{w'^2}) \\ &+ \left(\frac{\partial^2}{\partial z^2} - \frac{\partial^2}{\partial y^2}\right)\overline{v'w'} \end{aligned} \quad (1)$$

where

$$\begin{aligned} \xi &= \frac{\partial w}{\partial y} - \frac{\partial v}{\partial z} \\ \eta &= \frac{\partial u}{\partial z} - \frac{\partial w}{\partial x} \\ \varsigma &= \frac{\partial v}{\partial x} - \frac{\partial u}{\partial y}. \end{aligned}$$

The term

$$\begin{aligned} E_1 &= \eta\frac{\partial u}{\partial y} + \varsigma\frac{\partial u}{\partial z} \\ &= \frac{\partial u}{\partial z}\frac{\partial v}{\partial x} - \frac{\partial u}{\partial y}\frac{\partial w}{\partial x} \end{aligned} \quad (2)$$

represents the production of streamwise vorticity through skewing of the mean shear by a transverse pressure gradient. Among the other terms on the right hand side of Equation (4) the only significant term is

$$E_3 = \frac{\partial^2}{\partial y \partial z}(\overline{v'^2} - \overline{w'^2}). \tag{3}$$

This term represents the production of streamwise vorticity by the wall turbulence anisotropy. Based on measurements in a non-uniform, nominally two-dimensional boundary layer Perkins reported that it was adequate to use the relation

$$\frac{(\overline{v'^2} - \overline{w'^2})}{u_\tau^2} = f\left(\frac{z}{\delta}\right) = \left(1 - \frac{z}{\delta}\right) \tag{4}$$

for the determination of the direction of secondary vortices of the second kind. Then in our case we obtain

$$E_3 = -\frac{{u_\tau}^2}{\delta}\left[\frac{2}{u_\tau}\frac{\partial u_\tau}{\partial y} - \frac{1}{\delta}\frac{\partial \delta}{\partial y}\right]. \tag{5}$$

Although the above formulation is applicable to incompressible flows, compressibility should not change the direction of the vortex motion. Consider the boundary layer, inhomogeneous in the transverse plane, containing a transverse deformation in u_τ and δ, as shown in Figure 3.8. Application of Equation (5) leads to the following conclusions:

(i) In planes such as B-B′, $\partial u_\tau / \partial y = \partial \delta / \partial y = 0$ yielding $E_3 = 0$.

(ii) In planes such as A-A′, $\partial u_\tau / \partial y > 0$ and $\partial \delta / \partial y < 0$, giving E_3 less than zero and hence a clockwise secondary current. The reverse is true for planes such as C-C′.

From the δ distribution in the transverse plane (Figures 3.3, 3.7a and 3.7d), using the above explanation, it is obvious that the inhomogeneity of the cross plane boundary layer together with anisotropic wall turbulence leads to a pair of vortices that are clockwise for $y < 0$ and counter clockwise for $y > 0$.

Next consider the production of mean streamwise vorticity E_1 due to mean slow skewing given by Equation (2). For the present problem $\partial v / \partial x$ and $\partial w / \partial x$

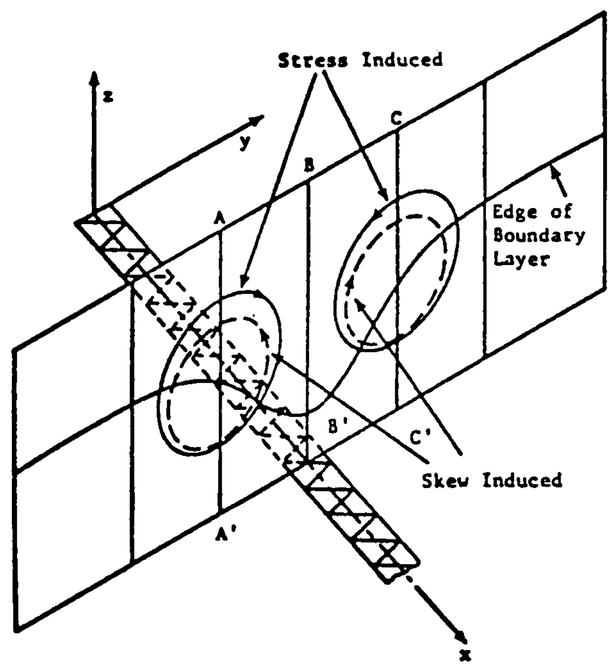

Figure 3.8. Rotational sense of skew and stress induced vortex motion in transverse plane.

are of the same order of magnitude while $\partial u/\partial z > \partial u/\partial y$ over most of the shear layer at moderate applied suction. While $\partial u/\partial y$ increases with applied suction there is a corresponding increase in $\partial u/\partial z$ due to the decrease in δ. Flow is always removed from the test section at the longitudinal station examined. This produces a lateral convergence of the streamlines towards the slot. Non zero values of $\partial v/\partial x$ and $\partial u/\partial y$ exist and have opposite signs on opposite sides of the slot. The above explanation yields $E_1 > 0$ (counter clockwise vortex for motion) for $y < 0$ and $E_1 < 0$ (clockwise vortex motion) for $y > 0$. The generation of streamwise vorticity by this mean flow skewing leads to a pair of vortices which expel fluid from the shear layer out into the mean flow. This mechanism of streamwise vorticity generation is explained in more physical terms in Figures (3.7a and 3.7d). With no applied suction the mean flow skewing source is dominant. The flow moves downward and toward the slot except near the wall where it must move parallel to the wall. Because of the low momentum in the wall shear layer, the influence of the slot suction is greatest near the wall. However, since the amount of removed air is very small with no applied suction only that portion of the flow near the wall is removed and that above it meets the air coming from the other side of the slot and moves upward, forming the secondary flow pattern shown. Note that the center of the secondary motion is far removed from the region of the boundary layer as it was defined previously.

The conclusion is that the two sources of streamwise vorticity generate secondary motion of the opposite rotation sense, for the present geometry, which tend to counterbalance each other. At no applied suction, since there is only a slight variation of δ with y, the contribution to the secondary flow is mainly from the mean flow skewing (Figures 3.7a and 3.7d). With moderate applied suction the influence of the inhomogeneous boundary layer is strong and the two secondary flow sources tend to cancel one another. Then no secondary pattern is discernible (Figures 3.7b and 3.7e). At the highest applied suction rate the suction effect overrides the secondary motions and the velocity vectors are directed toward the slot (Figures 3.7c, 3.7d and 3.7h).

Another plausible explanation for the disappearance of secondary motion with moderate suction (Figures 3.7b and 3.7e) is that the upward movement along the centerline from the secondary motion caused by mean flow skewing was balanced by the downward movement toward the slot caused by the increased suction. Only further experimentation can unambiguously determine the source of the streamwise vorticity that is observed and its change with amount of applied suction.

E. INFLUENCE OF THE APPLIED SUCTION UPON THE NORMAL COMPONENT OF VELOCITY AT THE EDGE OF THE BOUNDARY LAYER

A comparison of the measured normal velocity component above the slot, w_{slot}, with that at the edge of the boundary layer, $w_{z=\delta}$, above the slot is shown for $M_{\infty} = 0.6$ and $M_{\infty} = 0.76$ in Figures 3.9, respectively. For zero suction, (i.e., $w_{slot} = 0$), the value of $w_{z=\delta}$ reaches the flat plate value. With increased suction the w velocity component at the edge of the boundary layer reduces monotonically. The w–component of velocity in the regions close to the slot becomes negative, i.e., the flow is directed into the slot, but w is still positive at the outer part of boundary layer. With further increase in suction through the slot the w velocity component at the edge of the boundary layer becomes negative. This implies that the flow is directed into the slot through the shear layer at the measurement location. In other words, the influence of suction has stretched out across the entire shear layer at the slot.

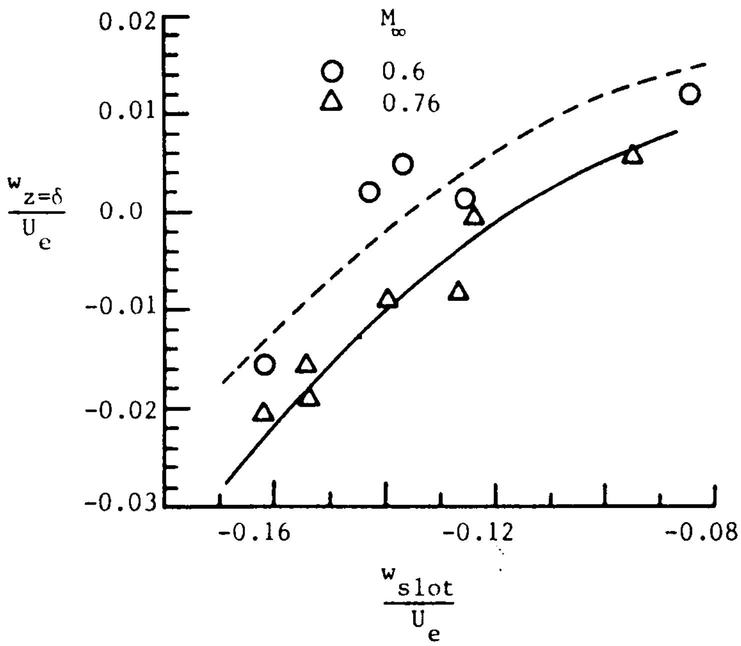

Figure 3.9. Variation of normal velocity at the edge of viscous layer over the slot with that at the slot for flow over the single slotted wall.

CHAPTER IV

RESULTS FOR FLOW ON SEGMENTED MULTI-SLOTTED WALL

Several test runs with different mass addition/removal rates through the chosen slot segments (see Figure 2.4) were made. The test section Mach number was maintained at 0.78 and Re/ft.= 7.1 $\times 10^6$. The applied suction and blowing varied from $Q \simeq 0$ CFM to $Q \simeq 400$ CFM ($m^* = 0.01$). Measurements were carried out at two longitudinal stations of x = 14.0 inches and x = 20.0 inches (see Figures 2.2, 2.4). At each longitudinal station, three probes were traversed through the flowfield close to the wall. In this way, measurements were conducted simultaneously at three lateral stations in the transverse plane. The measurements were conducted using five port cone probes. The cone probe data was reduced using an experimental calibration. The derived flow quantities from the measurements were 3–D flow angularity, total pressure, static pressure, Mach number and the magnitude of the velocity vector using the boundary layer analysis. The experimental data has been analyzed and the results are described in the following sections.

A. THREE DIMENSIONAL VELOCITY COMPONENTS

The velocity components, u, v and w were determined from the magnitude of the velocity vector and its 3–D angular orientation. Any contributions to these arising due to the initial mounting misalignments of the probe have been accounted for through the coordinate transformation discussed in Section J of Chapter II. A positive $v-$component represents the velocity component directed in the positive y–direction in a plane parallel to the tunnel wall and normal to the slot orientation (see Figures 2.2 and 2.7 for coordinate axis and slot orientation) and a positive w–component is the normal velocity component pointing away from the wall. The velocity components have been normalized by the magnitude of the freestream velocity. Many plots of these normalized velocity components have been obtained. A typical result of three velocity components is shown in Figure 4.1. It should be noted that in the immediate neighborhood of the wall the cone probe results become spurious due to the probe-wall interference. A detailed discussion on the flowfield velocity vector distribution is presented in Section C of Chapter IV. The flowfield features of the cross planeflow pattern are described next.

B. FLOW PATTERN IN THE CROSS-PLANE

The velocity vectors in the transverse planes at $x = 14$ inches and $x = 20$ inches are used to visualize the cross-plane flowfield pattern. The resultant of the v-and w-components at the corresponding distances y and z on these transverse planes of the segmented slotted wall have been plotted and their normalized magnitude indicated (see Section D of Chapter IV). The characteristics of these have been analyzed for various controlled blowing and suction conditions through the chosen plenum chambers. The details of the arrangement of the plenum chamber is given in Figure 2.4.

C. GENERAL CHARACTERISTICS OF THE CROSS-PLANE FLOW FIELD

For blowing and suction through the segmented slotted wall the following flow phenomena was observed.

In case of blowing through a segmented chamber, for moderate or low blowing rates (typically $Q \sim 150$ CFM, $m^* = 0.003$), the jet entering the test section had low momentum and formed a bubble-like flow pattern as has also been described by Berndt and Sorensen (1975). Berndt and Sorensen (1975) further observed that this bubble-like flow region spread laterally and farther outward into the boundary

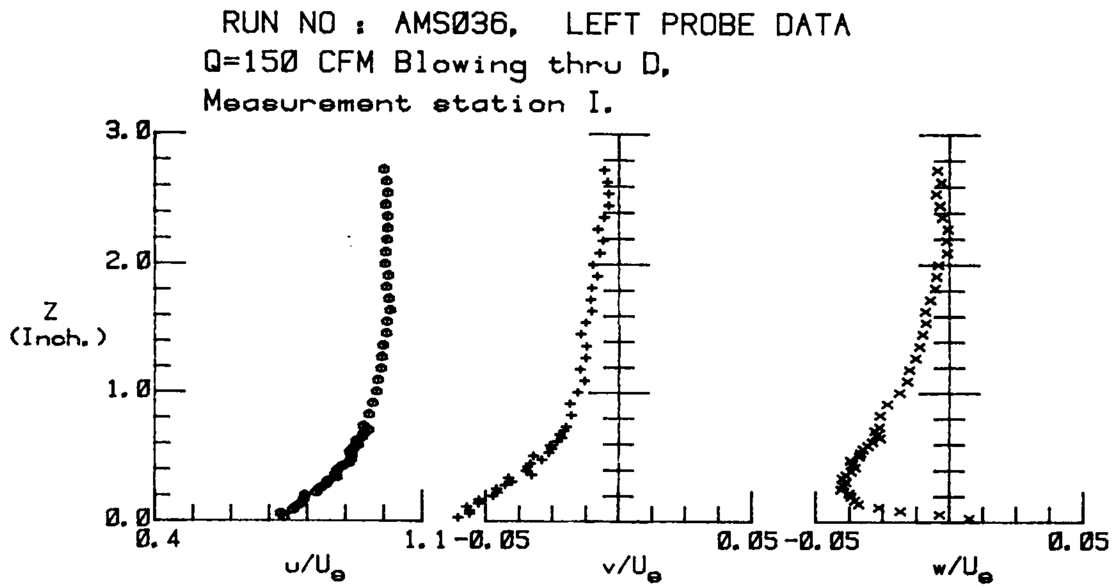

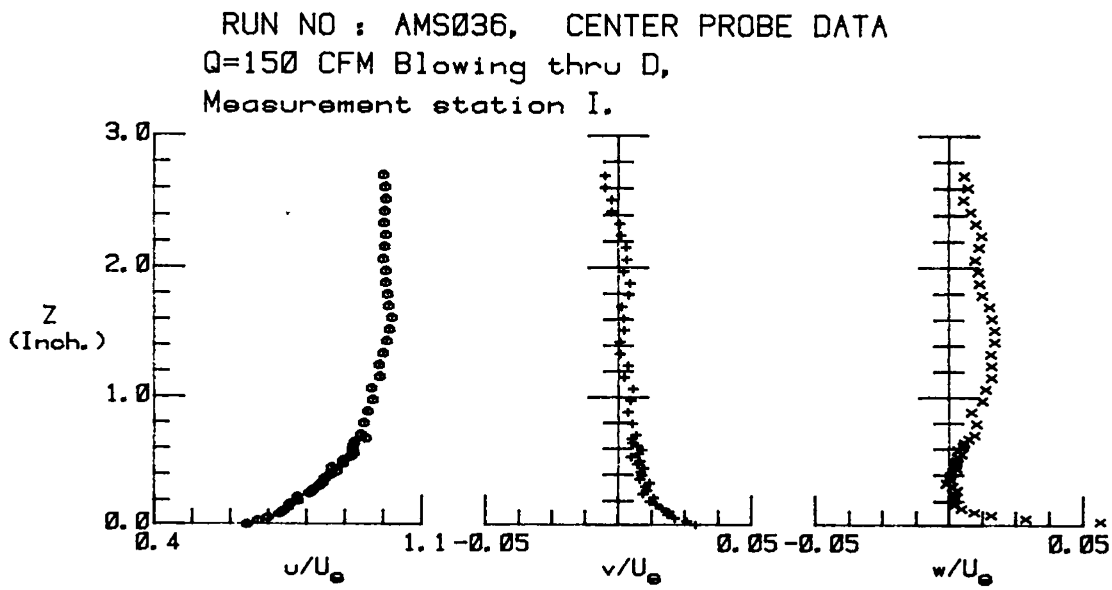

Figure 4.1. Typical velocity profile on segmented slotted wall at $M_\infty = 0.78$.

layer while being convected downstream. The diffusing "bubble" displaced the fluid mass and modified the flowfield by deflection. However, at high blowing rates (e.g., $Q \sim 400$ CFM), the blowing fluid entered the test section as a thin jet. This thin jet had higher momentum and moved upward with less lateral diffusion. While moving upward, the jet entrained main flow mass, creating a low pressure region close to the wall, and thereby pulling the fluid from the outer layers of the boundary layer away from the wall. A pressure gradient was thus built up which modified the local flow. The blowing through centrally located segmented compartments (i.e., compartments C and D) was observed to produce almost symmetric influence on the right and left probe measurements. This leads to the understanding that the blowing fluid displaced the fluid outside the boundary layer driving it away from the tunnel centerline while convecting it downstream. Larger resultant of v– and w–components at the left and right probe locations were measured.

A moderate suction (typically $Q \sim 150$ CFM, $m^* = 0.003$) through a segmented compartment resulted in drawing fluid mass from the boundary layer in the vicinity of the slot causing a local pressure gradient being built up, thereby modifying the flowfield. At high suction rates (e.g., $Q \sim 400$ CFM, $m^* = 0.01$), the boundary layer on the slot nearly disappeared (Chapter III) and the fluid was drawn mainly from the outside potential flow.

Both suction and blowing affect the boundary layer characteristics and the flowfield significantly. However the influence decays rapidly with transverse distance. The present studies showed that the measured magnitudes of w/U_e and v/U_e were rather small ($v/U_e, w/U_e \sim 0.05$). The present measurements were made at transverse locations that were far from the slots (about 0.75 inches). As described earlier (Chapter III) for flow on the single slotted walls, we observed that the magnitude of w/U_e on the slot ($y = 0.0$) at $M_\infty = 0.77, Re = 7.8 \times 10^6, Q = 87$

SCFM ($m^* = 0.0016$) was $w/U_e = 0.16$ while at $y = 0.5$ inches $w/U_e \simeq 0.042$. The rapid decay of the perturbation caused by the controlled suction is obvious.

D. DETAILED DESCRIPTION OF THE CROSS-PLANE FLOW PATTERN

The influence of controlled blowing and suction through individual chambers on the measured data at the two longitudinal stations is described below (for the Stations I and II, see Figure 2.4).

Since the blowing or suction through a set of segmented slots produces velocity field changes in its neighborhood, the flowfield analysis is divided into the following categories:

i) Lateral influence

ii) Downstream influence

iii) Upstream influence

iv) Interactive multiple compartment influence

The details of these are described below.

i) <u>Lateral influence</u>

The effect of blowing or suction through a compartment on the flowfield in the lateral direction (in the same transverse plane) is examined in this section. The results analyzed are for the controlled blowing or suction applied through chambers A or D and measurements made at transverse plane I (probe locations T1, T2 and T3). Also analyzed are the results obtained for applied control through chambers B or C and measurements made at transverse Station II (probe locations T4, T5 and T6).

The cross plane flowfield vectors for suction applied through side chamber A and that obtained for suction applied through central chamber D are shown in Figures 4.2 and 4.3 respectively. These results indicate that a low pressure

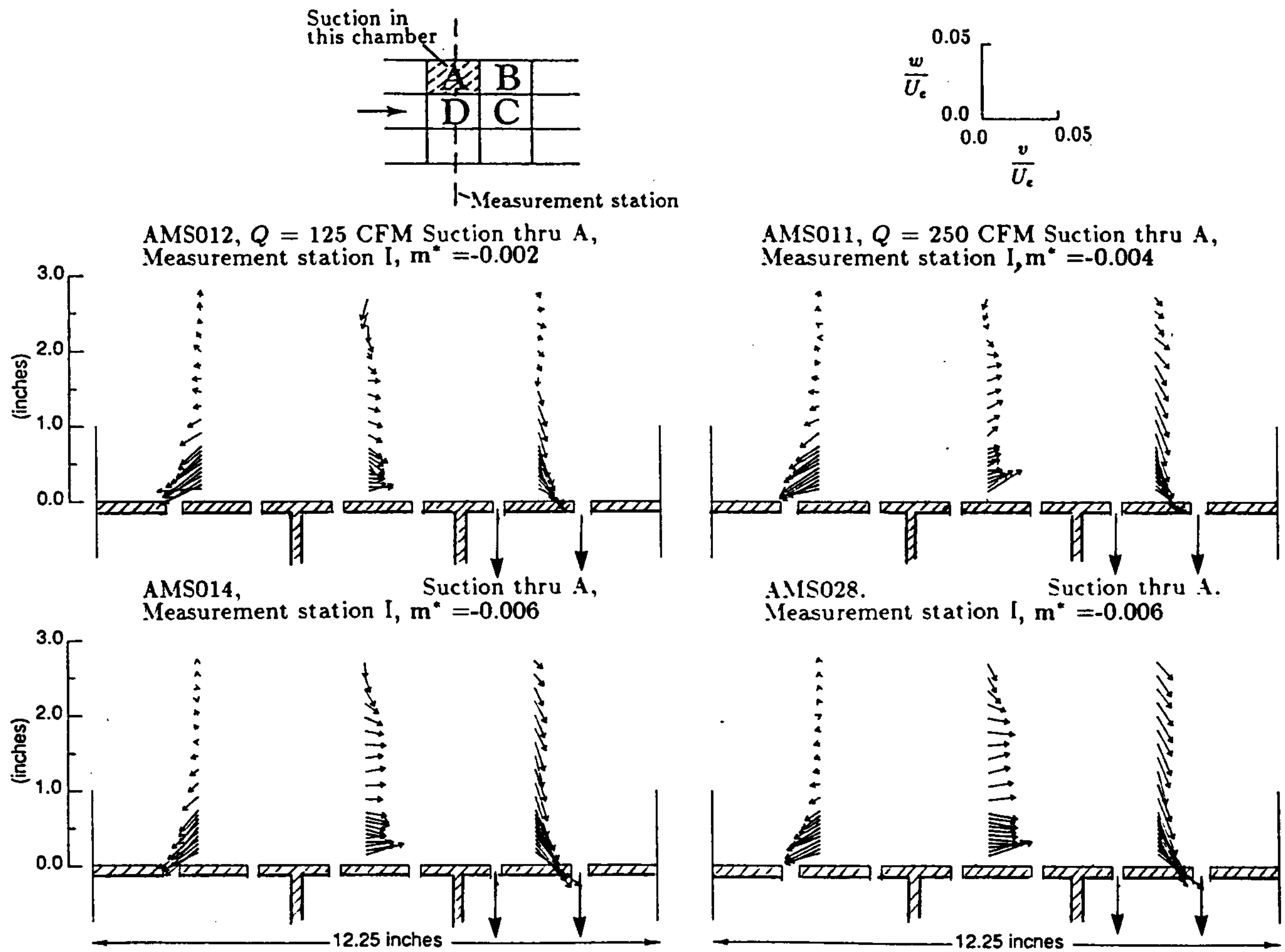

Figure 4.2. Cross plane velocity vectors in transverse plane I with suction applied through chamber A for flow on segmented slotted wall.

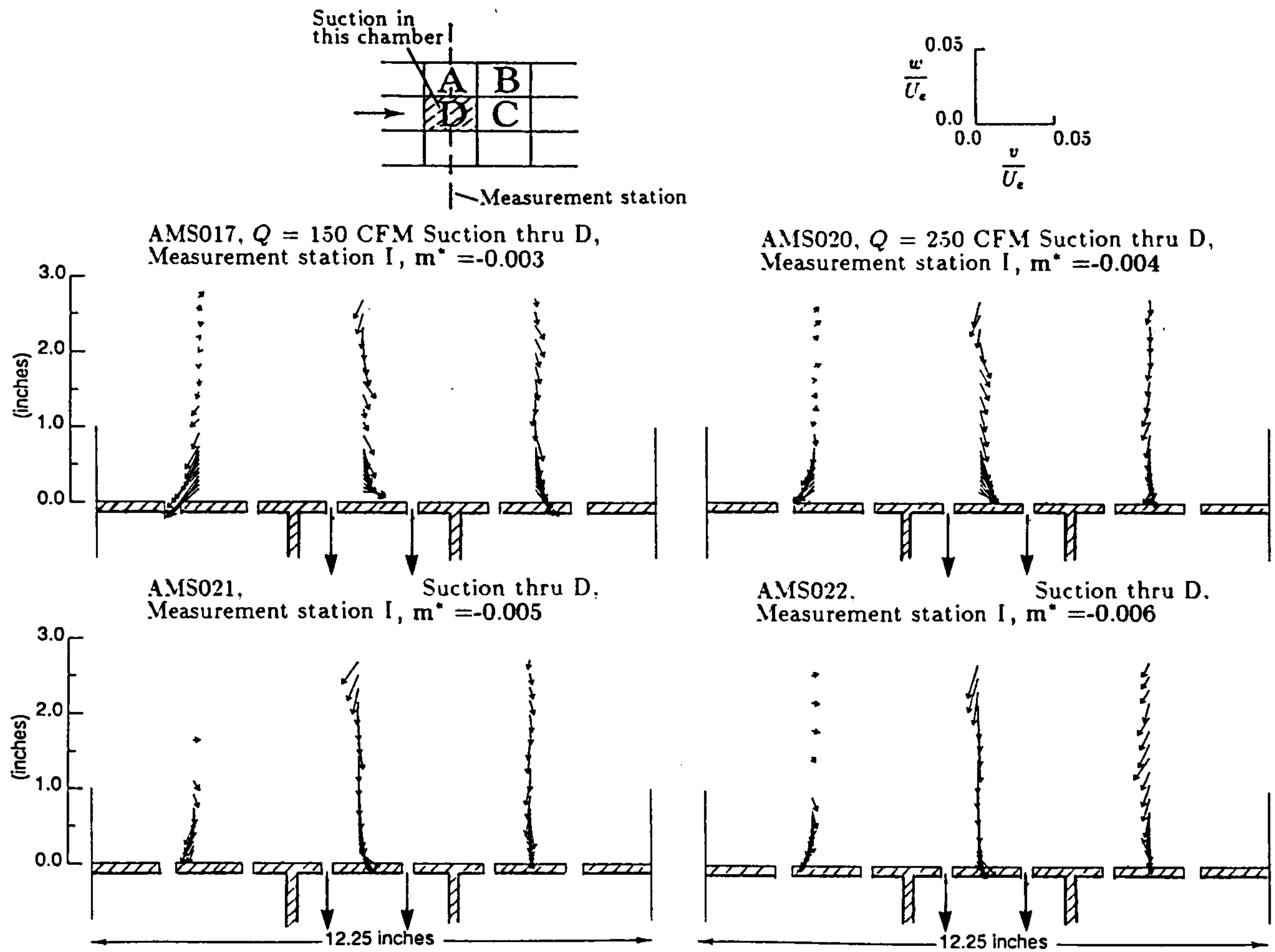

Figure 4.3. Cross plane velocity vectors in transverse plane I with suction applied through chamber D for flow on segmented slotted wall.

region formed near the suction slots and the perturbations due to this gradient extended to the adjacent probe locations and regions outside the boundary layer. For the case of suction applied through the side chamber, negligible velocity component changes at the farthest probe were observed. Moderate changes in $\Delta w/U_e$, about 2.5%, for measurements location between the suction slots itself and about 1% at the adjacent probe locations were observed. On the side compartments, the outer slot was wider and the narrow slot was placed toward one side of the compartment. This resulted in biased suction or blowing through the side compartments. The effect of this has been observed in the results.

The effect of blowing through side compartment B, and the central compartments D and C are illustrated in Figure 4.4, Figure 4.5 and Figure 4.6 respectively. As seen in Figure 4.4, the blowing through the side compartment was biased, that is there was a greater mass flow through the outer slot. The blowing fluid displaced the main stream fluid mass inducing v and w velocity components. The changes in velocity components were significant. The magnitude of $\Delta w/U_e$ is about 5% at a maximum blowing rate of about 40 lbm/min. The blowing through the central compartments had a nearly symmetric influence (somewhat biased to the right). The displacing of the main flow to the tunnel sides is observed. At the location between the blowing slots itself, the blowing fluid pushed upwards inducing upward velocity at moderate and low blowing rates. However at high blowing rates, the blowing fluid entering the test section as a high energy jet entrained fluid mass causing low pressure region to be formed between the blowing slots close to the wall. This resulted in downward velocity component within the sheer layer close to the wall.

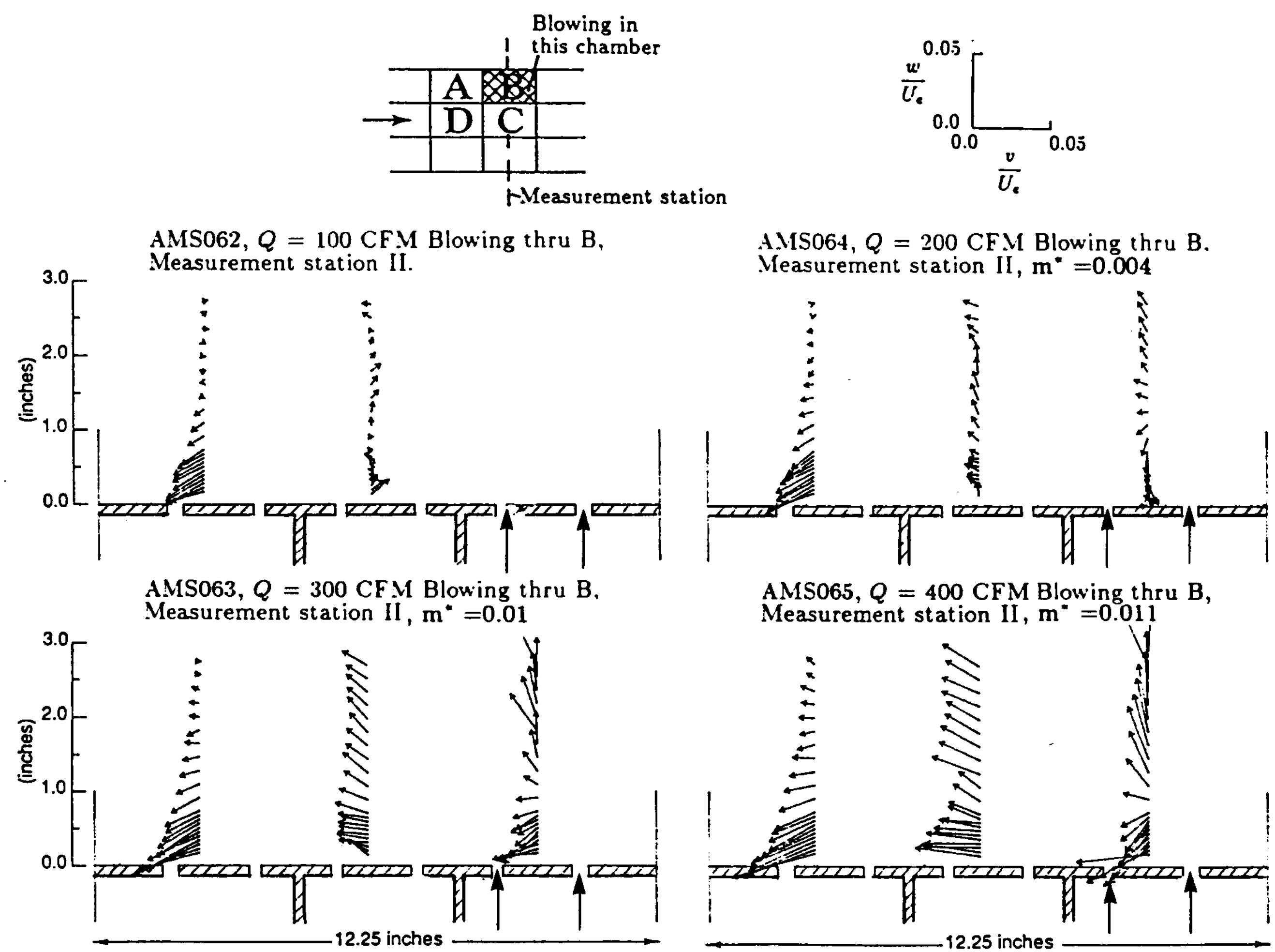

Figure 4.4. Cross plane velocity vectors in transverse plane II with blowing applied through chamber B for flow on segmented slotted wall.

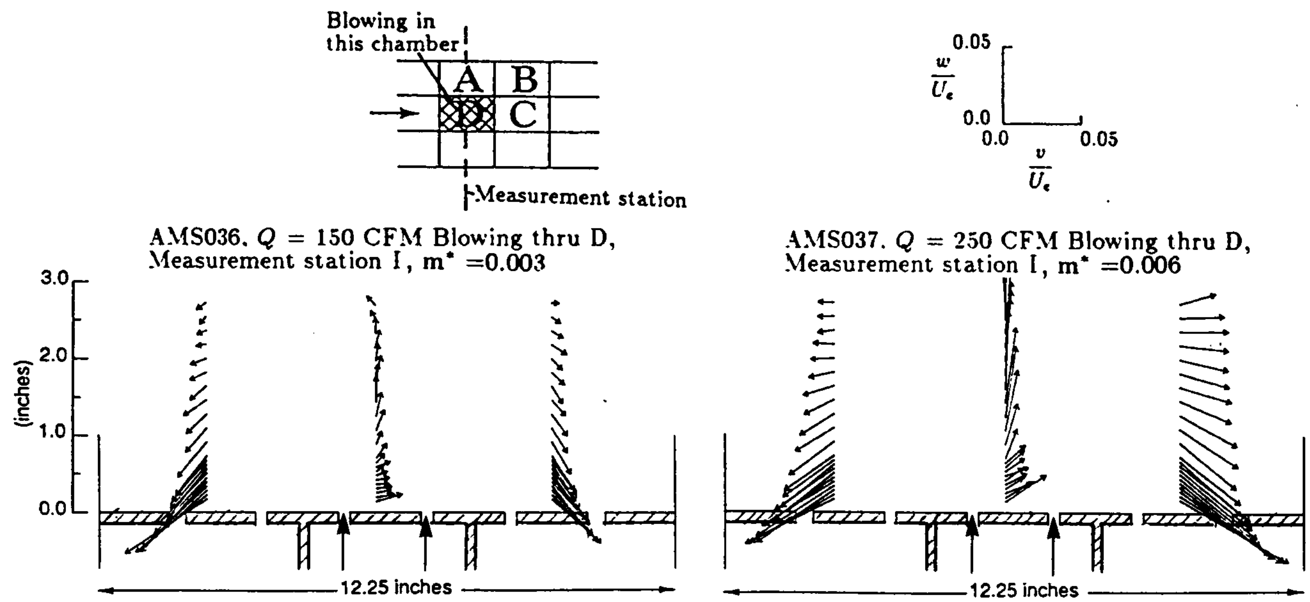

Figure 4.5. Cross plane velocity vectors in transverse plane I with blowing applied through chamber D for flow on segmented slotted wall.

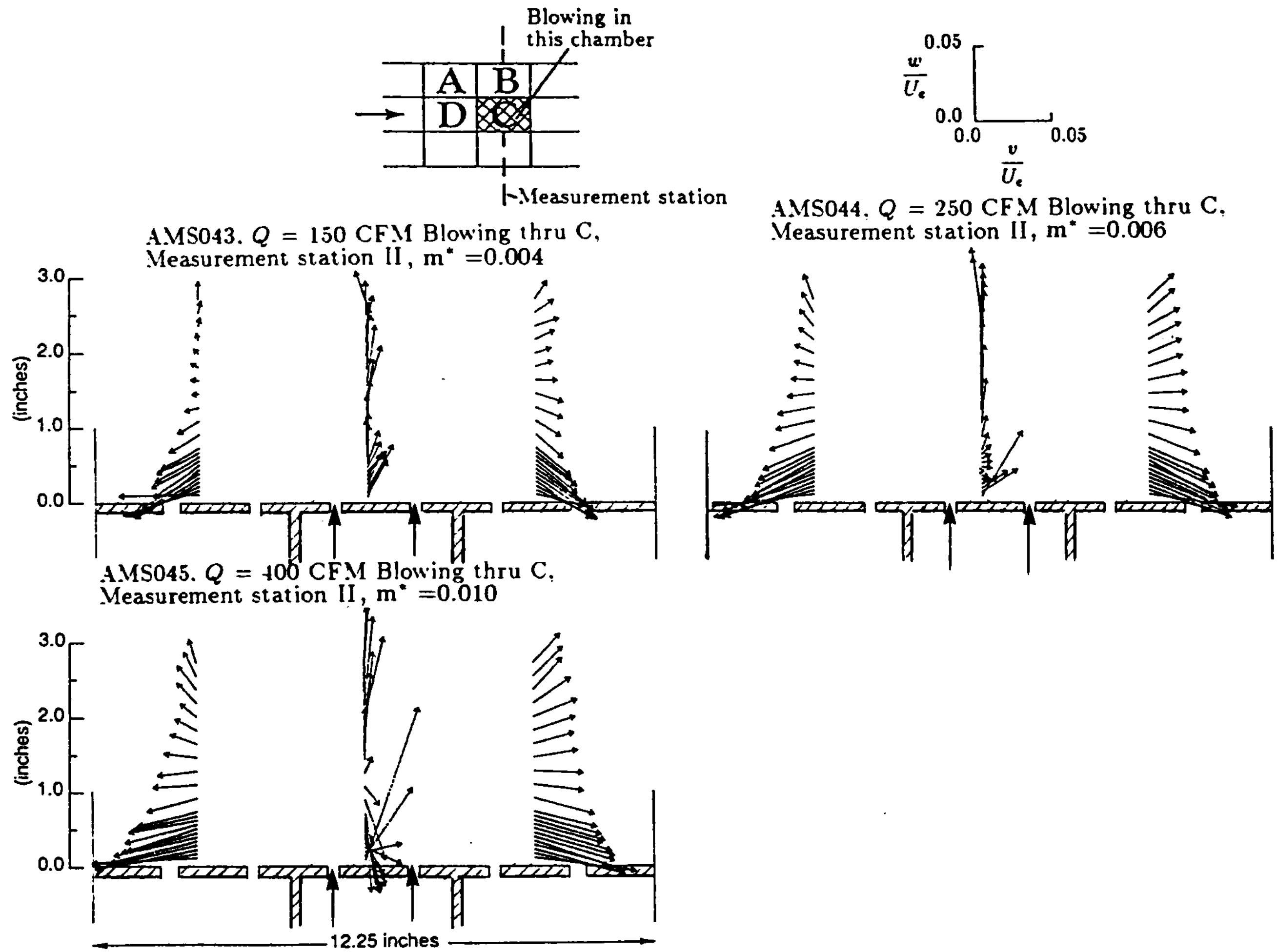

Figure 4.6. Cross plane velocity vectors in transverse plane II with blowing applied through chamber C for flow on segmented slotted wall.

ii) Downstream influence

In this section, the influence of blowing or suction through upstream compartments A or D on the flowfield measurements carried out at downstream transverse measurement plane, i.e., traversing locations T4, T5 and T6 is evaluated.

The cross plane flow velocity vectors for blowing through side chamber A or central chamber D are shown in Figure 4.7 and Figure 4.8 respectively. As is observed, immediately downstream of the blowing compartment the flow close to the wall within the shear layer was directed downwards. This result is consistent with that obtained by Satyanarayana et al. (1981) who observed that there was a reduction of pressure in the compartment immediately downstream of the blowing compartment. This reduction in plenum pressure in the downstream compartment caused a downward flow velocity component. The blowing fluid, from the side compartment, while pushing upwards moved away from the side wall toward the tunnel centerline as it convected downstream. The maximum magnitude of $\Delta w/U_e$ observed was about 2%.

The cross plane flowfield with suction applied through A or D are shown in Figure 4.9 and Figure 4.10 respectively. The cross plane flowfield in these cases looked distinctly different from that for the blowing case. Although there were velocity vector orientation changes, the magnitude changes of the cross plane velocity components remained small (less than 1%).

These results indicate limited downstream influence of the applied suction through an upstream compartment.

(iii) Upstream influence

The influence of suction through the downstream chambers B or C upon the measurements at the upstream station (T1, T2 and T3) are examined in this

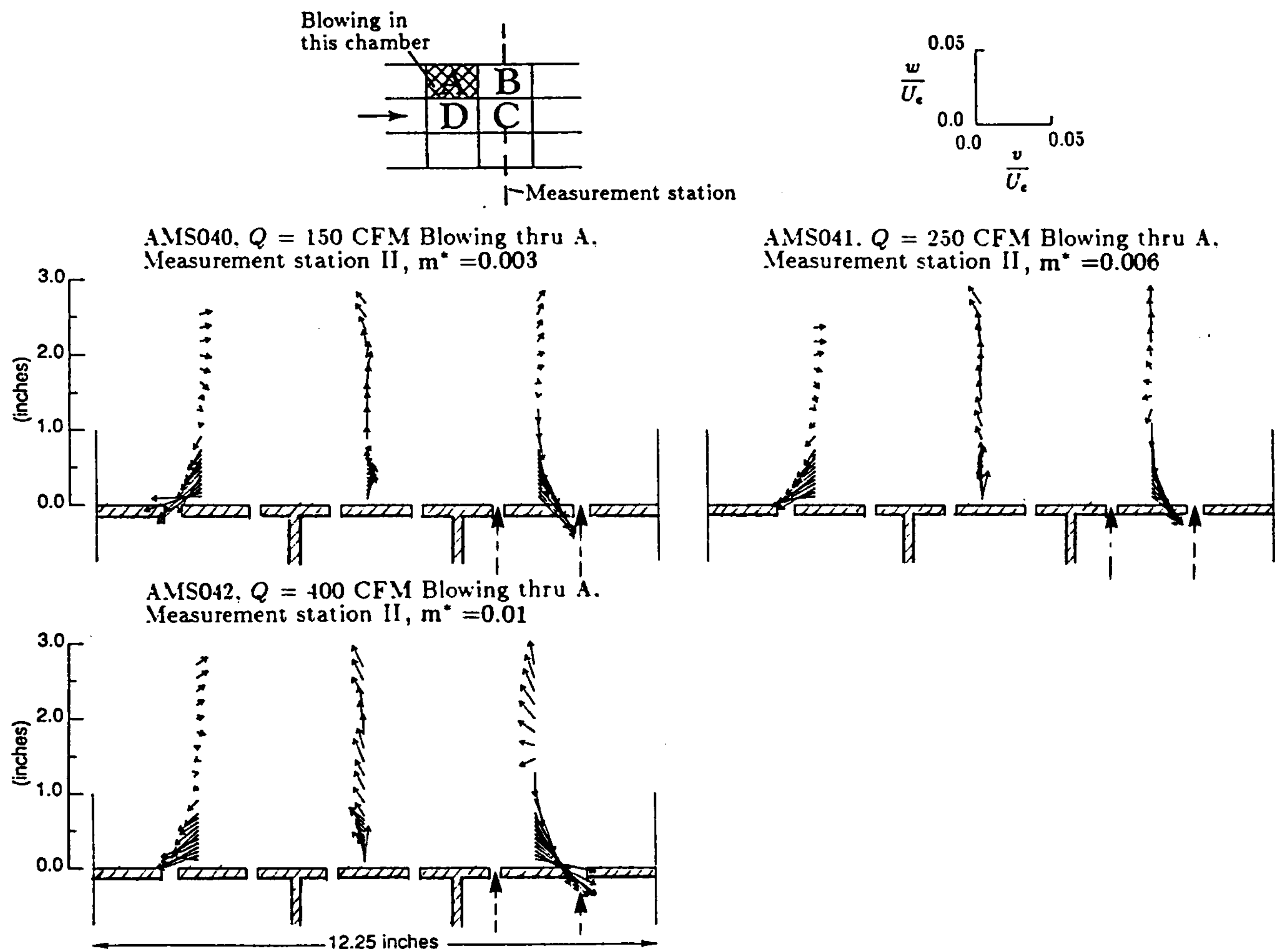

Figure 4.7. Cross plane velocity vectors in transverse plane II with blowing applied through chamber A for flow on segmented slotted wall.

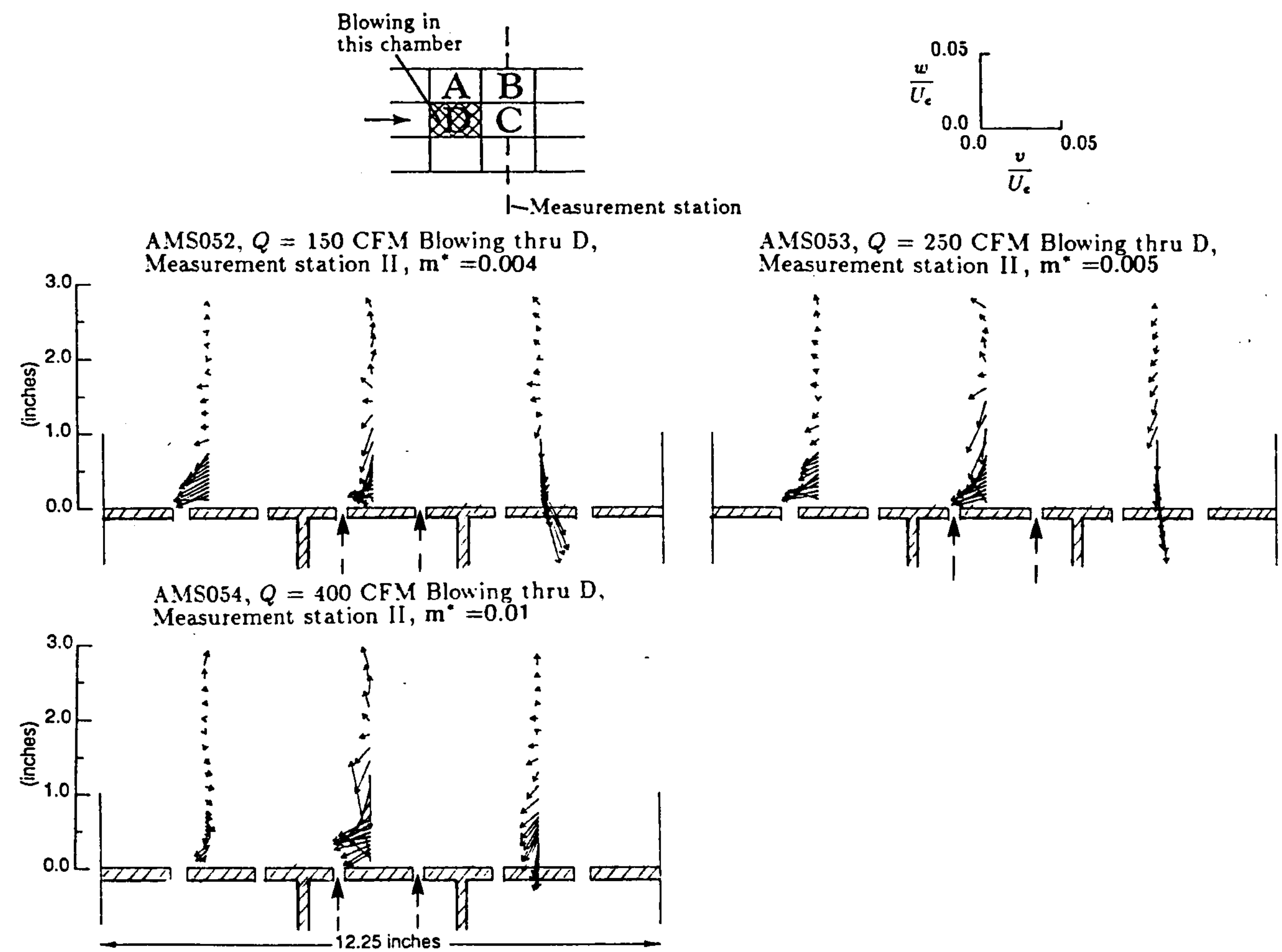

Figure 4.8. Cross plane velocity vectors in transverse plane II with blowing applied through chamber D for flow on segmented slotted wall.

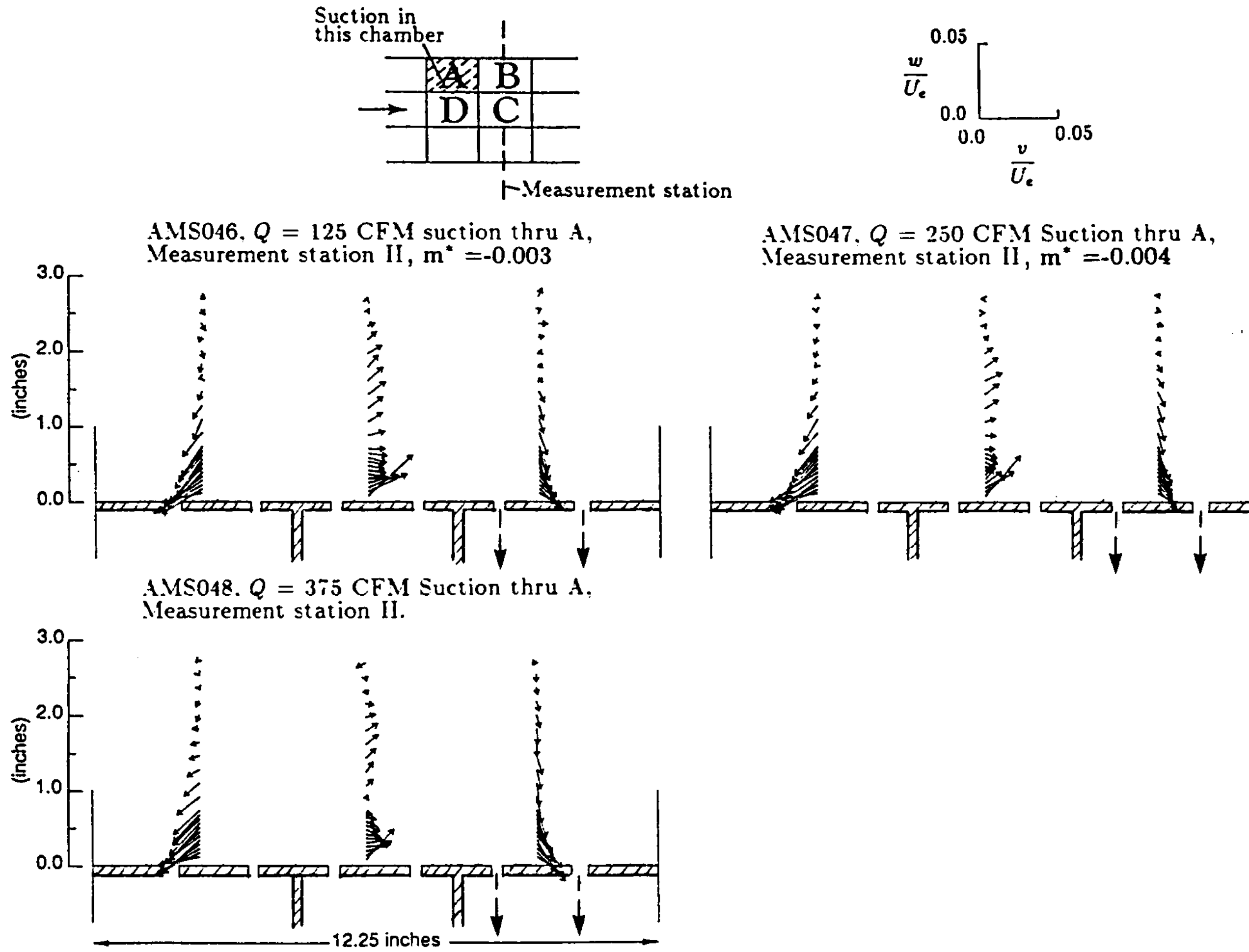

Figure 4.9. Cross plane velocity vectors in transverse plane II with suction applied through chamber A for flow on segmented slotted wall.

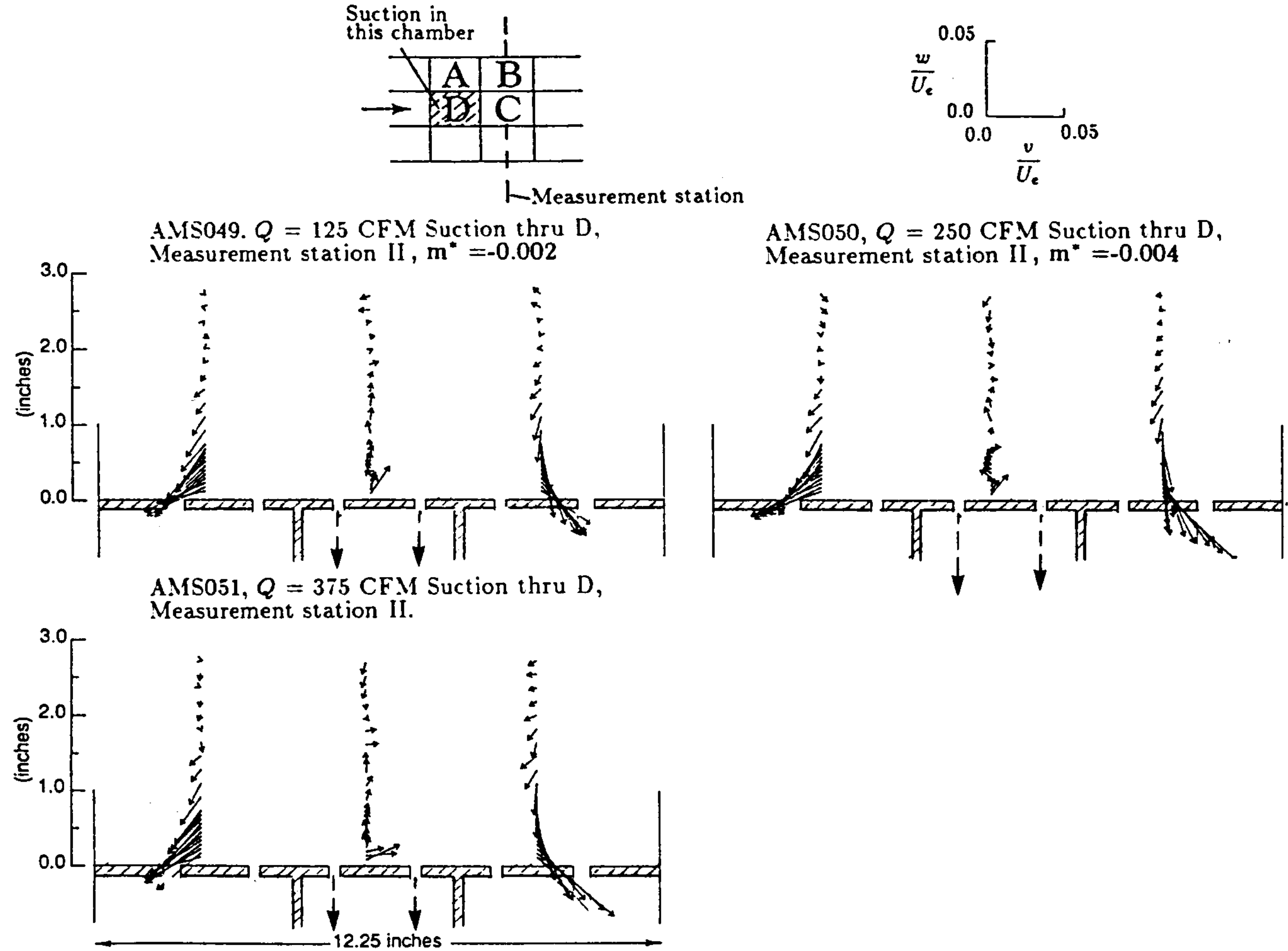

Figure 4.10. Cross plane velocity vectors in transverse plane II with suction applied through chamber D for flow on segmented slotted wall.

section.

The results for suction through the compartment B or the compartment C are shown in Figure 4.11 and Figure 4.12 respectively.

Very small changes in velocity components were observed. The change in $\Delta w/U_e$ was about 1%. The probe support, though slender and streamlined, was in the way between the measurement station and the applied control slot segment and therefore interfered with measurements. These observations reflect limited upstream influence of applied suction.

(iv) Interactive influence of suction and blowing applied through two compartments

The influence on measurements at the downstream transverse station with blowing through downstream chamber C and suction applied through upstream chamber D is shown in Figure 4.13. The flow pattern in this figure does show the combined interactive features of the two controls applied independently. As seen earlier, the blowing through C produces an upward velocity at the center probe (T5) and nearly symmetric outwards flow, i.e., away from tunnel centerline, at the two side probes (T4 and T6). The influence of suction through D caused a low pressure region at the edge of the boundary layer at the downstream location. This modified the flowfield in a region outside the boundary layer. From the present results Figure 4.13, the interacting characteristics of the two flowfields are obvious. The upward velocity components at the center probe (T5) are reduced in magnitude. At the side probes, the outward v-components are reduced. However, at high blowing rates through the downstream compartment C, the influence of this being greater at the measurement location, the flowfield exhibits the characteristics more like the independent flowfield of applied control through C. The flowfield had therefore characteristics of both the flowfields.

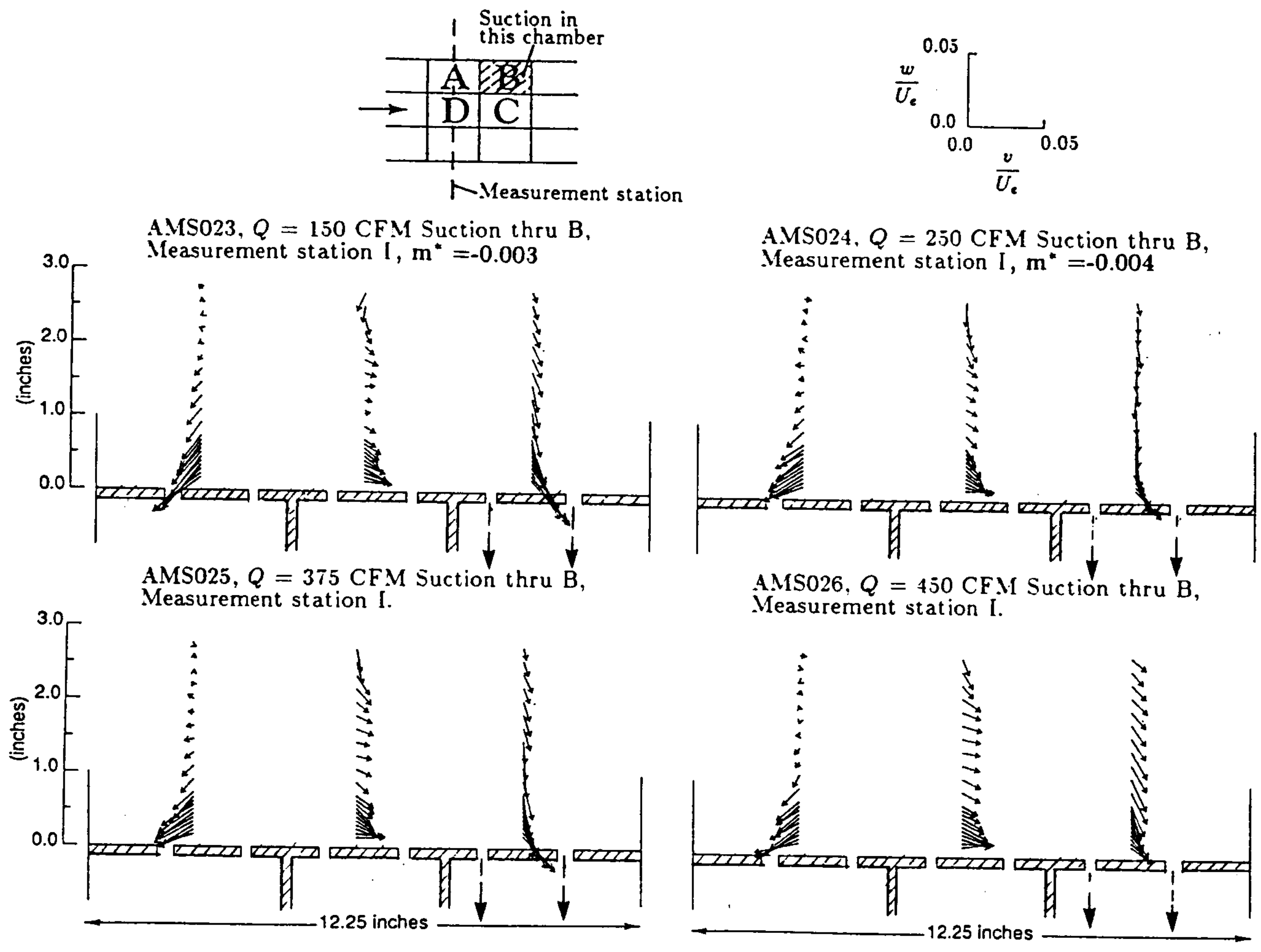

Figure 4.11. Cross plane velocity vectors in transverse plane I with suction applied through chamber B for flow on segmented slotted wall.

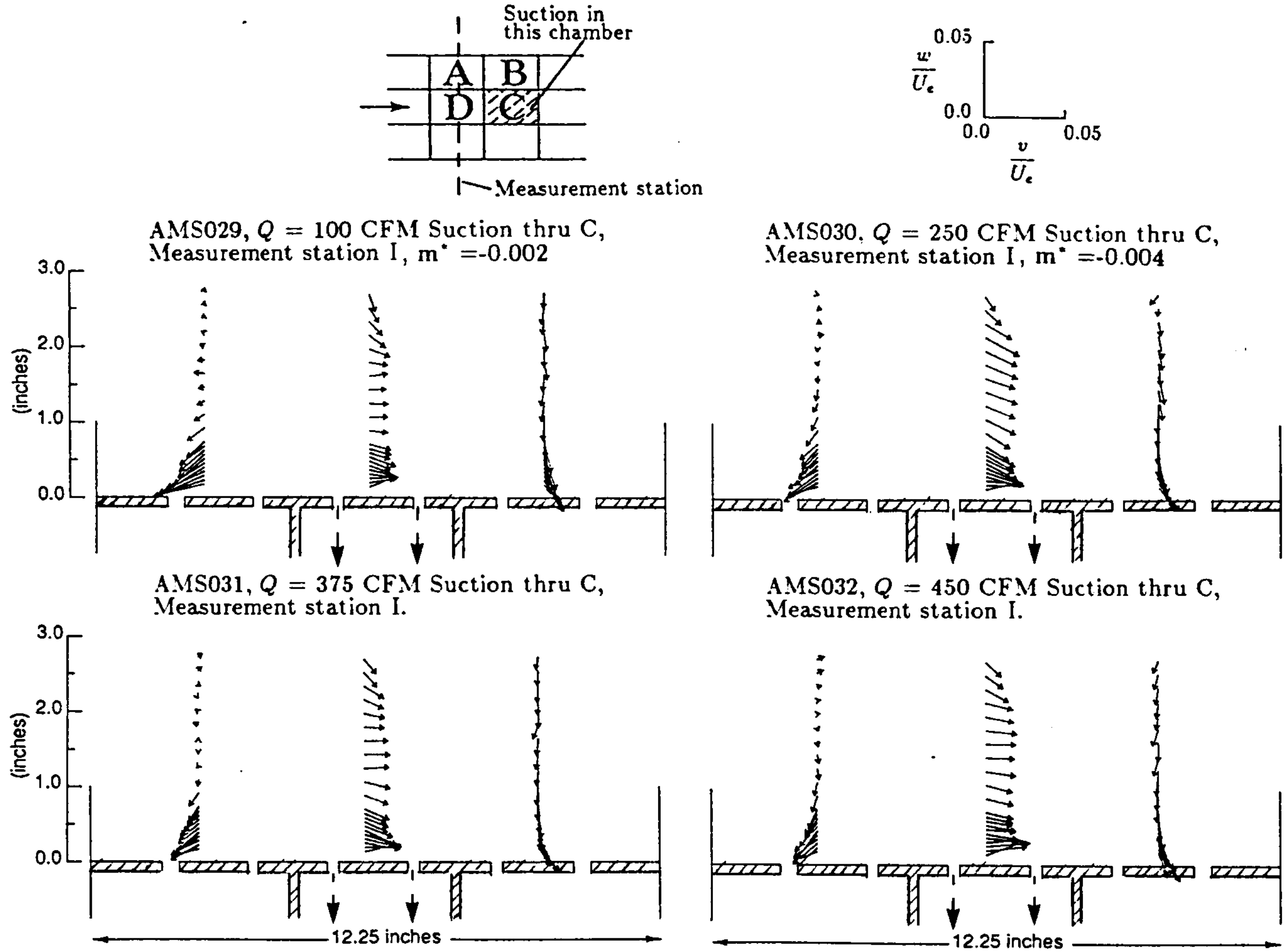

Figure 4.12. Cross plane velocity vectors in transverse plane I with suction applied through chamber C for flow on segmented slotted wall.

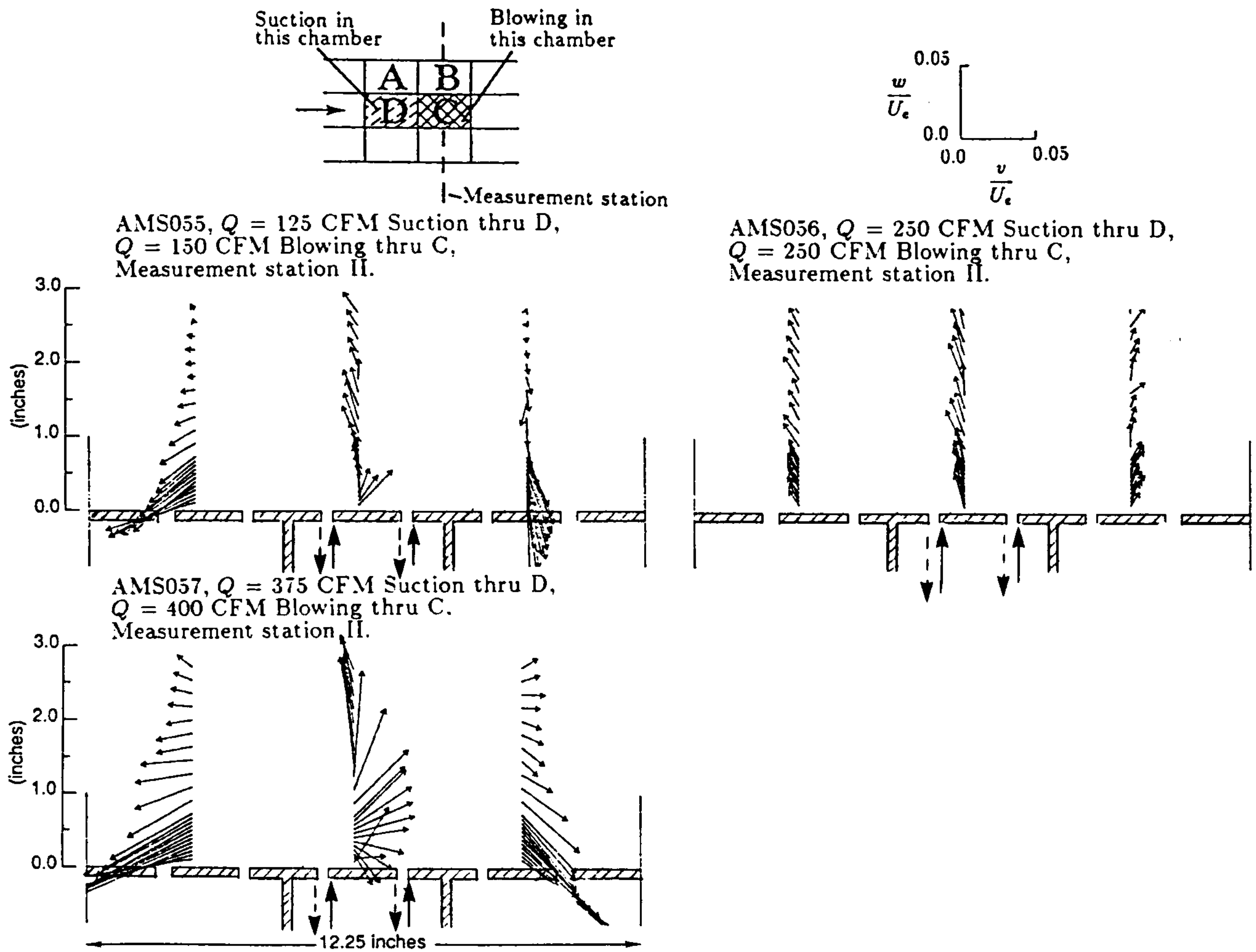

Figure 4.13. Cross plane velocity vectors in transverse plane II with suction applied through D and blowing applied through C for flow on segmented slotted wall.

The cross plane flow pattern for blowing through the downstream side chamber B and suction through the upstream central chamber D and measurements made at the downstream station (T4, T5 and T6) is shown in Figure 4.14. This flow pattern contains the features of the two flow patterns obtained by independent controls applied through D and B. The influence of blowing through the downstream chamber B has, as expected, more influence at this downstream measurement station.

E. INFLUENCE COEFFICIENT, VARIATION OF $\Delta w/U_e$ VELOCITY COMPONENT

The flowfield stream surface curvature, pressure, etc. are related to the wall boundary conditions through the influence coefficients. This implies that the flow close to the wall is directly related to the controlled blowing and suction applied at the segmented slotted wall. These flow variations in the z-direction are quantitatively represented by the w/U_e distribution. In this Chapter, the normalized velocity component $\Delta w/U_e$ vs. $\dot{m}$ are plotted and analyzed for control applied to the one and two segmented chambers.

The values of w/U_e, measured for no mass removed or added, at the corresponding height z have been subtracted so that the plotted w-component is a result of the pressure differential across the test section and the segmented chamber, due to the applied blowing or suction.

This implies that for no mass removal or addition i.e., $\dot{m} = 0$, the $\Delta w/U_e$ component must be zero.

The results of $\Delta w/U_e$ vs. $\dot{m}$ for blowing and suction applied through chambers A, B, C or D and measurements made at longitudinal Stations I or II are shown in Figures 4.15 to 4.22.

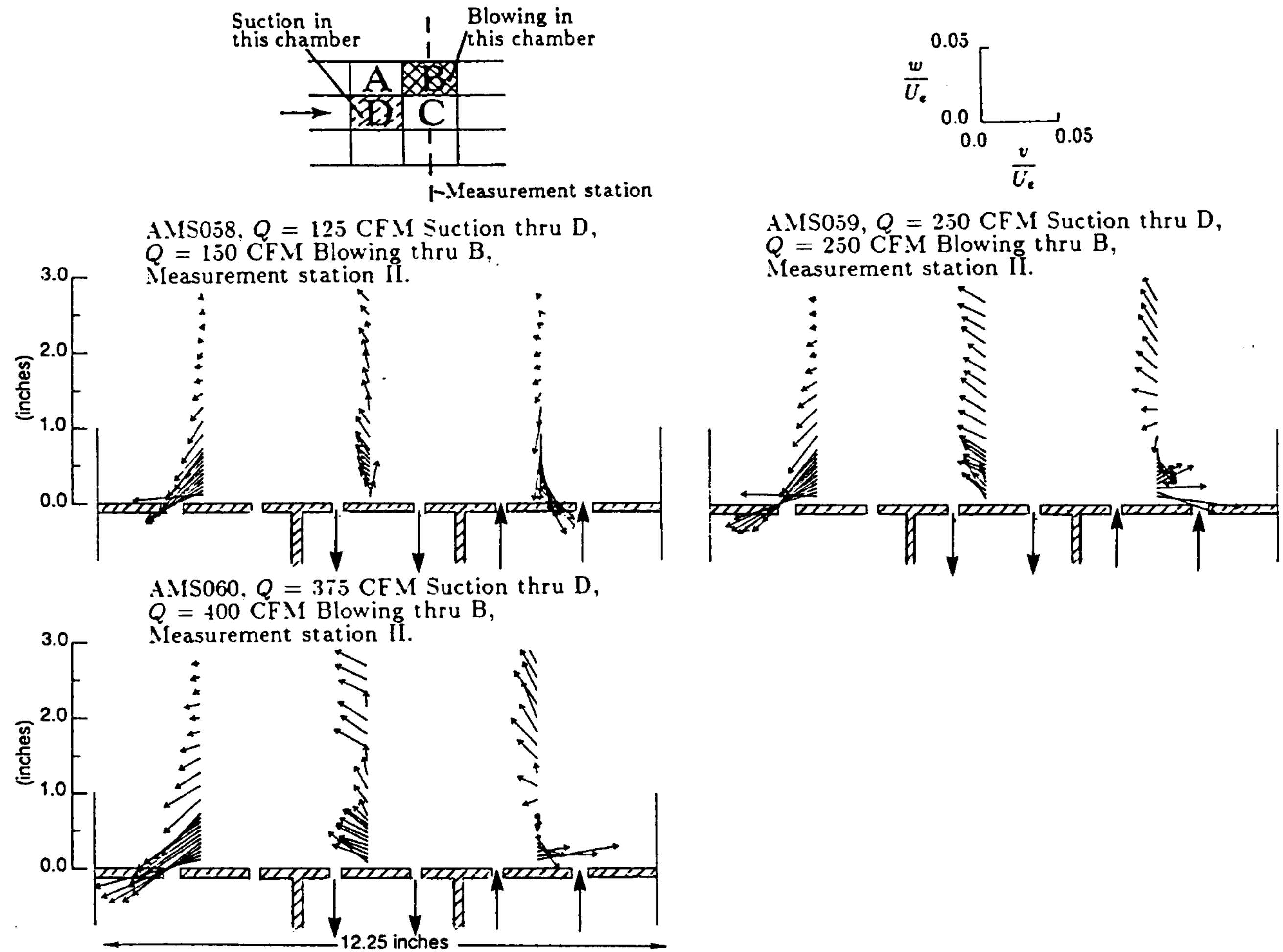

Figure 4.14. Cross plane velocity vectors in transverse plane II with suction applied through D and blowing applied through B for flow on segmented slotted wall.

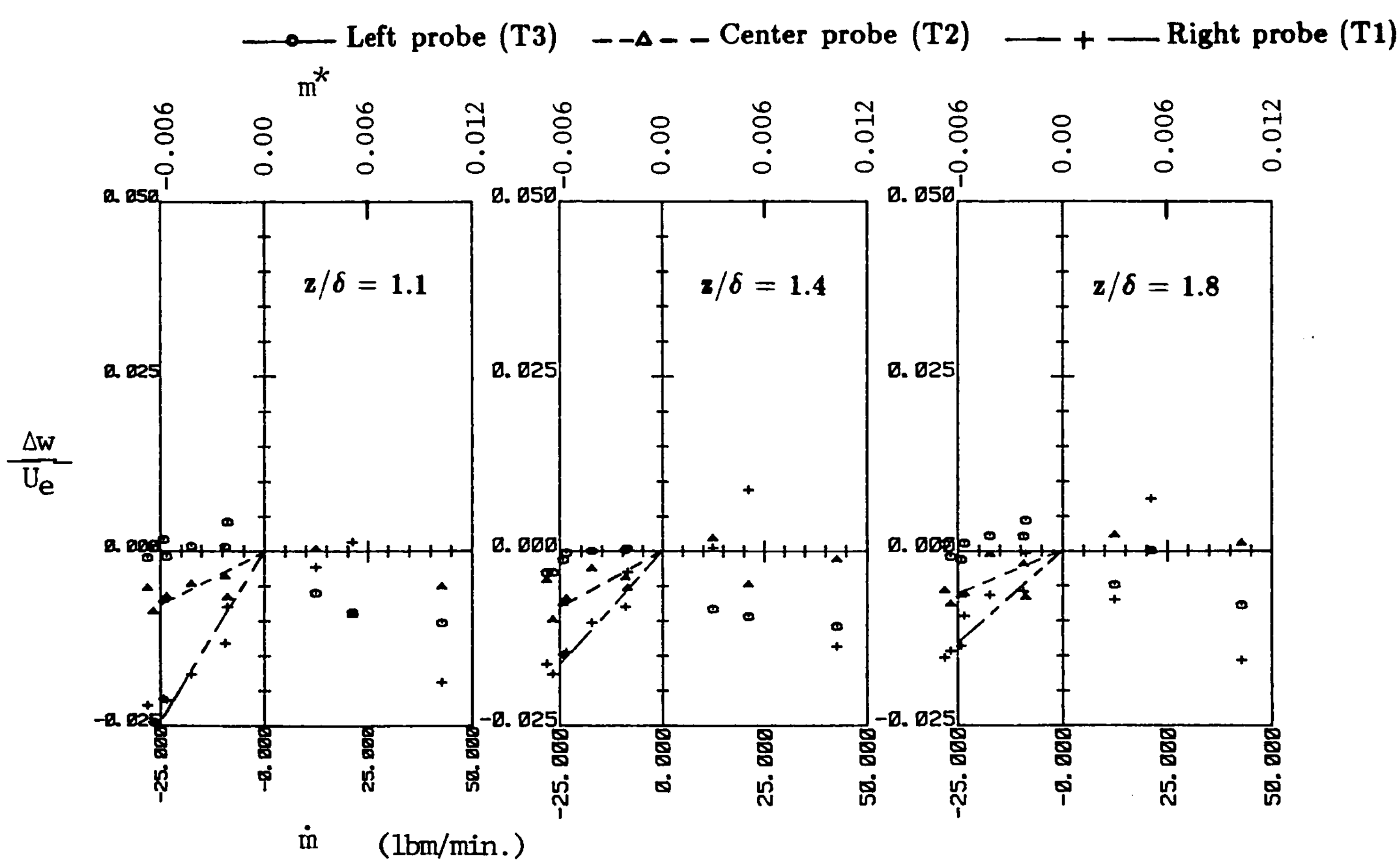

Figure 4.15. $\Delta w/U_e$. Variation at probe location in transverse plane I for blowing and suction applied through segmented chamber slots A.

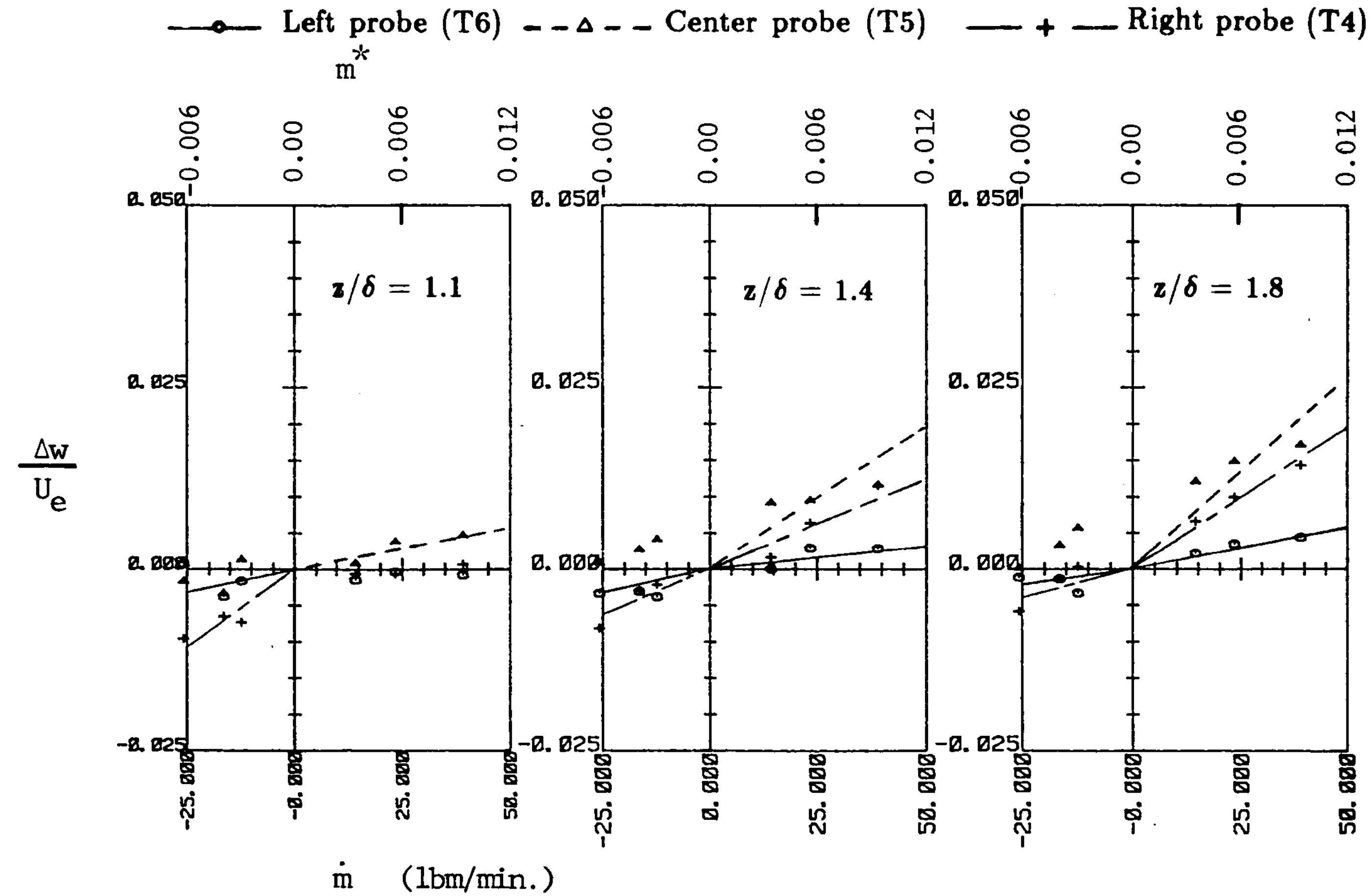

Figure 4.16. $\Delta w/U_e$. Variation at probe location in transverse plane II for blowing and suction applied through segmented chamber slots A.

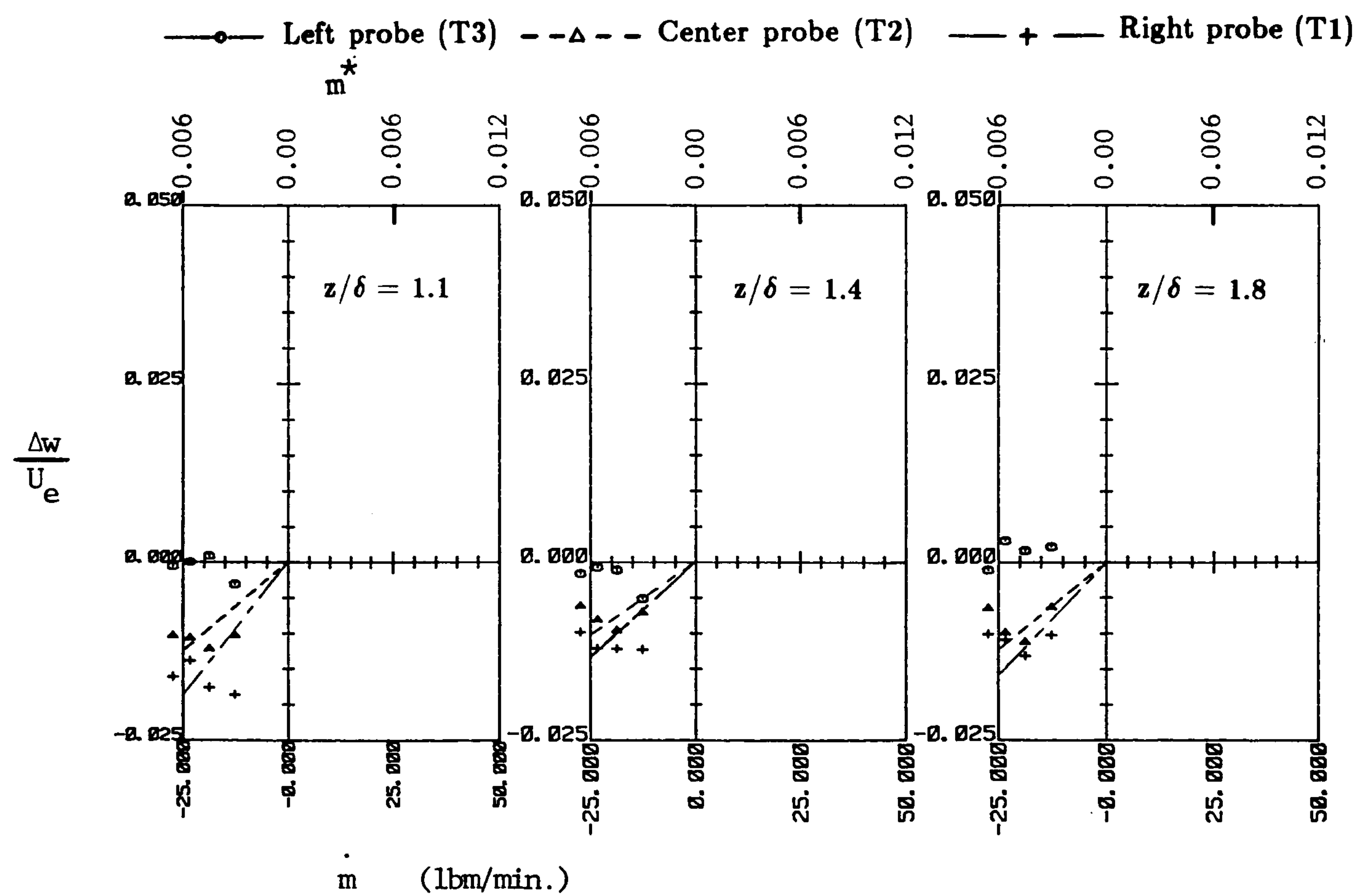

Figure 4.17. $\Delta w/U_e$. Variation at probe location in transverse plane I for blowing and suction applied through segmented chamber slots B.

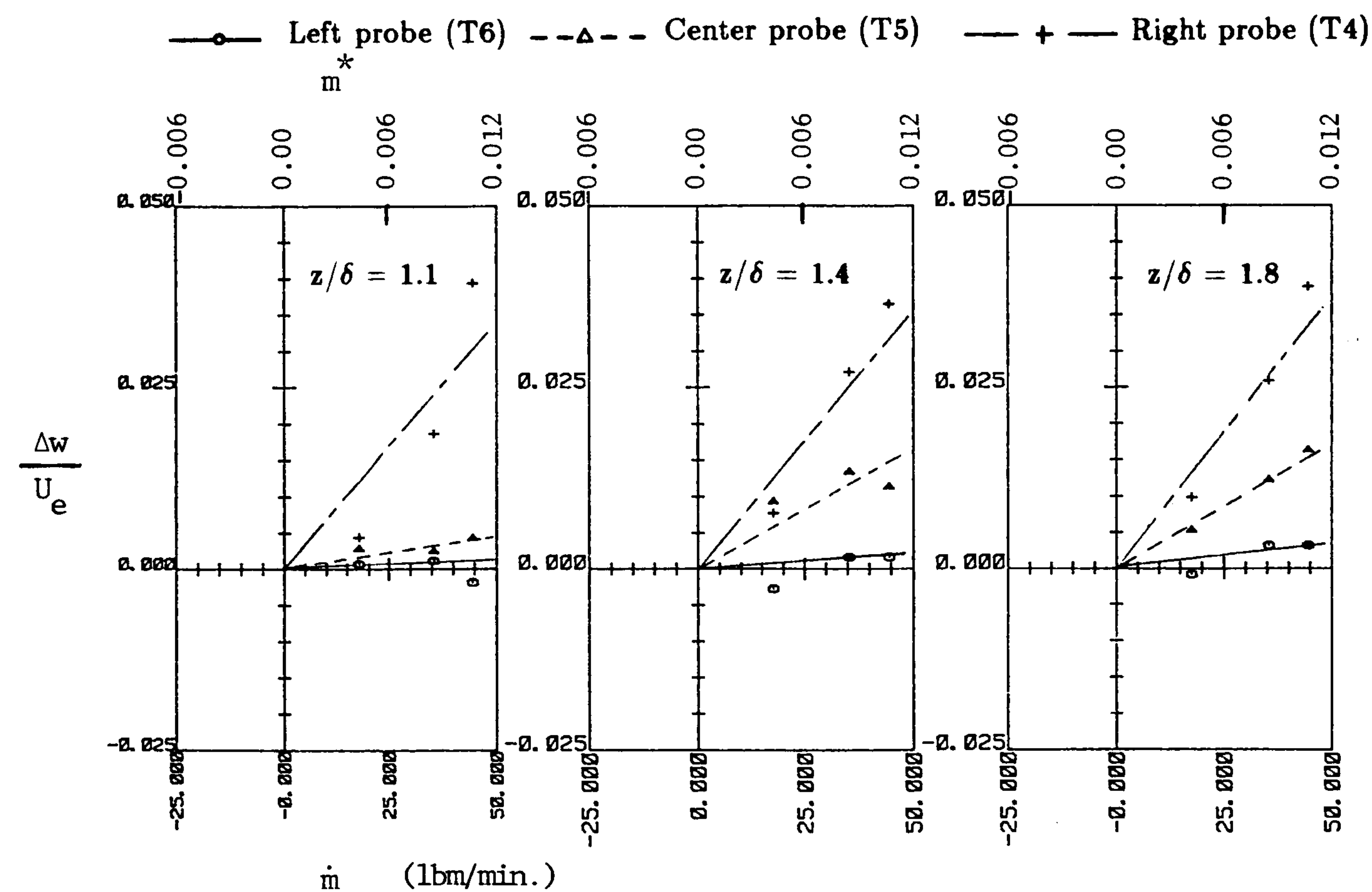

Figure 4.18. $\Delta w/U_e$. Variation at probe location in transverse plane II for blowing and suction applied through segmented chamber slots B.

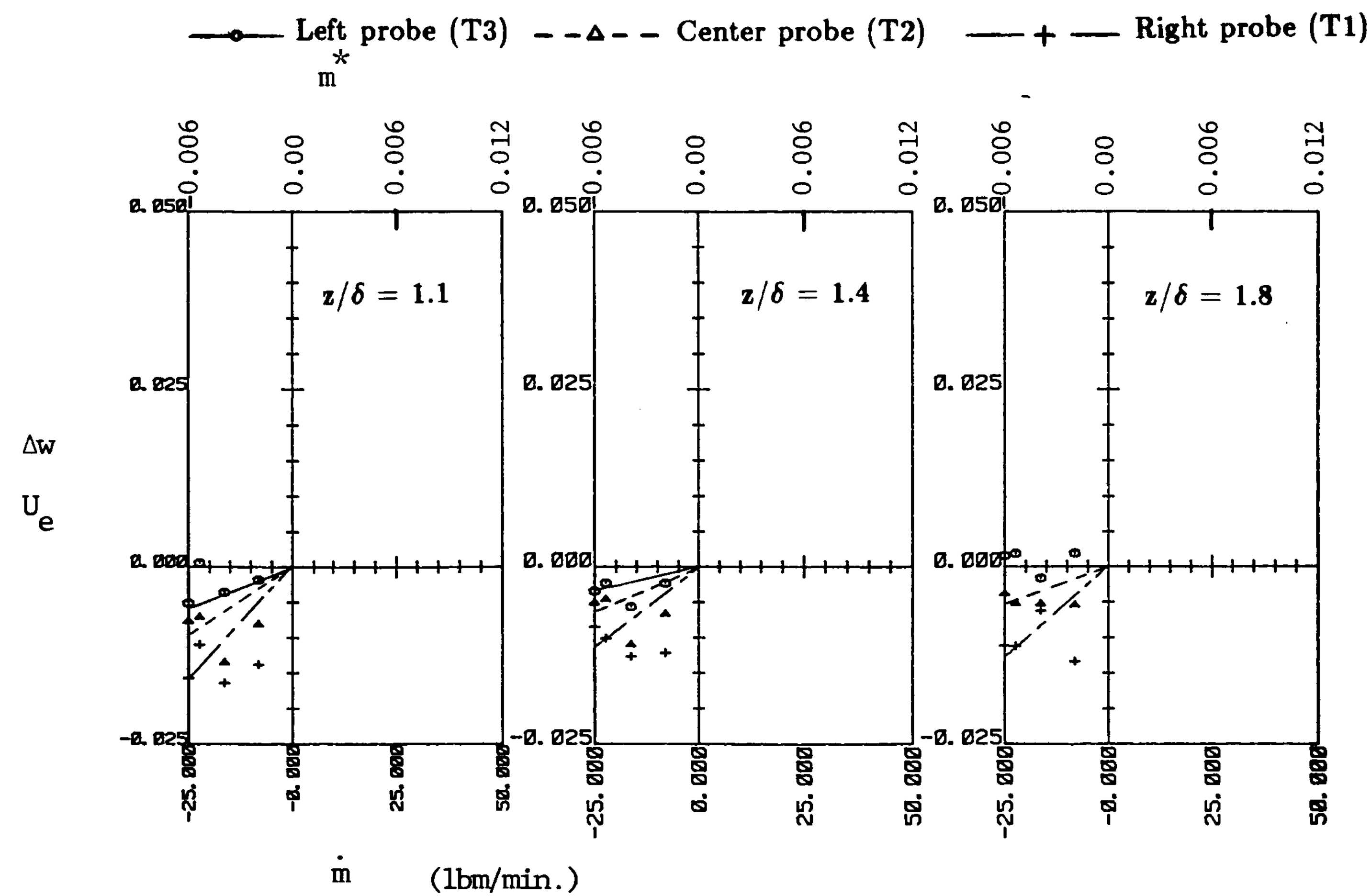

Figure 4.19. $\Delta w/U_e$. Variation at probe location in transverse plane I for blowing and suction applied through segmented chamber slots C.

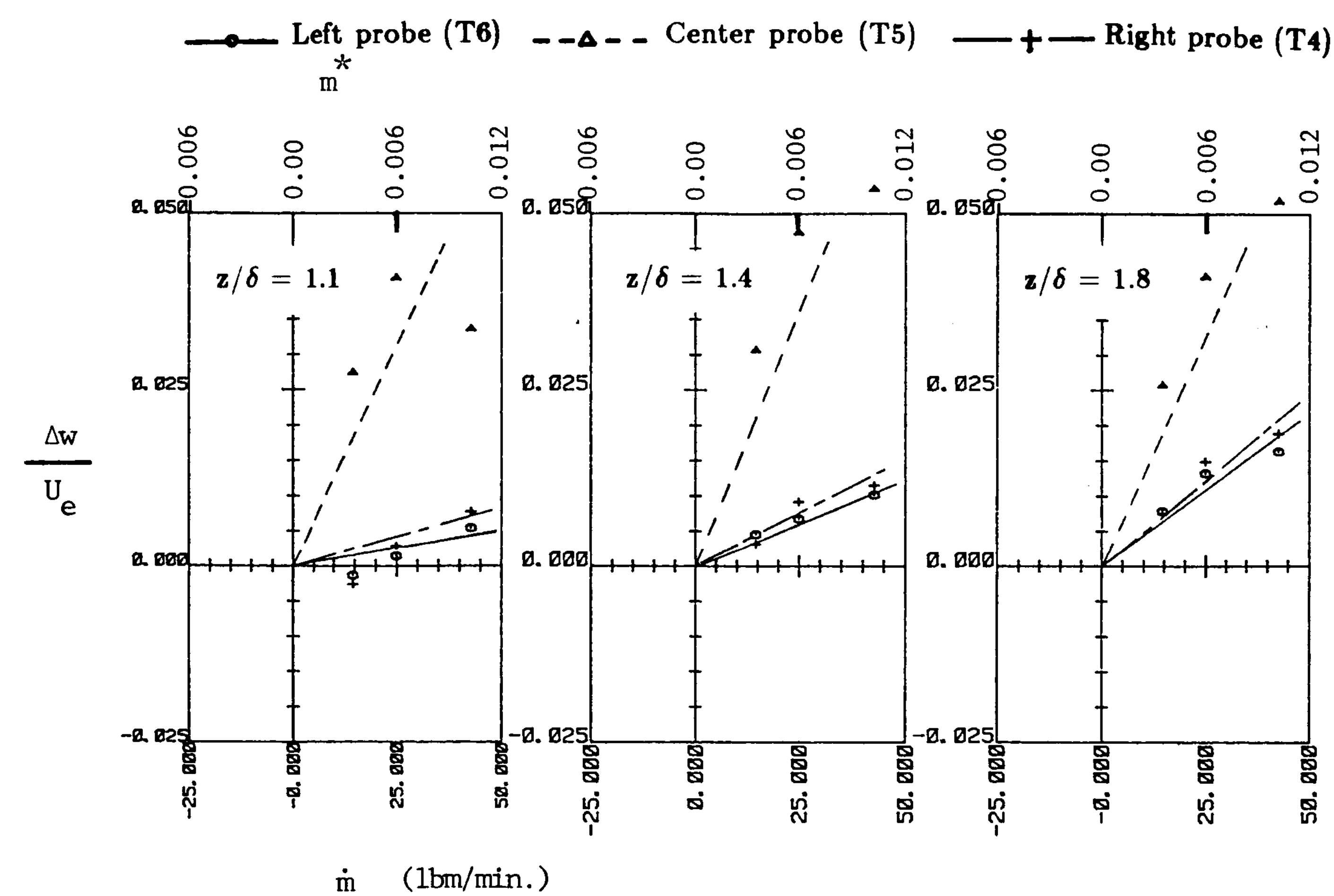

Figure 4.20. $\Delta w/U_e$. Variation at probe location in transverse plane II for blowing and suction applied through segmented chamber slots C.

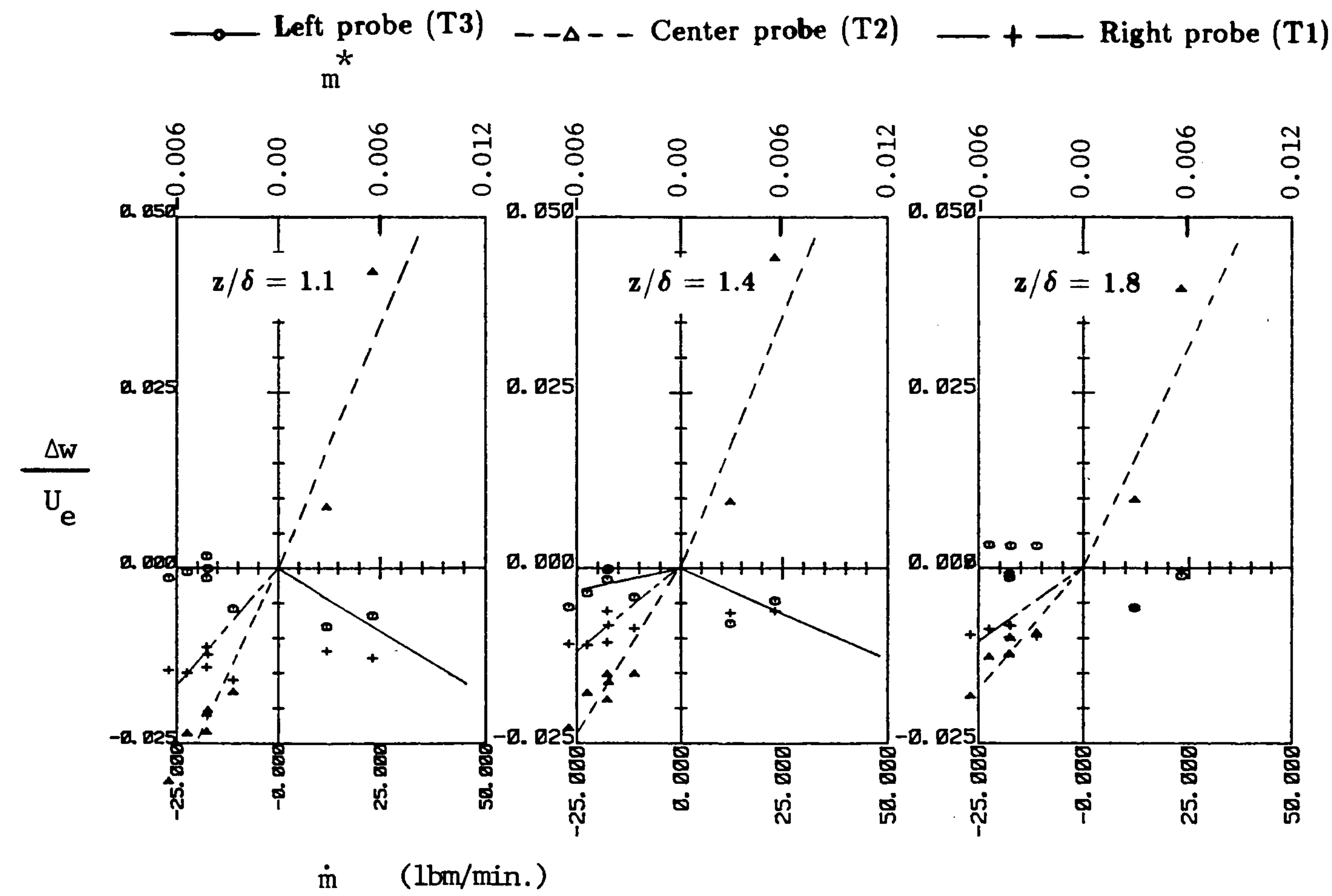

Figure 4.21. $\Delta w/U_e$. Variation at probe location in transverse plane I for blowing and suction applied through segmented chamber slots D.

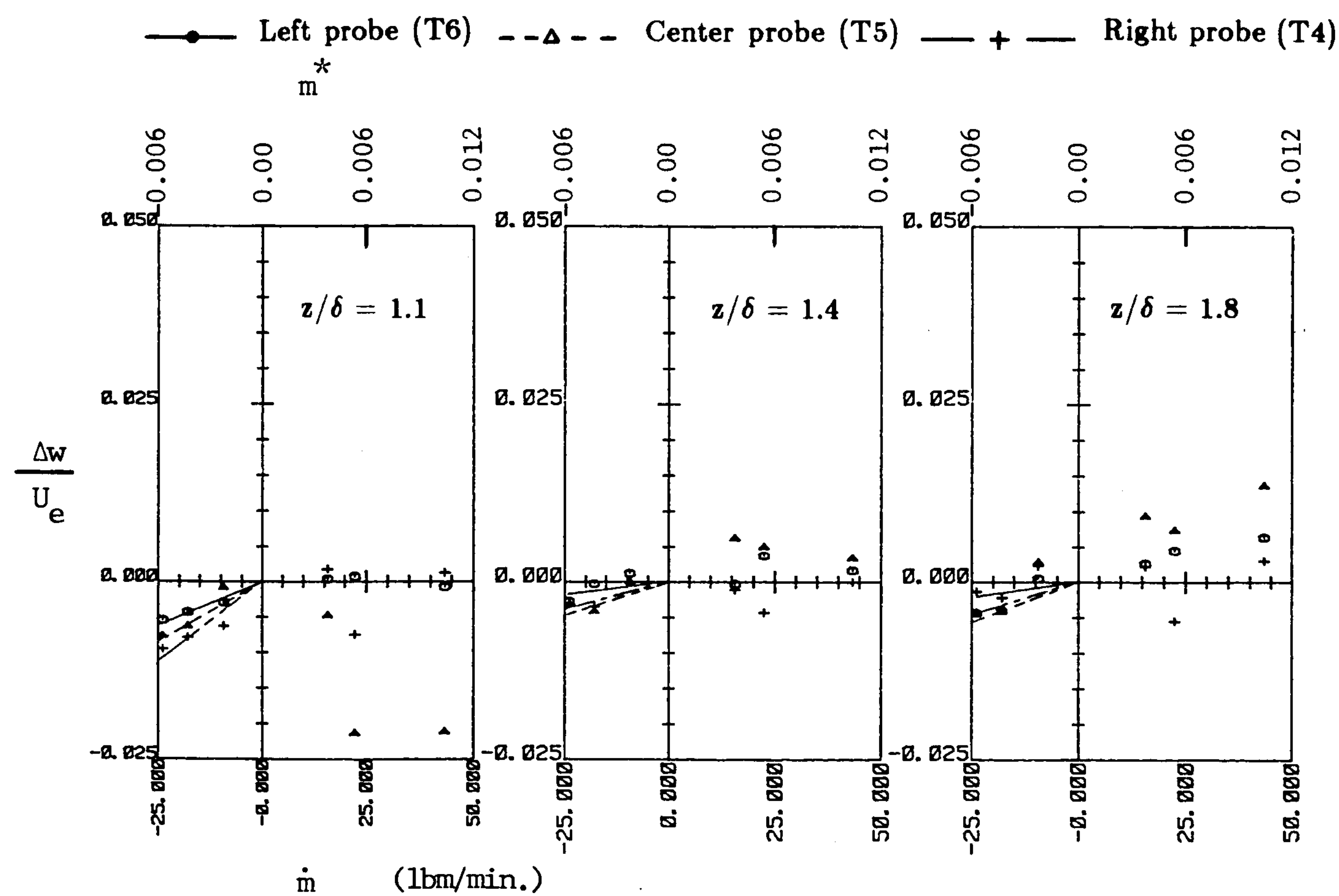

Figure 4.22. $\Delta w/U_e$. Variation at probe location in transverse plane II for blowing and suction applied through segmented chamber slots D.

Since the w/U_e velocity component is given by the relation

$$\frac{w}{U_e} = \sin\alpha \quad \cos B$$

where α and B are the pitch and yaw angles. The errors in α and B arising due to polynomial representations of calibration data, and that due to other measurement uncertainties is estimated to be about ± 0.5 degrees. The corresponding error in computed w/U_e is about $\pm 1\%$. Also during the test run the applied suction or blowing varied. The plotted values of $\dot{m}$ are averaged values over the test run. This introduces uncertainty into the values of $\dot{m}$.

$\Delta w/U_e$ vs. $\dot{m}$ is assumed to be linearly related. Straight lines have been passed through the data, independently for blowing and suction. The data in some cases shows considerable scatter from the straight line variation. These scatter are within the experimental error. However, nonlinear behavior should be expected for large $\dot{m}$. The slope of these curves, i.e.,

$$C = \frac{\Delta(\Delta w/U_e)}{\Delta(\dot{m})}$$

is a measure of the influence coefficient for control applied through one compartment at a time.

The velocity induced at a measurement location for applied suction or blowing through a compartment is then given by

$$\frac{\Delta w}{U_e} = C \cdot \dot{m}$$

The total velocity induced at a measurement location due to applied control at a number of compartments is assumed linearly related and therefore given by

$$\frac{\Delta w_T}{U_e} = \sum_{j=1}^{M} C_j \left(\frac{\Delta w}{U_e}\right)_j$$

where $\Delta w_T/U_e$ is the total velocity induced at the measurement station due to M number of active compartments. $(\Delta w/U_e)_j$ is the velocity induced at the measurement station by the jth compartment acting alone.

The C_j's are the influence coefficients for multi-compartment interactive applied blowing or suction control.

For N measurement locations we have in matrix notation.

$$[\Delta w_T] = [C][\Delta w]$$

If $M = N$, as also reported by Satyanarayana et al. (1981)

$$[\Delta w] = [C]^{-1}[\Delta w_T].$$

The above relation determines $[\Delta w]$ required to produce $[\Delta w_T]$ provided the influence coefficient matrix is known.

In the present case, blowing and suction was applied simultaneously through 2 compartments. In each case the applied blowing or suction rate was changed 3 times and the total induced velocity at the six measurement stations recorded. We therefore have

$$\underset{3\times 1}{[\Delta w_T]} = \underset{3\times 2}{[\Delta w]}\ \underset{2\times 1}{[C]}$$

or

$$[C] = \left[\Delta w^T \Delta w\right]^{-1}\left[\Delta w^T \Delta w_T\right].$$

where $[\Delta w^T]$ is the transpose of matrix $[\Delta w]$. In this manner the influence coefficients C are determined in a least square sense. The values of the C here have been obtained at each probe location for three values of z/δ. These values are given in Table I.

The total velocity induced at a measurement location is then computed from the following.

$$\Delta w_T = C_1 \Delta w_1 + C_2 \Delta w_2$$

Table I.

Influence Coefficients at measurement station II

	Probe	Chamber		Coefficients	
z/δ	Location	1	2	C1	C2
1.1	Left	D	C	6.811	10.412
1.1	Center	D	C	-9.017	-7.452
1.1	Right	D	C	10.415	17.053
1.4	Left	D	C	25.388	5.231
1.4	Center	D	C	-7.501	0.0698
1.4	Right	D	C	23.936	7.920
1.8	Left	D	C	3.923	1.796
1.8	Center	D	C	-4.121	0.3032
1.8	Right	D	C	24.367	3.341
1.1	Left	D	B	-0.1117	-6.455
1.1	Center	D	B	-0.7726	-0.1335
1.1	Right	D	B	4.344	2.347
1.4	Left	D	B	9.183	10.268
1.4	Center	D	B	-6.388	-1.426
1.4	Right	D	B	13.175	2.636
1.8	Left	D	B	0.2902	0.0880
1.8	Center	D	B	-6.106	-1.278
1.8	Right	D	B	6.995	1.187

The measured and computed total velocity at the downstream measurement station (II) for interactive suction applied through D and blowing applied through C are shown plotted in Figure 4.23 and the results for applied suction through D and blowing through B are shown is Figure 4.24. Also shown on these plots is (Δw_T) measured $=$ (Δw_T) computed data as a solid line. The closeness of the plotted data to this solid line is an indication of a better least square fit through the measured data and therefore a measure of the accuracy of the applicability of the influence coefficients.

The least square fit is expected to give better results for the data at measurement locations far from the wall where homogeneous conditions are expected and smooth monotonic variation of the w velocity component occurs.

It is observed from Figure 4.23 and Figure 4.24 that the calculated w_T data compares fairly well with the corresponding measured data. An accuracy of better than 30% in predicting the total induced velocity (w_T) for $z/8 = 1.8$ data is observed.

The magnitude of the influence coefficients thus determined (Table II) is not close to 1.0 (Satyanarayana et al. 1981) and differs considerably, depending upon the measurement location and the applied control compartments. It is thus inferred that the influence coefficients are only applicable for the measurement location and the active compartments from which they are determined.

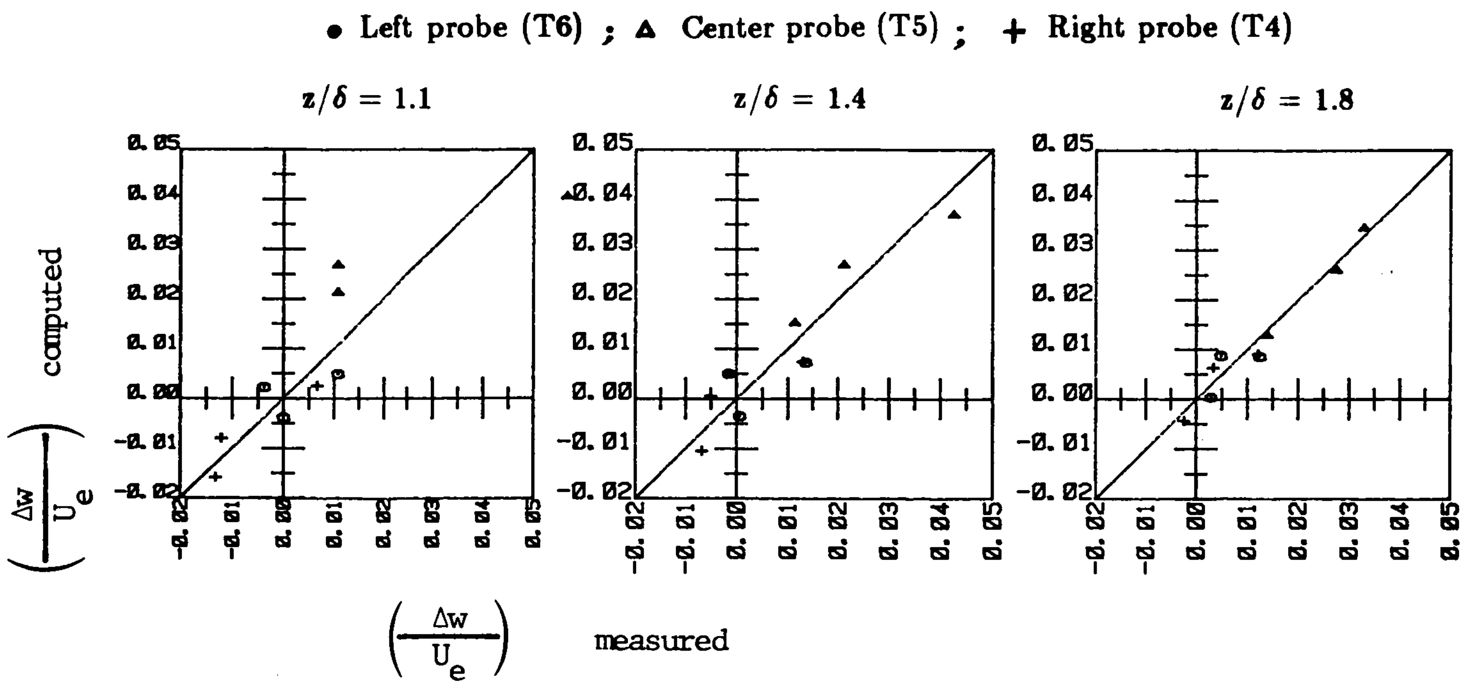

Figure 4.23. Comparison of measured and computed $\Delta w_T/U_e$ values for two compartment interactive applied blowing through C and suction through D.

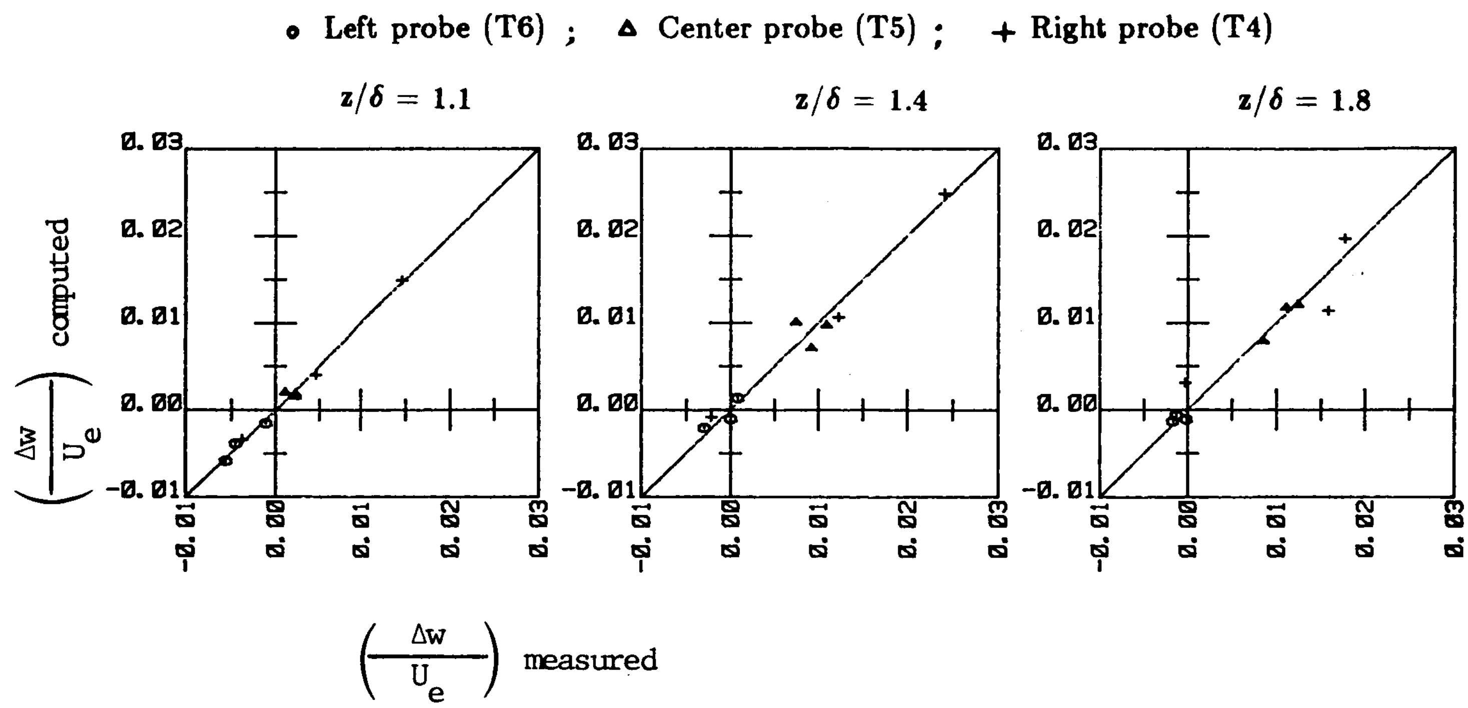

Figure 4.24. Comparison of measured and computed $\Delta w_T/U_e$ values for two compartment interactive applied blowing through B and suction through D.

CHAPTER V

SUMMARY OF RESULTS AND CONCLUSIONS

The problem of flow near a transonic slotted wind tunnel wall has been studied in two parts. In Part I, the flow on a single slotted wall at $M_\infty = 0.6, 0.76$ and 0.9, Re/ft $= 5 \times 10^6$ to 9.6×10^6 has been investigated with applied suction ranging from 0 to 250 SCFM ($m^* = 0.006$). The boundary layer traverses have been made at four transverse stations in one longitudinal location on the slot. In Part II, the flow on a multi-slotted segmented wall at $M_\infty = 0.78$, Re/ft $= 7.1 \times 10^6$ has been studied with suction or blowing applied through one or two compartments. The applied suction ranged from 0 to 25 lbm/min ($m^* = 0.006$). and the applied blowing ranged from 0 to 40 lbm/min ($m^* = 0.01$). Measurements have been made at two longitudinal stations. At each longitudinal station, measurements were conducted simultaneously at three transverse stations. All measurements have been made using five port cone probes.

The following observations were made from the single-slotted wall model results with and without applied suction.

The flowfield was found to be three-dimensional in nature with the flow velocity components inclined to the mainstream well beyond the conventionally defined boundary layer.

The natural ventilation through the slot (no applied suction) was found to have a strong influence upon the boundary layer displacement thickness and the character of the three-dimensional flowfield above the slot. Both the boundary layer and the displacement thickness distributions in the direction transverse to the slot were very sensitive to the applied suction rate through the slot. The boundary layer thickness was relatively constant in the transverse direction for no applied suction but decreased in the region of the slot with increased applied suction. The displacement thickness initially was considerably greater over the slot than away from it because of the natural ventilation at the transverse plane examined. For no applied suction, at $M_\infty = 0.76$ the displacement thickness at the slot was 3.3 times the corresponding flat plate value. The displacement thickness however diminished very rapidly with increased applied suction rate. The displacement thickness at the slot was reduced 5.32 times at $M_\infty = 0.76$ and $Q = 200$ SCFM ($m^* = 0.004$).The w–component perturbations produced by the applied suction were significant at the slot but decreased rapidly with lateral distance in the transverse plane. At $M_\infty = 0.77, Q = 87$ SCFM ($m^* = 0.0016$), w/U_∞ at the slot was 0.16, which reduced to 0.0423 at 0.5 inches from the slot centerline in the transverse direction. The boundary layer was almost removed over the slot at high suction rates.

The flow pattern in the transverse plane indicated the existence of a vortex-like secondary flow that contained streamwise vorticity. At high applied suction rates the suction effect diminished the secondary motions and the velocity vectors were directed towards the slot.

The change of the normal flow component (w) at the slot with that at the edge of the boundary layer above the slot showed a nearly linear variation. The w–component velocity at the edge of the boundary layer, $w_{z=\delta}$, can be either positive or negative depending on the rate of suction. An accurate knowledge of this relationship is required for determining the wall boundary conditions needed for the numerical calculation of the interference effect.

The following results were obtained for the flow on a segmented slotted wall:

Applied suction caused a low pressure region to be formed near the suction slots. The perturbations due to this pressure gradient extended to the tunnel wall or centerline and regions outside the boundary layer. The changes at adjacent and downstream direction were moderately small. The range of $\Delta w/U_e$ change, with maximum applied suction (about 25 lbm/min.), at the location between the two suction slots was about 2.5% and that at the adjacent or downstream locations decreased to about 1%. The changes in velocity components at the upstream measurement locations due to suction applied at the downstream chambers was less than 1%.

Blowing on the contrary had a marked influence on the flowfield. The blowing fluid displaced the adjacent mainstream fluid mass while convecting downstream. The maximum influence of the applied blowing was realized for measurement station located between the blowing slots themself. The blowing jet at higher blowing rates, by entrainment effect, resulted in a reduced w–component close to the edge of the boundary layer. In regions outside the boundary layer, a monotonic variation of $\Delta w/U_e$ was observed.

Blowing from side chambers resulted in significant cross plane velocity vector changes. The range of change of the $\Delta w/U_e$ component at the slot location between suction was about 3–4% and that in $v-$ and $w-$components at the adjacent center probe of order of 1–2%. The extent of the lateral influence was significant.

At the downstream station, blowing from the upstream side chamber induced upward motion on the fluid outside the boundary layer ($\Delta w/U_e$ changed about 1–2%) and in regions close to the wall introduced low pressure. Also the blowing fluid moved towards the tunnel centerline.

Blowing through the central compartments produced a large magnitude for $\Delta w/U_e$ at the center probe (about 5% change) and a nearly symmetrical influence on the side probes in the same transverse plane.

The downstream influence with blowing through the upstream compartment

$\Delta w/U_e$ changed about 1%. This indicated that the influence in the lateral direction exceeded (only slightly) that in the downstream direction.

The blowing and suction applied through the downstream compartments did not produce appreciable velocity component changes at the upstream measurement stations.

Applied blowing had stronger influence than that due to applied suction.

Two-compartment interactive blowing and suction produced results that included the characteristics of both the individual flowfields.

Influence coefficient $\Delta(\Delta w/U_e)/\Delta\dot{m}$ obtained assuming a linear variation of $\Delta w/U_e$ with $\dot{m}$ approximates the influence of blowing or suction through a compartment reasonably well.

The values of $\Delta w/U_e$, calculated using the influence coefficients obtained in a least square sense and assuming a linear combination of the individual velocity components for blowing or suction applied through 2 compartments simultaneously, compare reasonably well with the measured values.

The following conclusions were drawn from the results obtained for flow on single slotted wall:

(1) As expected, the flowfield in the vicinity of the slot is three dimensional in nature that extended into the freestream.

(2) Both the boundary layer and displacement thickness were very sensitive to the applied suction at the slot. The boundary layer displacement thickness was considerably greater over the slot for natural ventilation and diminished rapidly with increased suction. Far from the slot (in the lateral direction) in about five slot widths the boundary layer displacement thickness approached flat plate value.

(3) A vortex like flowfield existed in the vicinity of the slot for natural ventilation

or low suction. However at high suction rates the suction effects diminished these secondary motions. The streamwise vorticity was attributed to both the mean flow skewing and that induced by the turbulent stresses.

(4) The variation of the w velocity component at the edge of the viscous layer over the slot with that at the slot exhibited a nearly linear variation.

The following conclusions were made for flow on a segmented slotted wall:

(1) For suction and blowing applied through a given compartment, the resultant velocity component changes were maximum at points located between the active slots associated with that chamber.

(2) The lateral influence of applied suction or blowing exceeded only slightly that in the downstream direction.

(3) The upstream influence due to an active compartment was limited.

(4) The influence coefficients determined in a least square sense for two active compartments predicted the total velocity induced at a point that compared reasonably well with the measured values. However, the magnitude of the influence coefficients depended strongly on the location of the measurement point and active compartments. Therefore, the influence coefficient so determined were applicable only to the measurement and compartment locations from which they were determined.

(5) Finally it is concluded from the influence coefficients, for blowing and suction through individual chambers and simultaneously through multiple chambers, that changes in stream surface slope can effectively be controlled if the chambers are small and close enough to the location at which the desired change is sought.

BIBLIOGRAPHY

BIBLIOGRAPHY

Bean, H. S. (1971). "Fluid Meters: Their Theory and Application", 6th edition, ASME, New York.

Berndt, Sune B. (1977). "Transonic Flow at a Slotted Test Section Well", AD A035308, AFOSR-TR-77-0035.

Berndt, Sune B. (1982). "Flow Properties of Slotted-Wall Test Sections", AGARD Conference Proceedings No. 335, Paper NO. 6.

Berndt, Sune B. and Hans Sorenson. (1975). "Flow Properties of Slotted Walls For Transonic Test Sections", AGARD Conference Proceedings No. 174, Paper No. 17.

Dowgwillo, R. M. (1977). "An Analysis of Data Quality in Transonic Wind Tunnel Testing", M.S. Thesis, The University of Tennessee, Knoxville, Tennessee.

Firmin, M. C. P. and P. H. Cook. (1984). "Disturbances From Ventilated Tunnel Walls in Aerofoil Testing", AGARD Conference Proceedings No. 348, Paper No. 8.

Ganzer, U. (1984). "A Short Note on Recent Advances in the Adaptive Wall Technique for 3D-Model Tests at the TU-Berlin", AGARD Conference Proceedings No. 348, Paper No. 6A.

Goethert, B. H. (1961). "Transonic Wind Tunnel Testing", Pergamon Press.

Goodyer, M. J. (1985). "Derivation of Jack Movement Influence Coefficients as a Basis for Selecting Wall Contours Giving Reduced Levels of Interference in Flexible Walled Test Sections", NASA CR 177992.

High, M. D. (1970). "Turbulent Boundary-Layer Profiles Measured in a High Enthalpy Supersonic Channel Flow", AEDC TR-70-209.

Kemp, W. B. Jr. (1978). "Toward the Correctable-Interference Transonic Wind Tunnel", Proceedings of the AIAA 9th Aerodynamic Testing Conference, pp. 31–38.

Lighthill, M. J. (1958). "On Displacement Thickness", Jl. of Fluid Mechanics, Vol. 4, p. 383.

Matyk, G. E. and Y. Kobayashi (1977). "An Experimental Investigation of Boundary Layer and Cross-Flow Characteristics of the Ames 2-by 2-fot and 11-by 11-foot Transonic Wind Tunnel Walls", NASA TM 73257.

Neyberg, S. E. (1976). "Some Results From an Investigation of the Slot Flow in a Transonic Slotted Test Section Wall", AGARD Conference Proceedings No. 187.

Reed, T. D., T. C. Pope and J. M. Cooksey (1977). "Wind Tunnel Calibration Procedures Manual", NASA CR 2920.

Rittenhouse, L. E. (1969). "Flow Separation on Cone-Cylinder-Frustrums at Transonic Mach Numbers", M.S. Thesis, The University of Tennessee, Knoxville, Tennessee.

Satyanarayana, B., E. Schairer and S. Davis (1981). "Adaptive-Wall Wind-Tunnel Development for Transonic Testing", Jl. of Aircraft, Vol. 18, No. 4, p. 273.

Shan, L. (1974). "On Transonic Wind Tunnel Design Consideration", M.S. Thesis, The University of Tennessee, Knoxville, Tennessee.

Smith, J. (1982). "Measured Boundary Conditions Methods for 2D Flow", AGARD Conference Proceedings No. 335, Paper No. 9.

Stahara, S. S. and J. R. Spreiter (1979). "A Transonic Wind Tunnel Interference Assessment-Axisymmetric Flows", AIAA Paper 79-0203.

Tuttle, M. H. and E. B. Plantovich (1982). "Adaptive Wall Wind Tunnels-A Selected, Annotated Bibliography", NASA TM 84526.

Whitfield, D. L. (1976). "Analytic, Numerical and Experimental Results on Turbulent Boundary Layers", AEDC-TR-76-62.

Wu, J. M., F. G. Collns and M. K. Bhat. (1981). "Transonic Slotted Wind Tunnel Wall Boundary Layer Flow Study", Final Report for NASA NSG 2379, NASA Ames Research Center, Moffett Field, California.

Wu, J. M. and R. C. Lock (1974). "A Theory for Subsonic and Transonic Flow Over a Cone– With and Without Small Yaw Angle", U.S. Army Missile Command, Technical Report RD-74-2.

APPENDIX

APPENDIX

CALIBRATION OF FIVE PORT CONE PROBE

Very often in aerodynamic experiments measurements of flow speed and angularity are required. Pressure probes provide convenient, reliable and robust means to carry out these measurements. Cone probes present many desirable properties of pressure probes. Among these are ease of precision manufacture, infrequent and convenient calibration, high sensitivity and less variation with changing test conditions. Among disadvantages are their relatively large size. Two modes of operation to conduct flow angularity measurements using a cone probe are possible. These are null and fixed methods. In the null method, the cone probe is repositioned for every measurement to null all the differential pressures measured on opposing cone probe ports. The method requires 3-D orientation adjustment of the probe and therefore is not desirable in situations where rapid measurements are needed. In the fixed mode of operation pressures both differential (on symmetrically opposing ports) and static and total pressure on cone ports are measured. The flow conditions are then derived from the measurements of the calibration data. This later method is advantageous to conduct measurements rapidly (such as is needed in a blow down tunnel) but the derived data may not be as accurate as the null method.

In the present study calibration of cone probe at transonic and low subsonic speeds is carried out with the motivation to subsequently use it to carry out flow measurements.

DESCRIPTION OF EXPERIMENTAL SET-UP

Brief description of the probe geometry, calibration facility, probe orientation mechanism and instrumentation are given below.

PROBE GEOMETRY DETAILS

Using the computer program, Wu et al. (1974) the properties of various cones at incidence at transonic speeds were compared. Figure A.1 shows the differential pressure distribution on cone surface for various cone geometries. For optimum performance properties i.e., with reasonable high sensitivity, cone angle high enough but not to introduce separation at cone cylinder shoulder, small probe dimensions and position of probe ports such that the pressure distribution at these locations remain nearly constant, the cone probe with a 40 degree included angle and dimensions as indicated in Figure A.2 was chosen.

OPEN JET TUNNEL

The schematic of the experimental set-up is shown in Figure A.3 and the nomenclature of the probe at incidence is shown in Figure A.4. The calibration runs were made with an open jet. The nozzle exit diameter of the tunnel was 2.0 inches. The probe tip was located at the center of the jet 1.5 nozzle diameters downstream from the nozzle exit. In this way the probe was located in the inviscid core of the jet.

The total pressure inside the stilling chamber upstream of the nozzle and in the jet using a pitot probe were compared at various jet Mach numbers. The difference was found to be negligible.

The static pressure within the jet was assumed to be atmospheric pressure and the jet Mach number, in which the probe was placed, was calculated using the stilling chamber total pressure and the atmospheric pressure.

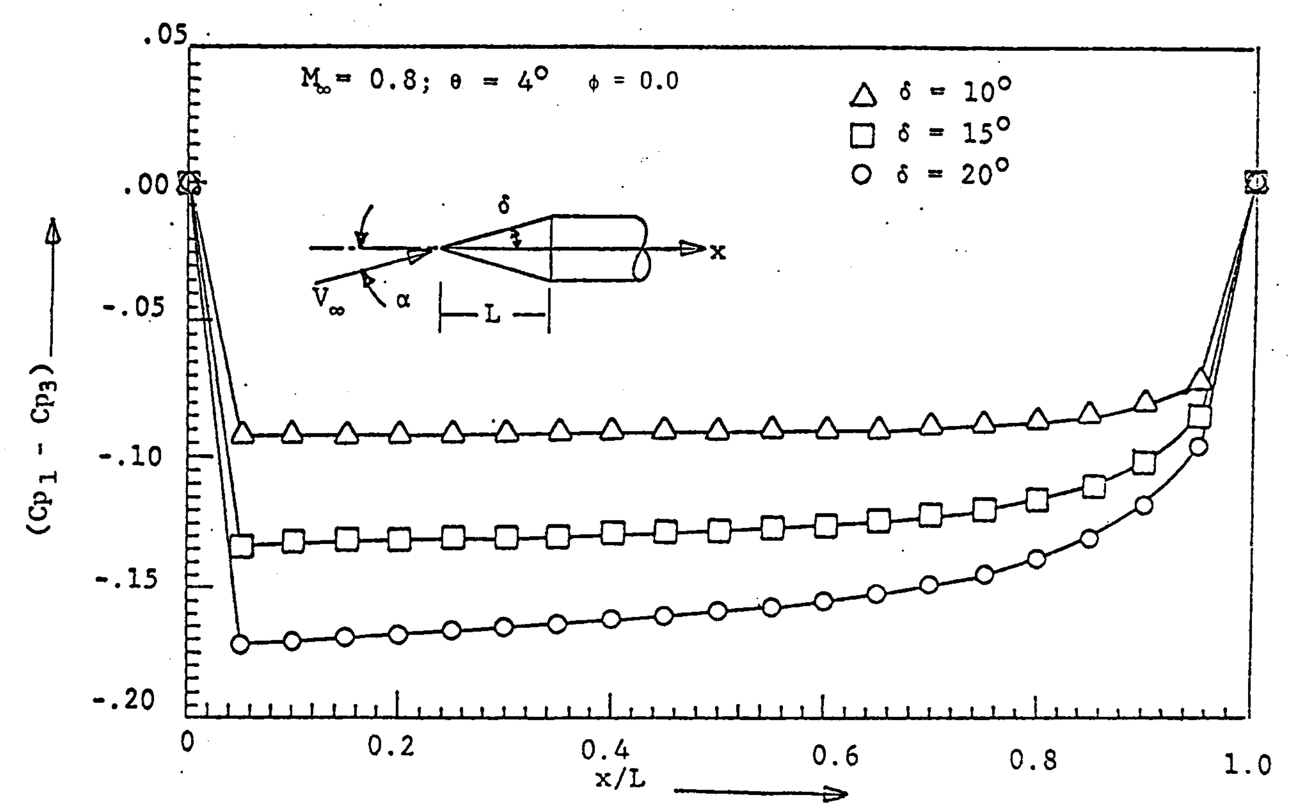

Figure A.1. Differential pressure distribution for various cone geometries (Wu et al. 1974).

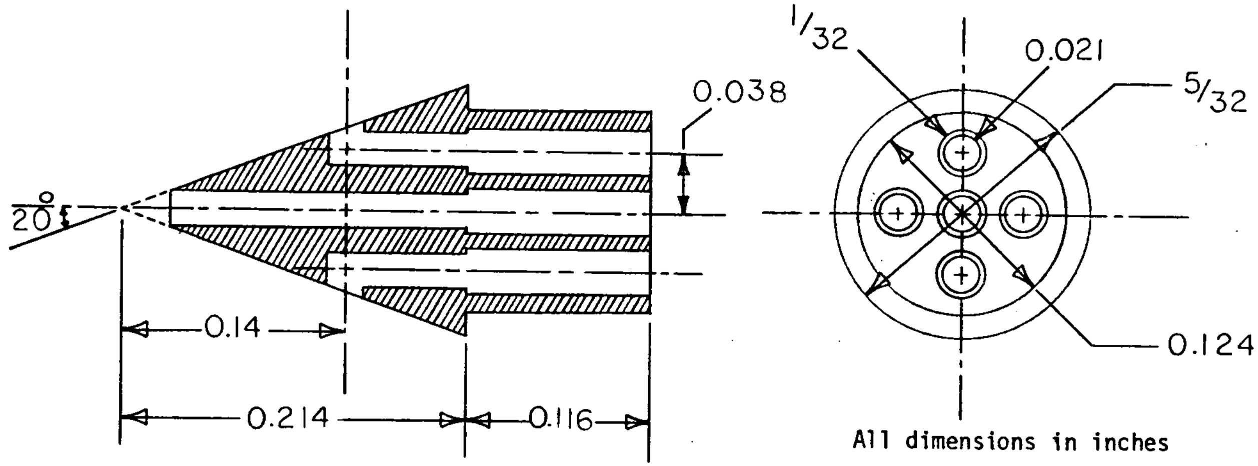

Figure A.2. Schematic of five port cone probe.

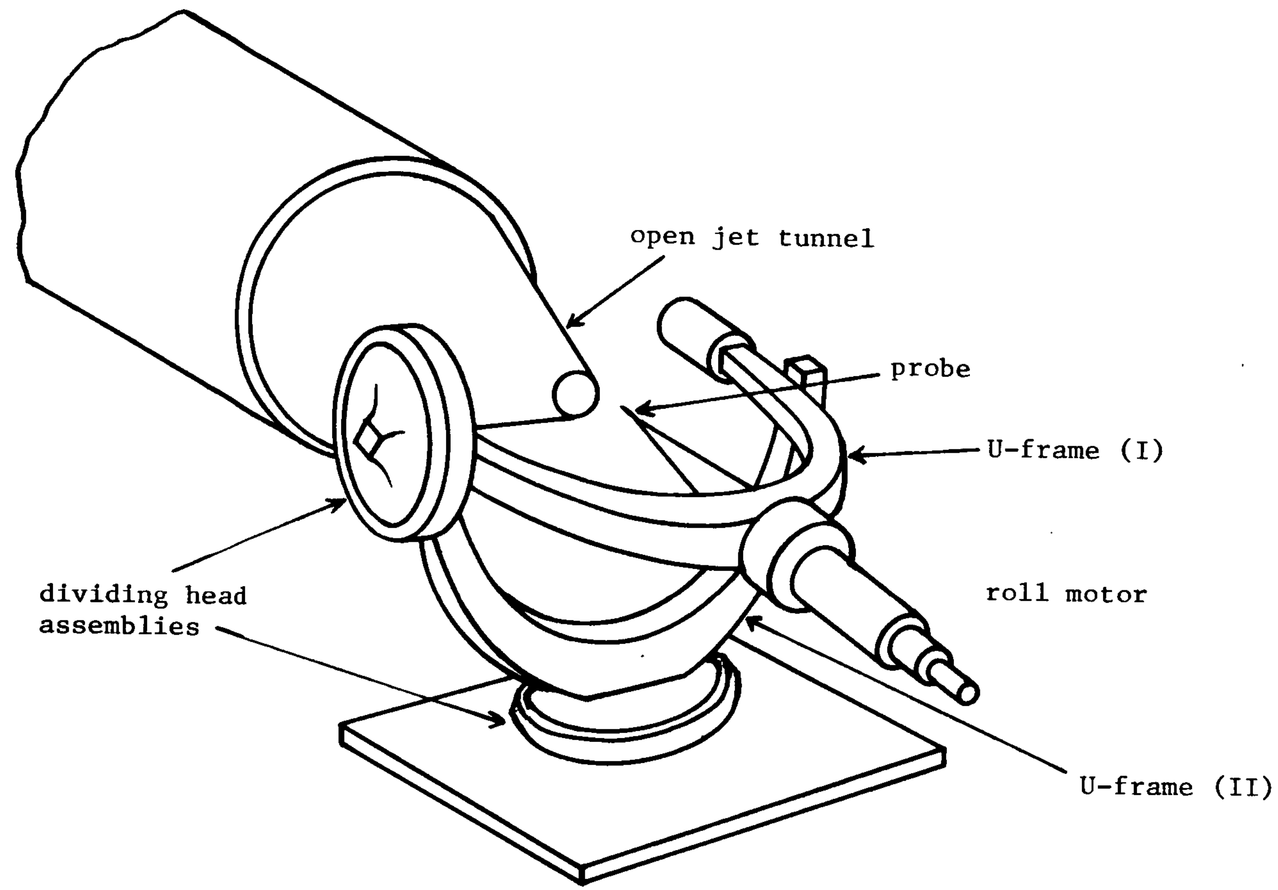

Figure A.3. Schematic of experimental set-up.

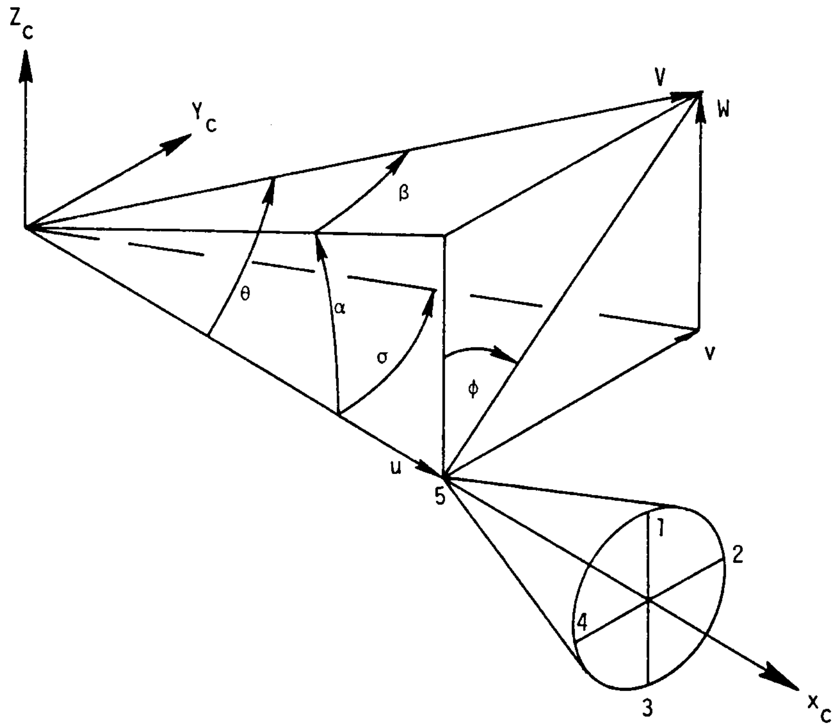

Figure A.4. Cone probe nomenclature.

PROBE ORIENTATION MECHANISM

The cone probe to be calibrated was glued on the forward part of the sting stem. Further downstream the sting enlarged into a slender conical body of revolution for added stiffness and strength. The sting was built in 2 parts. The joint was such that it introduced minimum wobble when the probe was rolled. The sting was supported into a U–frame on 2 bearings and was connected to a computer controlled roll motor. The probe stem and sting were hollow to allow carrying the pressure port tubes through them. The pressure tubes were finally taken out of the sting tube through a cut before the sting tube attached to the roll motor.

The U–frame (I) carrying the roll motor and the probe was mounted through a dividing head device on another U–frame (II). The U–frame (II) was fixed on a shaft at its center which was held, through a dividing head assembly, in a bearing on an adjustable platform.

The U–frames (I) and (II) could be rotated to introduce pitch and yaw flow angularities to the probe. The dividing heads permitted angular changes in both pitch and yaw in increments of 1 degree. The dividing head assemblies also allowed limited angular adjustments required for initial setting up of the probe. The U–frames (I) and (II) and the probe sting were so designed that with pitch, yaw or roll angularities the probe tip always remained at the center (same physical location) of the set-up.

It has been our experience that there will always be some wobble when the probe is rolled. To minimize the wobble angularity the probe and its stem were uniquely attached to the probe sting. Further the initial angular adjustments in pitch and yaw permitted the probe to be set-up for constant wobble with roll, i.e., wobble axis or the roll axis coincided with the freestream. For minimum jet blockage the probe stem had same dimensions as the probe and enlarged sting was made slender. In order to minimize the probe vibrations at incidence and higher Mach numbers (transonic Mach numbers) damper weights were added on the extended U–frame (I) arms.

INSTRUMENTATION

The measurements required were the probe pressures, tunnel pressures, tunnel temperature and probe angular orientations.

The tunnel total pressure, inside the stilling chamber upstream of the nozzle exit, was measured using a pitot probe. All the pressures, i.e., tunnel total pressure, tunnel static (at the tip of the nozzle exit), cone probe pressures at ports 1 and 2, cone probe differential pressures ΔP_{1-3}, ΔP_{2-4}, cone probe total pressure at port 5 were measured using Validyne DP series transducers. The transducers were calibrated using MKS – Barotron system and were expected to yield accuracy to within $\pm 0.5\%$. The differential pressure transducers were calibrated to ± 5 psid for lower angularity orientations and then to ± 10 psid for higher flow angularity orientation measurements.

The tunnel temperature was measured inside stilling chamber using Chromel–Alumel (C-A) thermocouple giving temperature measurement accuracy to within $\pm 1^{o}C$.

A precision inclinometer (with accuracy within 1 minute) was used to measure the angular position changes of the pitch orientation frame i.e., U–frame (I).

The computer controlled roll motor used to role the probe to the desired azimuthal orientation had a resolution of 0.08 degrees.

CALIBRATION PROCEDURE

(i) The angular orientation position of pitch and yaw on the dividing head assemblies were set to zero.

(ii) Next using the adjustable platform the probe was approximately aligned with the freestream flow.

(iii) The limited adjustments in pitch and yaw dividing head assemblies permitted nulling the probe, i.e., the probe orientation was adjusted until the differential pressures ΔP_{1-3} and ΔP_{2-4} were approximately zero (to an acceptable tolerance value).

(iv) Next using pitch angularity dividing head, the probe was pitched to moderately large incidence (say 15^o). This introduced changes in ΔP_{1-3} and ΔP_{2-4}.

(v) The probe was rolled until ΔP_{2-4} was nulled. This step makes the plane containing the ports 1 and 3 parallel to the pitch incidence plane. This position of role angle is noted and the computer program initialized the probe role angle to zero.

With further incidence in pitch ΔP_{2-4} changed slightly from previously nulled value. This may be caused due to the following: (a) The role angle is slightly off, (b) the ports 2-4 and 1-3 are not exactly perpendicular of independent, (c) asymmetry in the probe, (d) pitch mechanism introducing yaw. In the present experiments these changes were negligible within our accepted tolerance of ΔP within 0.05 psid.

The probe was brought back to zero pitch incidence and next the probe was yawed relative to the freestream. For moderately large incidence ΔP_{1-3} remained negligibly small while ΔP_{2-4} changed.

(vi) The probe was brought back to zero incidence. Next the probe was rolled through 360^o in increments of 90^o and the differential pressures ΔP_{1-3} and ΔP_{2-4} recorded. It was noted that the pressures ΔP_{1-3} and ΔP_{2-4} changed from the previously nulled values at $\phi = 0$. This was attributed to the small wobble that arises when the probe is rolled. The objective next was to set the probe orientation such that with role angle the wobble remained constant, i.e., the axis of wobble coincided with the freestream direction. This was done by slightly adjusting the pitch and yaw of the probe such that with role the differential pressures ΔP_{1-3} and ΔP_{2-4} remain constant. The wobble misalignment was small. By interpolating across the data obtained for incidence in pitch or yaw, the wobble misalignment was determined to be about $\theta = 0.33^o$.

(vii) The probe was now set to be calibrated. The calibration procedure consisted of the following steps:

(a) The probe was set at incidence using the pitch incidence U–frame (I). The angle of this U–frame (I) relative to the gravity was measured using a precision inclinometer.

(b) At each incidence the probe was rolled from $\phi = -90^o$ to $\phi = 90^o$ in increments of $\Delta\phi = 5^o$.

(c) At each incidence θ and azimuthal orientation ϕ the probe and tunnel pressures and other data were digitized and recorded on computer.

(d) The steps (a) - (c) were repeated for various incidence angles and jet Mach numbers. The jet Mach number was calculated using the tunnel total pressure and the ambient pressure which was the static pressure within the jet.

RESULTS

Figure A.5 shows C_α vs. C_β for various free conditions. In these figures θ and ϕ angularities have the nominal values i.e., θ and ϕ shown have not been corrected for small wobble angularity. However the wobble pitch and yaw angularities have been accounted for determining the true incidence of cone probe and these true incidence in pitch (α) and yaw (β) have been used in polynomial approximation of data. The method of polynomial approximation of data follows.

POLYNOMIAL APPROXIMATION OF CALIBRATION DATA

Third degree polynomials as used by other investigators were used to fit through the calibration data in the least square sense.

Polynomials were fitted through α, β, P_T and P_∞ data independently. The following procedure was used.

The normalized coefficients of independent and dependent variables were formed. The dependent variables were $\alpha = \alpha,\ \beta = \beta$.

$$C_O = \frac{P_5 - P_T}{P_5 - \overline{P}}$$

$$C_q = \frac{P_5 - \overline{P}}{P_T - P_\infty}$$

The independent variables were

$$C_\alpha = \frac{P_1 - P_3}{P_5 - \overline{P}} = \frac{\Delta P_{1-3}}{P_5 - \overline{P}}$$

$$C_\beta = \frac{P_2 - P_4}{P_5 - \overline{P}} = \frac{\Delta P_{2-4}}{P_5 - \overline{P}}$$

$$C_M = \frac{P_5 - \overline{P}}{P_5}$$

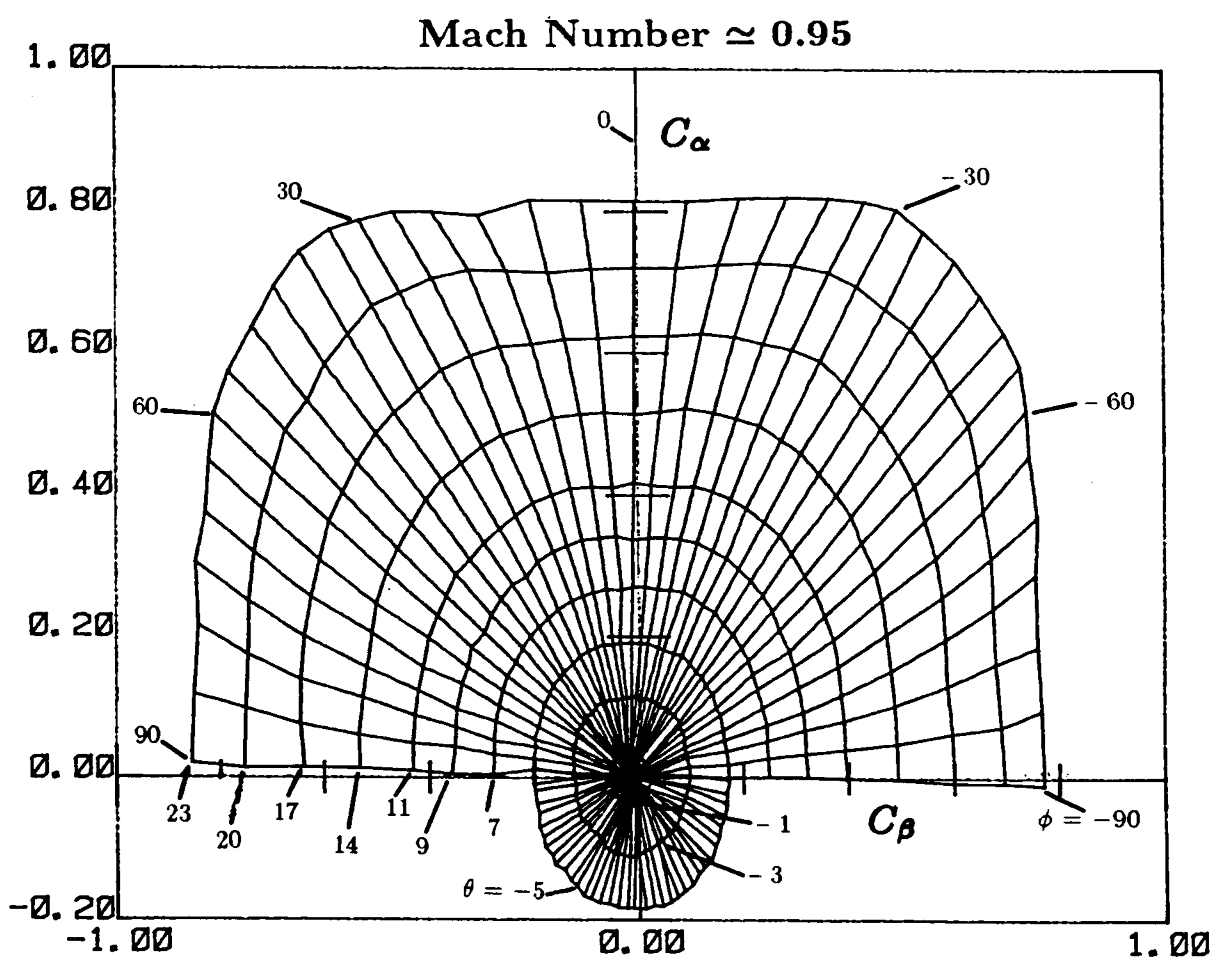

Figure A.5. C_α vs. C_β fornominalvaluesof θ and ϕ.

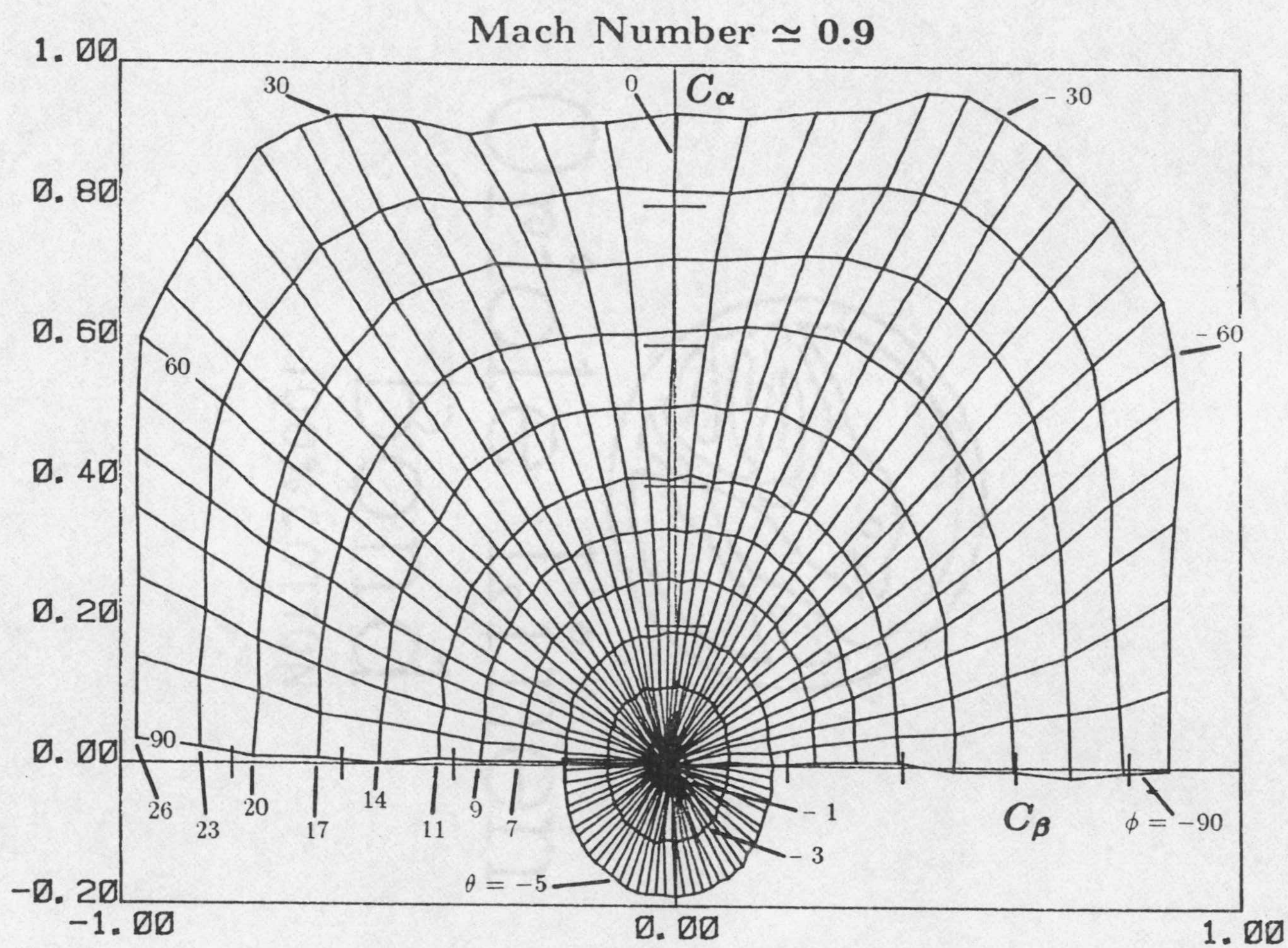

Figure A.5. (continued)

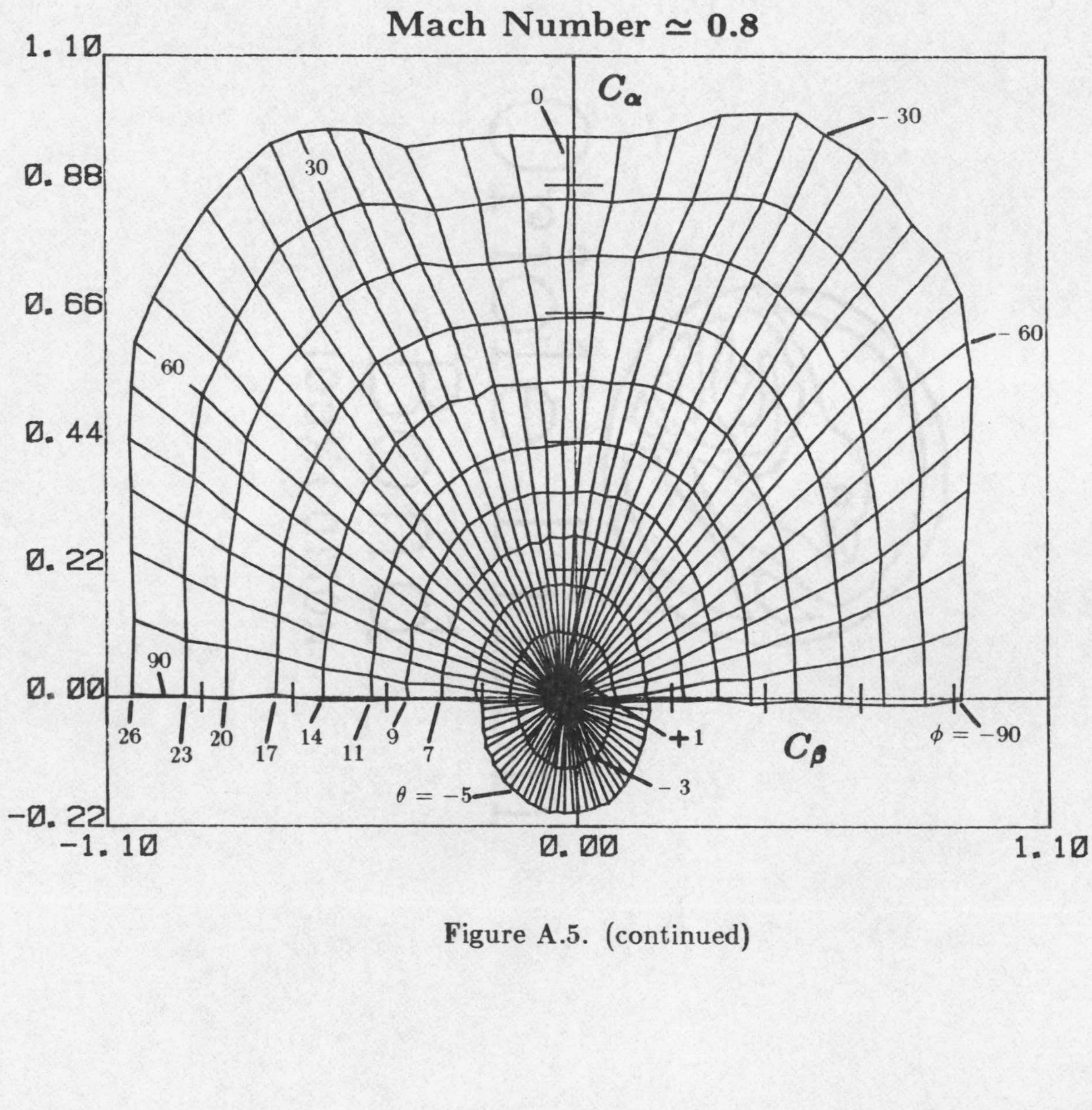

Figure A.5. (continued)

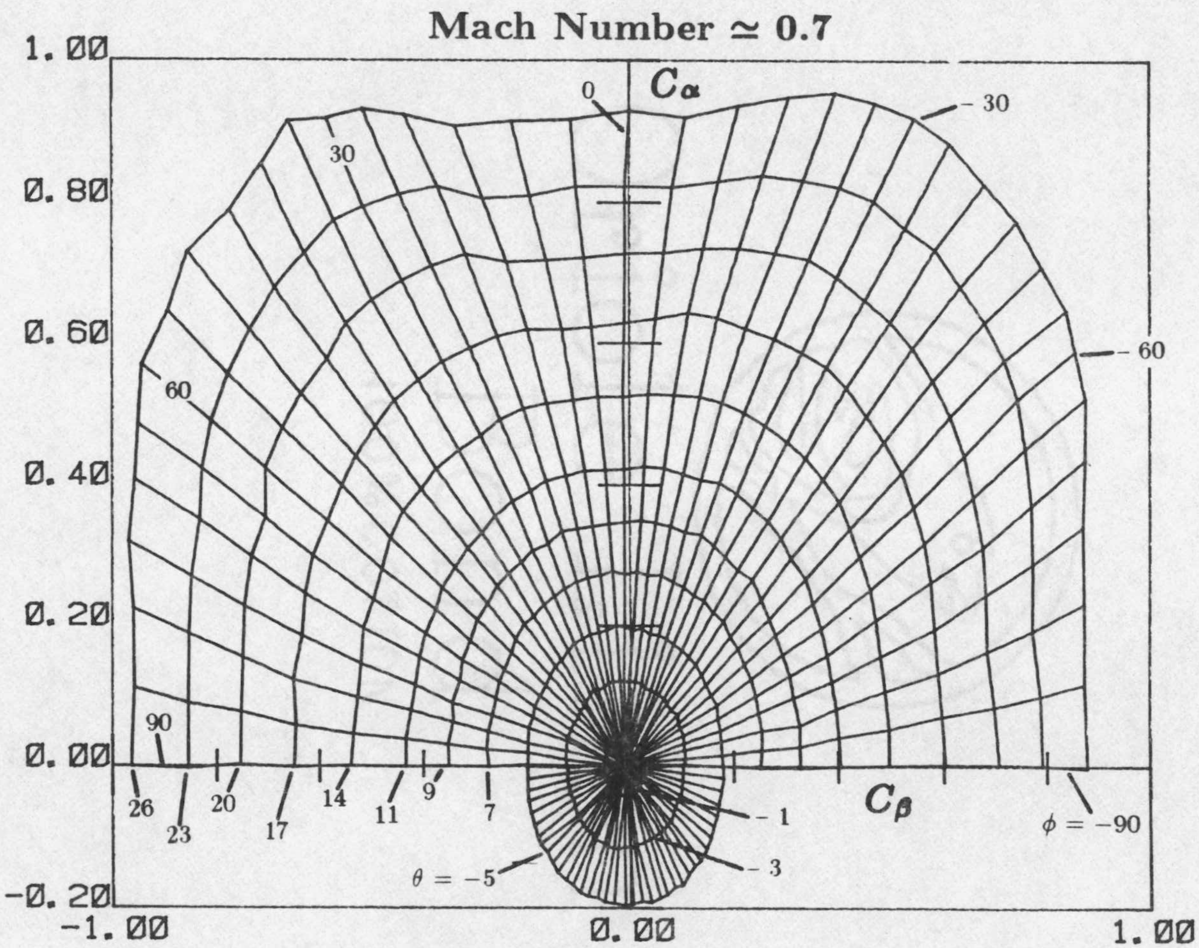

Figure A.5. (continued)

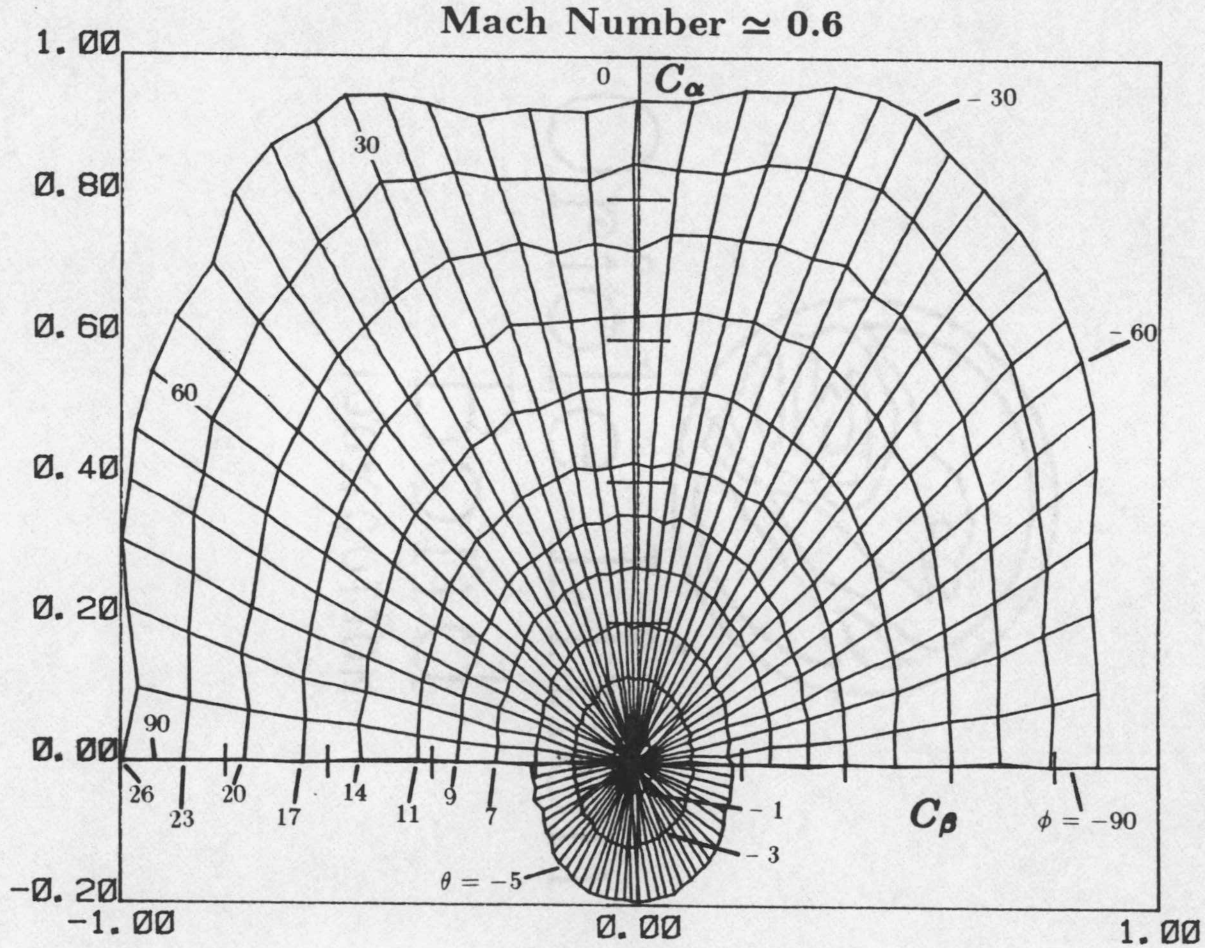

Figure A.5. (continued)

Mach Number $\simeq$ 0.5

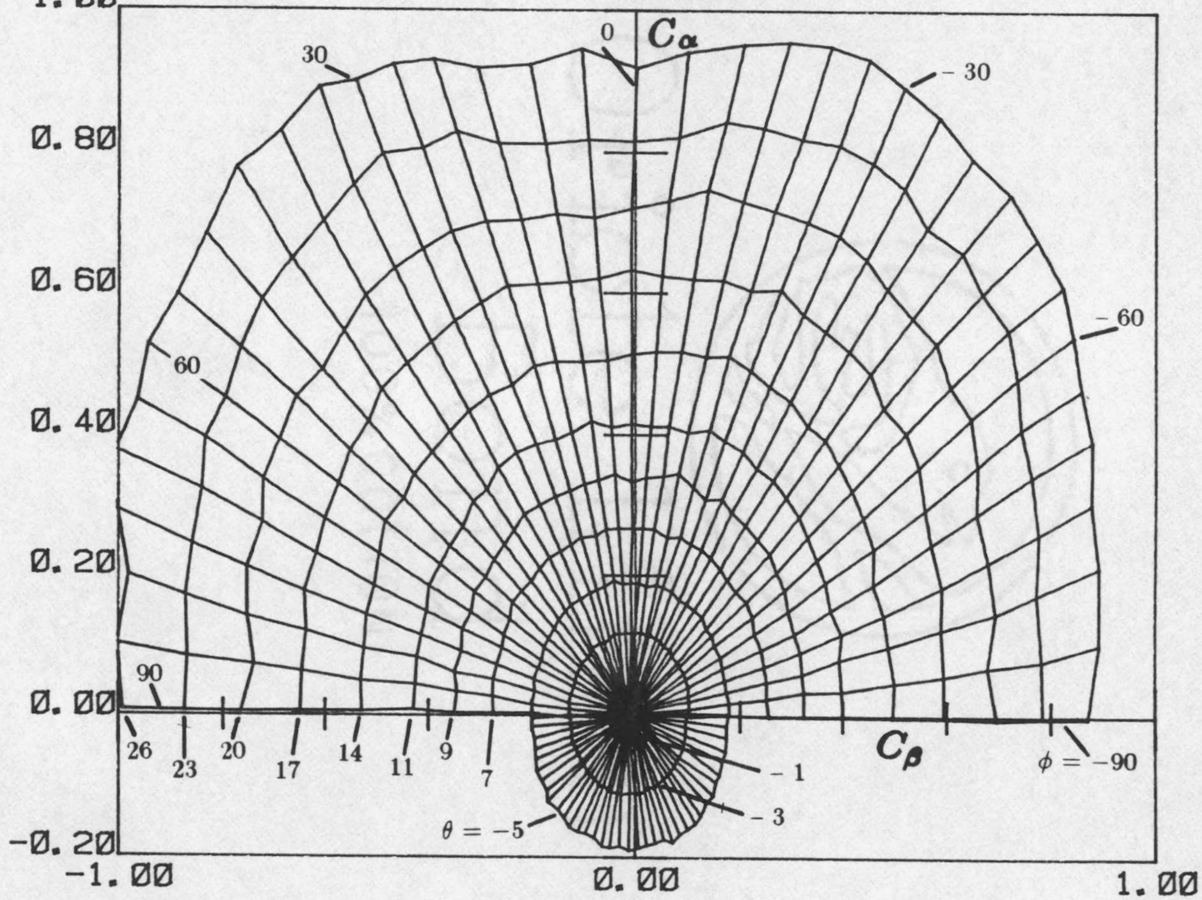

Figure A.5. (continued)

where

$$\overline{P} = \frac{P_1 + P_2 + P_3 + P_4}{4}$$

C_0 and C_q permitted the determination of P_T and P_∞.

Third order polynomial of the following form to represent the calibration data was used.

$$\begin{aligned}
F = {} & K_0 + K_1 C_\alpha + K_2 C_\beta + K_3 C_M \\
& + K_4 C_\alpha^2 + K_5 C_\beta^2 + K_6 C_M^2 \\
& + K_7 C_\alpha C_\beta + K_8 C_\alpha C_M + K_9 C_\beta C_M \\
& + K_{10} C_\alpha^3 + K_{11} C_\beta^3 + K_{12} C_M^3 \\
& + K_{13} C_\alpha^2 C_\beta + K_{14} C_\alpha^2 C_M + K_{15} C_\beta^2 C_\alpha \\
& + K_{16} C_\beta^2 C_M + K_{17} C_M^2 C_\alpha + K_{18} C_M^2 C_\beta \\
& + K_{19} C_\alpha C_\beta C_M
\end{aligned} \tag{1}$$

The above polynomial have 20 unknown coefficients and represents the functional form

$$F[C_\alpha,\ C_\beta,\ C_M].$$

The function F is one of the variables α, β, P_T or P_∞.

At each point $i = 1$, NPTS (total # of data points).

$$F_i[C\alpha_i, C\beta_i, CM_i]$$

In matrix notation, we then have

$$\underset{(\text{NPTS} * 1)}{[F]} = \underset{(\text{NPTS} * 20)}{[A]} \quad \underset{(20 * 1)}{[K]}$$

In order to determine the coefficients $[K]$ the following procedure which also assures a least square fit through the data is adopted.

$$\underset{(20 * 1)}{[A^T][F]} = \underset{(20 * 20)}{[A^T A]} \quad \underset{(20 * 1)}{[K]}$$

therefore

$$\underset{(20 * 1)}{[K]} = \underset{(20 * 20)}{[A^T A]^{-1}} \quad \underset{(20 * 1)}{[A^T F]}$$

A computer program that determines the coefficient vector $[K]$ each for α, β, P_T and P_∞ from the calibration data was written.

VITA

Maharaj Krishen Bhat was born at Srinagar, Jammu and Kashmir, India on August 18, 1946. He graduated from National High School, Srinagar in 1961. He received the Bachelor of Science in Mathematics and Physics from Kashmir University in 1966. In 1970, he received the Bachelor's degree in Mechanical Engineering from Allahabad University.

He joined the Indian Institute of Technology, Madras, India in 1971 and obtained an M.S. in Aeronautical Engineering in 1973. In 1973, he joined the Indian Space Research Organization as an aerodynamics engineer. He then joined The University of Tennessee Space Institute in September of 1976.

Mr. Bhat is an associate member of Sigma Xi, student member of the American Insitute of Aeronautics and Astronautics (AIAA) and the Society for Industrial and Applied Mathematics (SIAM).